AN ABSTRACT OF THE THESIS OF

Aaron K. Goodwin for the degree of Master of Science in Chemical Engineering presented on February 2, 2007

Title: Conversion of Glucose to Hydrogen Gas by Supercritical Water in a Microchannel Reactor.

Abstract approved:

_____

Gregory L. Rorrer

Glucose was gasified in supercritical water within a microchannel reactor at 650°C – 750°C, and 250 bar to yield H_2 rich gas with a low concentration of CO. The feed glucose concentration was 0.1 M. Two microchannel reactor configurations were tested at fluid residence times ranging from 0.5 sec to 24 sec. The first was a single tube microchannel reactor that consisted of a 2.0 m serpentine stainless steel tube imbedded within a heating block. Inner diameters of the tubing were 254 μm and 508 μm. The second was a serpentine microchannel reactor configuration, which consisted of a serpentine parallel array of 75 μm by 500 μm channels. It was fabricated in stainless steel by a combination of micromachining, laser cutting, and hotpress microlamination bonding techniques. Hydrogen yields averaged 5.7 ± 0.29 and peaked at 6.3 moles of hydrogen gas produced per mole of glucose fed in the serpentine microchannel reactor at 750°C and 250 bar. Typical gas compositions at 750°C and 250 bar were 52.5 % H_2, 35.0 % CO_2, 12.1 % CH_4, and 0.4 % CO. Gas composition and H_2 yield were not dependent on residence time, indicating that the gas products

were moving toward equilibrium. Complete glucose conversions were obtained in less than a 1.0 sec fluid residence time, and minimal organic acids were detected in the liquid products. Glucose, which subsequently decomposed to H_2, CO_2, CH_4, and CO, first decomposed to organic acids, rather than reformed by water directly to H_2, and CO_2. Acetic acid was the major intermediate. Measured hydrogen yield and gas composition were similar to stoichiometric hydrogen yield and gas composition based on the decomposition of glucose through an acetic acid intermediate. The presence of acetic acid in the liquid product and CH_4 present in the gas product confirms that glucose was being decomposed to organic acids that were further gasified to H_2, CO_2, CO, and CH_4.

Conversion of Glucose to Hydrogen Gas by Supercritical Water in a Microchannel Reactor

by

Aaron K. Goodwin

A THESIS

submitted to

Oregon State University

in partial fulfillment of

the requirements for the

degree of

Master of Science

Presented February 2, 2007

Commencement June 2007

Master of Science thesis of Aaron K. Goodwin presented on February 2, 2007

APPROVED:

Major professor, representing Chemical Engineering

Chair of the Department of Chemical Engineering

Dean of the Graduate School

I understand that my thesis will become part of the permanent collection of Oregon State University libraries. My signature below authorizes release of my thesis to any reader upon request.

Aaron K. Goodwin, Author

ACKNOWLEDGEMENTS

I would like to thank my advisor Dr. Gregory L. Rorrer, whose patients and support helped me complete this project. His guidance provided me a road map to successes.

I would like to thank my girlfriend Johannah Cervantes. Her unconditional support and ability to make me smile regardless of my stress level was invaluable to me. I would like to thank my lab mates and friends Clayton Jeffryes and Tavi Cruz-Uribe for their support, help, and encouragement whenever a problem arose. I would like to thank my friend and lab mate Thad Ivey for motivating me to get up in the morning on weekends to go kayaking with him. I would like to thank my parents for their moral support, encouragement, and willingness to always listen.

I would like to thank Bend Research for supporting me financially and having the confidence in me to send me to graduate school. Also I would like to thank Bend Research for donating a HPLC auto-sampler to the Rorrer laboratory.

Finally I would like to thank the Army for supporting this project.

TABLE OF CONTENTS

TABLE OF CONTENTS (Continued)

TABLE OF CONTENTS (Continued)

Page

LIST OF FIGURES

LIST OF FIGURES (Continued)

LIST OF FIGURES (Continued)

Figure Page

LIST OF FIGURES (Continued)

LIST OF FIGURES (Continued)

LIST OF FIGURES (Continued)

LIST OF TABLES

LIST OF TABLES (Continued)

Introduction

With crude oil prices continually on the rise and a growing concern for global warming, there has been a recent push for the development of alternative renewable energy sources. Biomass is a clean and renewable source for the production of H_2 gas. Currently it is estimated that biomass makes up 10% - 14% of the world's energy supply (McKendry et al. 2002). Unlike fossil fuels, biomass is CO_2 neutral. The CO_2 used to grow the biomass during photosynthesis is released when the biomass is gasified. The released CO_2 is used to grow more biomass, thus making the process renewable and clean. This paper focuses on supercritical water gasification of glucose.

Biomass

Plant biomass is a complex mixture of organic materials derived from CO_2, water, and sunlight. The main components of biomass produced via photosynthesis are starch and cellulose (Berg et al. 2002). Starch is a complex carbohydrate used by plants to store excess glucose, and is made from amylose and amylopectin. Amylose is a linear polymer of glucose joined by an α-1,4 glycosidic linkage. Amylopectin is a highly branched polymer of glucose, where branching occurs every 24 to 30 monomer units (Berg et al. 2002). Cellulose is a polysaccharide carbohydrate that forms the primary structural elements of green plants. It is also made up from glucose monomers that are linked together through a β-1,4 glycosidic bond (Berg et al. 2002). Cellulose combined with lignin is termed lignocellulose, and is the most abundant biopolymer

on earth. When glucose, starch, or cellulose is reformed with water, H_2 and CO_2 are the major products. The overall reaction for glucose is

$$C_6H_{12}O_6 + 6H_2O \rightarrow 6CO_2 + 12H_2 \qquad (1.1)$$

where stoichiometrically it is possible to produce 12 moles of H_2 for every one mole of glucose reacted.

Current Technologies Used to Convert Biomass to Hydrogen

There are three major technologies currently used to convert biomass to H_2 gas.

Gasification

Gasification is the process by which biomass is converted to gas by heating in a media such as air or water. The first step in this process is the partial oxidation of biomass in air to synthesis gas at 800°C and 35 bar to yield

$$Biomass + O_2(g) \rightarrow CO(g) + H_2(g) + CO_2(g) + energy \qquad (1.2)$$

The products are further reacted by the water gas shift reaction to decrease the concentration of CO in the product stream. The water gas shift reaction

$$CO(g) + H_2O(g) \rightleftharpoons CO_2(g) + H_2(g) \qquad (1.3)$$

can be carried out in a high temperature reactor, or a low temperature catalytic reactor. Two major advantages of gasification are: it is a robust well understood process, and it is able to utilize lignocellulose as a feedstock. Two major disadvantages to this

process are product gas cleanup and an expensive pre-treating step. As biomass heats up during the partial oxidation reaction it goes through pyrolysis that produces unwanted tar and char. The tar and char can be cleaned up by further gasification or reacted on a nickel catalyst to increase the conversion of condensable hydrocarbons (Sutton et al. 2001). Secondly there will be high levels of CO in the reactor product stream after the water gas shift reaction due to thermodynamic constraints. The residual CO must be removed from the gas stream if the H_2 is to be used in a PEM fuel cell given that CO poisons fuel cell catalysts. The biomass must go through an expensive drying step before the biomass can be gasified. Depending on the moisture content of the biomass, the drying step can severely add to the cost of gasification.

Aqueous Phase Reforming

The second process being investigated for hydrogen production from biomass is aqueous phase catalytic reforming (Huber et al. 2006). The process takes place over a bi-functional catalyst usually, Pt/SiO_2-Al_2O_3, at approximately 225°C and 32 bar - 35 bar. The reaction for hydrogenated glucose, sorbitol, is

$$(COH_3)_2(COH_2)_4\,(aq) \xrightarrow{Pt} 6\,CO(ads) + 7\,H_2(g) \xrightleftharpoons{Pt,H_2O} 6\,CO_2(g) + 13\,H_2(g) \tag{1.4}$$

The process begins when sorbitol is dehydrated over a solid acid or aqueous mineral acid catalyst, followed by dehydrogenation and selective C-C bond cleavage over a platinum catalyst. CO and H_2 gas are released as products. Adsorbed CO on the platinum catalyst surface further reacts with water via the water gas shift reaction to

form H_2 and CO_2. The gas streams for oxygenated hydrocarbons i.e. glycerol and sorbitol, at low concentrations (1 wt% in water), contained less than 300 ppm of CO, and produced high hydrogen yields. However hydrogen yields obtained from glucose were low and significant amounts of CH_4 and ethane were formed. Major disadvantages of aqueous phase reforming are expensive catalyst, long residence times, and decreased hydrogen yield for carbohydrates.

Supercritical Water Reforming

The third process used to produce H_2 from biomass is gasification in supercritical water. Water is supercritical when it is above its critical point on its phase diagram. That is any combination of temperature and pressure above 374.4°C and 217.7 bar. The properties of supercritical water vary from those of either water in the liquid or gas state. The dominant characteristic that makes supercritical water gasification so feasible is its extremely low dielectric constant. As water is heated well past its critical temperature its dielectric constant dramatically decreases. As a result its ionic character and its ability to hydrogen bond decrease. The density of supercritical water is one tenth of liquid water, and has practically no surface tension (Johanson et al. 2001). Under supercritical conditions, water solubility is similar to that of high pressure steam. Larger organic molecules, including polymers, hydrolyze to smaller organic molecules. These small volatile organic molecules, regardless of polarity, will be completely miscible in the supercritical water (Johanson et al. 2001). The characteristics of supercritical water including low viscosity, relatively high density,

and the ability to solubilize both small polar and non-polar volatile organic compounds, make it an ideal choice for reforming carbohydrates with no catalyst.

Over the last decade several groups of researchers have studied supercritical water gasification of biomass. Yu et al. (1993) gasified low concentrations of a glucose solution, 0.1 molar, at 600°C, 345 bar, and a 30 sec residence time. The gas contained H_2, CO_2, CO, CH_4, and small amounts of ethane, ethylene, and other larger hydrocarbons. The gasification efficiency, defined as the fraction of recovered carbon in the gas, decreased in both Hastelloy and Inconel reactors when feed concentrations were greater than 0.4 M glucose. Yu et al. observed that the type of reactor material has a strong influence on the gasification efficiency. They concluded that Inconel strongly catalyzes the water gas shift reaction, and that corroded Hastelloy behaves more like Inconel with glucose as a reactant. The result of this catalytic activity was an increase in CO_2 yields and a decrease in CO yields. The group was able to achieve a hydrogen yield of 7.7 moles of hydrogen per mole of glucose in the corroded Hastelloy reactor.

Xu et al. (1996) determined that at 600°C and 345 bar, a 1.2 M glucose solution could be completely gasified in the presence of various carbon catalysts. The gas was comprised of H_2, CO_2, CO, CH_4, and C_{2+}. C_{2+} is defined as any hydrocarbon containing 2 or more carbons. The carbon catalyst was shown to increase the gasification efficiency, decrease CO levels, and increase hydrogen yields. At 600°C, hydrogen yields in the presence of a carbon catalyst ranged from 2 – 2.25 mole of

hydrogen per mole of glucose, compared to 0.56 without the catalyst. Decreasing the reactor temperature in the presence of carbon catalyst decreased the hydrogen yields to 0.62 at 550°C and 0.46 at 500°C. The CO concentration in the gas at 600°C in the presence of the carbon catalyst was 10.1 %, as compared to 62.4 % without the catalyst.

Lee et al. (2002) investigated temperature dependence on the gasification of 0.6 M glucose solution at 280 bar in a Hastelloy reactor. At 750°C and a 19 sec residence time the gas composition was 46.4 mole % H_2, 2.6 % CO, 34.2 % CO_2, 12.2 % CH_4, and 0.4.5 % C_{2+}. The hydrogen yield was 4.78 moles of hydrogen per mol of glucose fed, and the gasification efficiency was 99.7 %. The gasification efficiency remained constant at 700°C over a residence time ranging from 10 to 50 sec. When the temperature was decreased to 600°C with a residence time of 16 sec, there was an increase in the CO concentration to 50.8 mole %. This was accompanied by a decrease in the hydrogen yield from 4.78 to 0.52 moles of H_2 per mole of glucose fed. Gasification efficiency also fell to 39.2 %. When the residence time was increased to 50 sec at 600°C, they observed a CO concentration of 9.7 mole %, and a hydrogen yield of 2.63, and the gasification efficiency increased to 67.3 %. Lee et al. hypothesized that the water soluble intermediates formed by the decomposition of glucose were rapidly converted to gas at reactor temperatures greater than 500°C. They also concluded that low CO concentrations above 660°C were due to the strong temperature dependence on the water gas shift reaction. Based on these results Lee et al. proposed a simplified model for hydrogen production from glucose. Pseudo first

order kinetics were obtained for the decomposition of glucose with activation energy of 67.6 kJ/mol.

Kertsen et al. (2006) gasified glucose in supercritical water using a quartz capillary batch reactor. They used a quartz reactor in order to study the process in the absence of metal that was thought to potentially catalyze the reaction. The gasification efficiency was 70 % when 0.1 M glucose was reacted at 600°C, and 300 bar. The gas was comprised of 13.3 % H_2, 20.0 % CO_2, 53.0 % CO, 6.0 % CH_4, and 7.4 % C_{2+}. When the glucose concentration in the feed solution was increased to 0.56 M the gasification efficiency remained approximately constant at 69 %. The gas composition was also similar and consisted of 11.7 % H_2, 8.9 % CO_2, 60.5 % CO, 12.9 % CH_4, and 6.0 % C_{2+}. Kertsen et al. concluded that the higher nickel content in both Inconnel and Hastelloy reactors improve carbon conversion and increase water gas shift activity. They noted that carbon conversion was unaffected by pressure, but was a strong function of temperature below 650°C. They also concluded that the addition of K^+ and Na^+ promoted the water gas shift reaction and led to increased hydrogen yields and decreased CO concentrations. However, the addition of K^+ and Na^+ did not increase carbon conversion.

Holgate et al. (1995) studied glucose hydrolysis and oxidation in supercritical water. The group concluded that at very low concentrations, 0.001 molar, glucose was completely gasified at 600°C, 246 bar, and a 6 sec residence time. The gas produced was comprised of H_2, CO, CO_2, CH_4, and C_{2+}. The major intermediates for

gasification of glucose were acetic acid, acetonylacetone, propenoic acid, and acetaldehyde.

Antal et al. (2000) gasified feed stocks of corn, potato starch gels, and wood sawdust in a tubular reactor. They reported that with rapid heating above 650°C, pressures of 280 bar, and activated carbon catalyzation, they produced clean reactor liquid effluent, as well as gas containing CO_2, CO, CH_4, H_2, and small amounts of C_{2+}. At temperatures, greater than 745°C, they report H_2 compositions as high as 57 % from cornstarch. Even though no tar formation was found, the reactor had to be shutdown periodically to remove coke and ash buildup which plugged the reactor. The group concluded that the nickel in Hastelloy catalyzes the gasification and reforming reactions.

Lu et al. (2006) successfully gasified a 0.2 M solution of glucose in a stainless steel reactor at 650°C, 250 bar, and 2.9 min residence time. The gas consisted of 33.5 mole % H_2, 14.5 % CO, 11.7 % CH_4, 36.3 % CO_2, and 4.0 % C_{2+}. The group concluded that high excesses of water lead to the selective formation of H_2 and CO_2. Secondly they observed that K_2CO_3 found in biomass catalyzes the reforming reaction leading to lower CO concentrations in the gas effluent. Lu et al. (2006) then gasified a 0.28 M glucose solution at 500°C, 300 bar, and a residence time of 5.3 min in the presence of 0.5 wt % K_2CO_3. The concentration of CO was decreased from 14.5 % at 650°C and 250 bar to 0.2 mole %.

Based upon previous work described above, and Williams and Onwudili (2005), Williams and Onwudili (2006), Yan et al. (2006), Penninger and Rep (2005), Matsumura et al. (2006) and Watanabe et al (2005) biomass can be gasified in supercritical water to produce H_2 rich gas that has the potential for use in hydrogen fuel cell technology. There are several major advantages that supercritical water reforming of carbohydrates offer compared to other biomass to hydrogen processes. The first advantage is simplicity. Supercritical water reforming is a one step process that involves no pre-processing or catalyst. In traditional gasification wet biomass can not be processed, and thus an expensive drying step is used to reduce the water content. Aqueous water reforming uses expensive catalyst which must be regenerated and monitored for fouling. The second advantage is short processing times. Nearly 100 % conversion of glucose was achieved with residence times shorter than 7 seconds (Holgate et al. 1995). Aqueous phase reforming requires residence times in excess of 6 min. The third advantage of supercritical water reforming is the resulting compressed product gas containing low levels of CO. Cleaning small amounts of CO from the product gas for use in a PEM fuel cell is easily attainable.

In order for commercial hydrogen generation from biomass in supercritical water to be realized, two technical barriers must be overcome. First a high heat flux reactor is needed. A high heat flux reactor will minimize the heating period of the reactants, and keep the reaction temperature constant in the presence of endothermic reforming reactions. Reaction temperature is a key process variable that significantly influences gas composition and hydrogen yield (Antal et al. 2000). Above 600°C and 250 bar

glucose is completely gasified and hydrogen yields range from 1.8 to 7.7 moles of hydrogen per mole of glucose fed. At temperatures above 650°C, the water gas shift reaction favors low CO concentrations in the gas. Decreases in reactor temperature due to the endothermic reforming reaction would lead to increased CO concentrations and lower hydrogen yields due to the formation of organic acid intermediates (Lee et al. 2002). A high heat flux reactor would allow a minimal heating period, producing greater hydrogen yields and decreased CO concentrations in the product gas.

The second barrier is reactor fouling. Gasification of biomass feed stocks eventually led to a build up of coke and ash in the heating zone of the reactor, which had to be taken off line periodically for clean up (Antal et al. 2000). Increased pressure drops through the reactor due to the buildup of char and coke, can cause excess stress on the system. Lu et al. (2006) concluded that furfurals and phenols formed during the heat up period were the key components causing the reactor plugging.

Based on previous work of Holgate et al. (1995) and Yu et al. (1993), a reaction pathway for the decomposition of glucose was proposed and is presented in Figure 1.1. There exist two major mechanisms for the decomposition of glucose, a high temperature pathway and a low temperature pathway. The low temperature pathway occurs when the temperature of the reactants is between 400°C and 600°C at pressures greater than 218 bar. One intermediate of the low temperature pathway proceeds through the formation of acetic acid and acetaldehyde that further decomposes to CO_2, CO, H_2, and small amounts of CH_4. Lastly, the gas products undergo water-gas shift

and methanation reactions. The water-gas shift reaction is presented in Equation 1.3, and the methanation reaction is

$$CO + 3\,H_2 \rightleftharpoons CH_4 + H_2O \qquad (1.5)$$

The second intermediate formed via the low temperature pathway is propenoic acid, which is further reacted to CO_2, CO, H_2, and small amounts of ethylene. The ethylene further reacts with H_2 to form ethane.

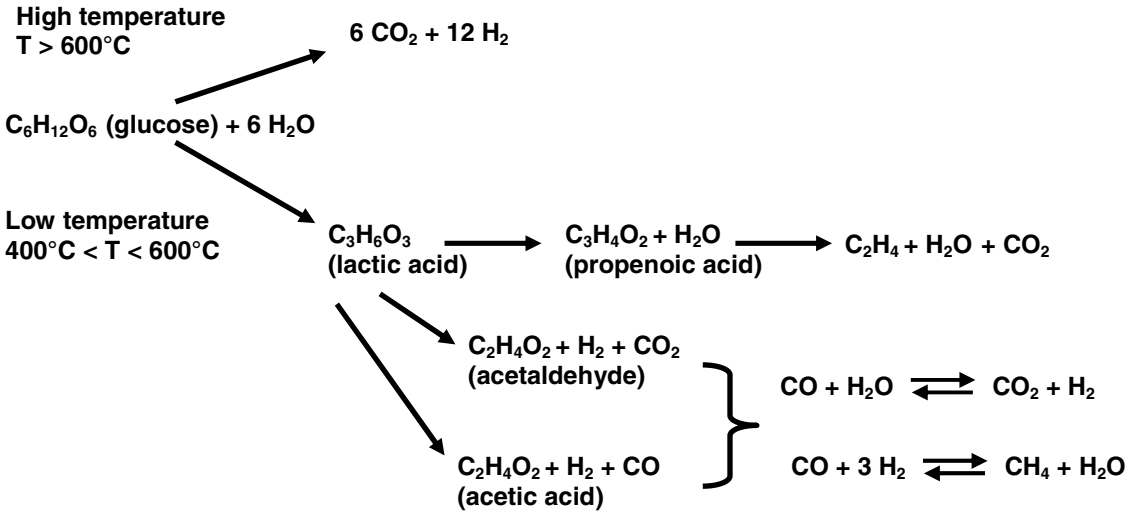

Figure 1.1. Reaction pathway for decomposition of glucose in supercritical water

At temperatures greater than 600°C in the supercritical state, glucose may be reformed via the high temperature pathway. The gas products CO_2 and H_2 are formed from un-stabilized free radicals that react with water Holgate et al. (1995). Equation 1.1 gives the reaction stoichiometry. The reaction is endothermic and has a standard enthalpy of reaction of +620 kJ/mol of glucose.

Microchannel Reactors

Microchannel reactors gained popularity in the 1970s as a result of process intensification concepts and manufacturing methods derived from the electronic industry (Holladay 2004). Thrusts towards the miniaturization of electronics led to novel manufacturing techniques allowing for micron sized complex geometries to be realized. Manufacturing techniques include etching, vapor deposition, micromachining, and lithography. Advances in manufacturing methods ultimately led to advances in micro reactor design. A micro reactor is a reactor whose channels hydraulic diameter is less than 1 mm (Palm 2001). Types of micro reactors include coated wall reactors, packed bed reactors, structured catalyst reactors, and membrane reactors (Holladay et al. 2004). Micro reactor technology has been used to realize such innovations as lab on a chip, microsensors, and advanced rapid chemical and catalyst screening tools (Wang and Holladay 2005). Improvements in micro reactor design and fabrication has enabled chemical and biological processing in microchannels to emerge as a dominate technology for diffusion limited and temperature sensitive processes.

Microchannel technology offers several advantages compared to traditional tubular reactors. They have been shown to increase yields and selectivity by exploiting high heat and mass transfer rates (Wang and Holladay 2004). Microchannel reactors can facilitate reaction pathways difficult to control in tubular reactors. They offer an

alternative approach to batch processing temperature sensitive reactions (Jensen 2005). Microchannel processing uses fewer utilities, has increased throughput for rapid screening processes, produces less waste, and has increased safety advantages (Jensen 2005). Microchannel reactor size plays an integral role for device miniaturization, and on board H_2 generation. Close temperature control, increased throughput due to smaller residence times, and small reactor size make microchannel processing a promising alternative to tubular and batch reactors.

Currently microchannel reactor design is focused around H_2 generation from hydrocarbons. Combustible fuels such as methanol and other hydrocarbons are able to store up to 100 times more energy per weight than batteries (Jensen 2005). Since H_2 gas is difficult to store due to its low compressibility, there is a need for portable H_2 production for devices such as laptop computers, cellular phones, GPS, and electric powered vehicles (Norton et al. 2005). The H_2 produced is fed into a PEM fuel cell and in the presence of oxygen is used to generate power. Presently methanol is widely used as a fuel for catalytic steam reforming in microchannel reactors due to its low sulfur content, and low activation temperature (Shah et al. 2005). Microchannel reactors have unique characteristics that could allow them to be used for on board power generation.

Several factors need to be overcome for microreactors to be realized commercially for H_2 production from hydrocarbons. The first is reactor fouling. Processing high energy density fuels such as natural gas, propane, diesel, ect. contain sulfur which eventually

leads to reactor fouling (Holladay et al. 2004). Processing biomass feed stocks also leads to a build up of coke in the reactor heating zone eventually plugging the reactor as previously discussed. The second factor to be overcome is catalyst fouling. Hydrocarbon reforming processes including steam reforming, partial oxidation, and autothermal reforming are carried out in the presence of iron or copper catalysts (Holladay et al. 2004) Catalysts must be able to be regenerated *in situ*, or extremely long lived due to the difficulty to remove or replace the catalyst (King et al. 2005). Lastly the integration of several unit operations is needed to determine the overall efficiency of the system. The first unit op needed is feed pre-treatment. Whether it is the hydrolysis or solubilization of biomass, or the de-sulferization of fuels, pretreatment of the feed will prevent fewer problems downstream. Secondly, there is a need for CO removal. CO poisons PEM fuel cells, and must be reduced below 10 ppm (Shah et al. 2005). Finally a PEM hydrogen fuel cell needs to be integrated to produce electrical power and determine the overall efficiency of the system.

Characteristics of microchannel reactors have been proven as an ideal platform for catalytically reforming methanol and other hydrocarbons to produce H_2 gas for electrical power generation in a PEM fuel cell. Glucose has successfully been reformed by supercritical water in tubular and batch reactors to produce H_2 gas with CO concentrations less than 1 mole %. The development of a high pressure microreactor would be able to facilitate the non-catalytic reforming of glucose to H_2 gas with little need for downstream processing due to low CO concentrations.

Rationale for Current Investigation

Due to the endothermic nature of glucose reforming to H_2 gas, and the need for a fast heating rate in the reactor entrance (Lu et al. 2006), a microchannel reactor was used to facilitate the reaction. In a microchannel reactor there is a large surface area to volume ratio. This ratio allows the fluid to have a high heat flux, and keeps the radial temperature profile above 600°C in the presence of the highly endothermic reaction. Minimization of the reactant heating period, along with accurate control of the reactor temperature, may promote the gasification of glucose via the high temperature pathway with the potential for low levels of CO, and little to no organic acid formation.

Research Goals and Objectives

The overall goal of this research was to develop a process to reform glucose in supercritical water using a microchannel reactor to produce H_2 rich gas low in CO. Glucose was used as a model compound because it is the monomer unit of cellulose and starch. To achieve this goal the research has 5 objectives: 1) Design and fabricate a high pressure microchannel reactor capable of operating at temperatures greater than 600°C and pressures of 250 bar, 2) Determine how residence time affects glucose conversion, gasification efficiency and gas composition in a microchannel reactor, 3) Determine the affect tubing diameter and reactor geometry has on gas composition, gas production, and organic acid formation, 4) Determine the affect reactor

temperature has on gas composition, gas production, and organic acid formation in a microchannel reactor, 5) Compare experimental gas compositions to predictions of thermodynamic equilibrium.

Two prospective areas for future work beyond the scope of this study are an investigation of potential feedstocks, including cellulose based biomass, and determination of catalytic activity resulting from reactor material on glucose decomposition and the water gas shift reaction.

Supercritical Reactor Test Loop Design

A schematic of the supercritical flow reactor is presented in Figure 2.1. Pictures of the reactor are presented in Figures 2.2 - 2.3.

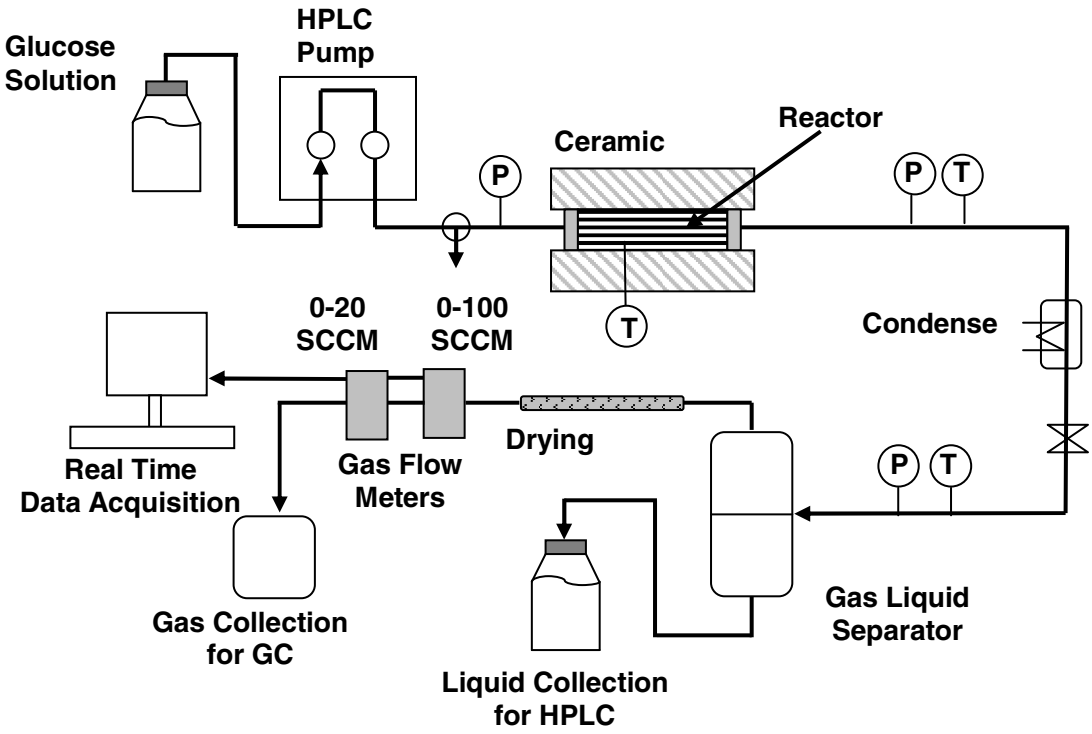

Figure 2.1. Supercritical flow reactor and test loop schematic

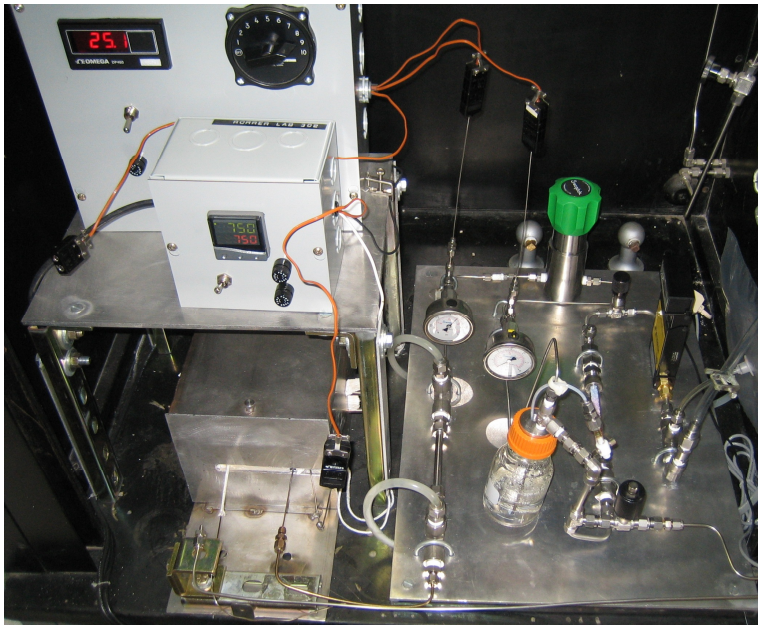

Figure 2.2. Supercritical flow reactor and test loop

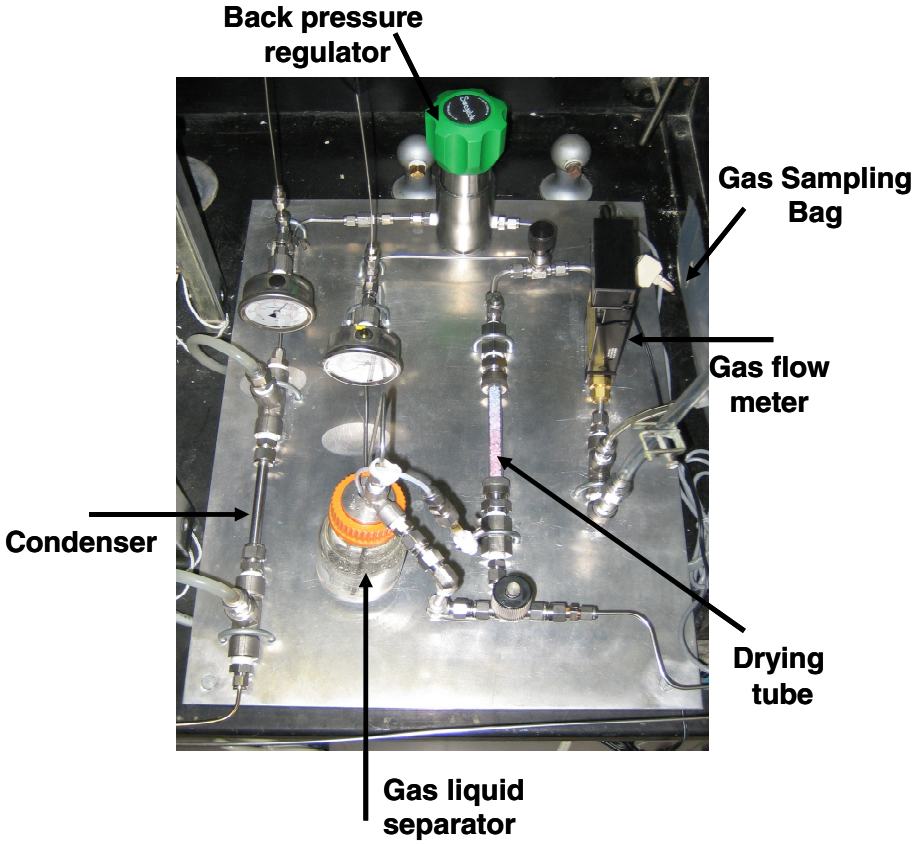

Figure 2.3. Reactor test loop

Pump

An Agilent 1100 series isocratic high performance liquid chromatography (HPLC) pump was used to deliver water and aqueous glucose solutions to the reactor. The reactants were pumped through a 40 µm glass frit to filter out large particles. Figures 2.4 – 2.7 show flow calibration curves for flow rates between 1 µl/min and 5 ml/min. Pump precision was determined by running 5µl/min of water for 23 hours and is presented in Figure 2.6. The delivery of 80 µl/min of water at 250 bar is presented in Figure 2.7. The flow range used in this study was 40.0 µl/min - 1.5 ml/min.

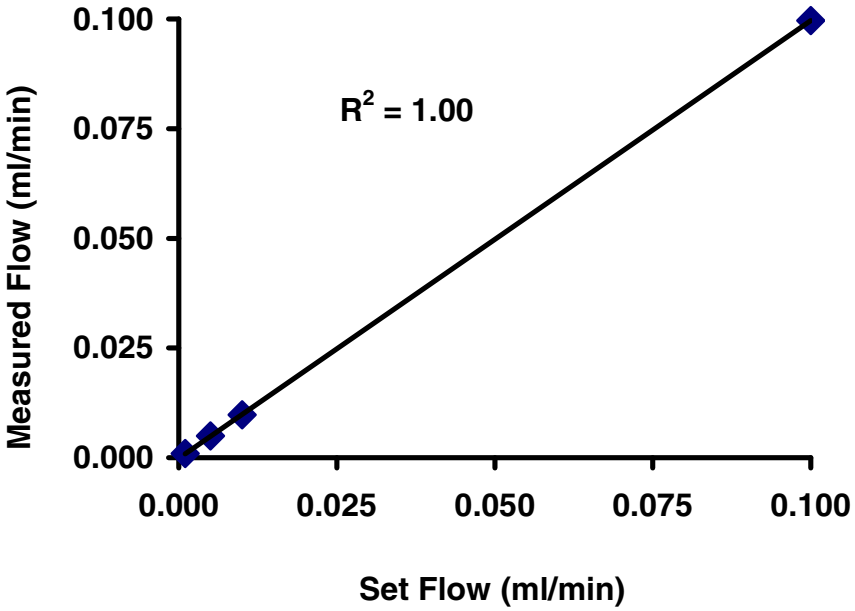

Figure 2.4. Measured pump flow rate as a function of set point at ambient conditions (0.001 ml/min-0.1 ml/min)

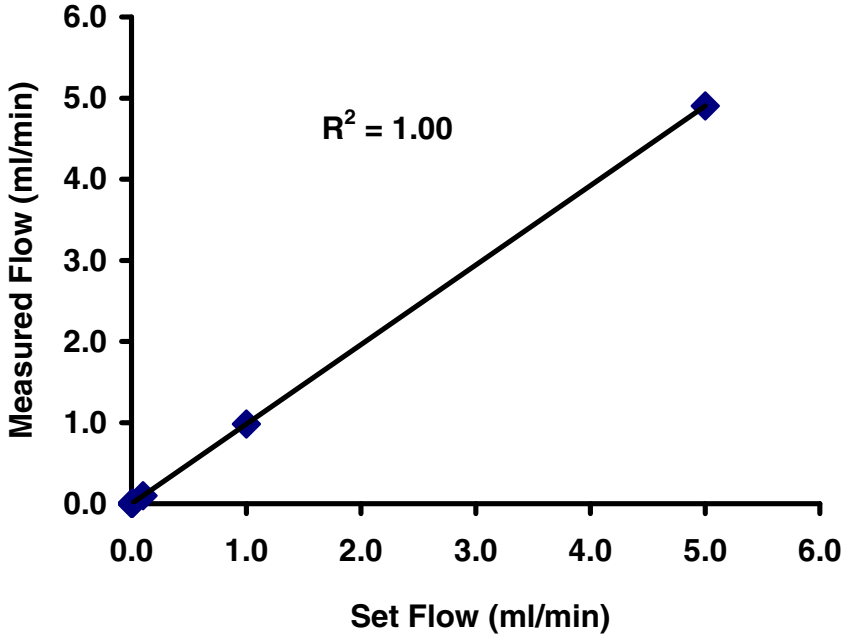

Figure 2.5. Measured pump flow rate as a function of set point at ambient conditions (0.1 - 5.0 ml/min)

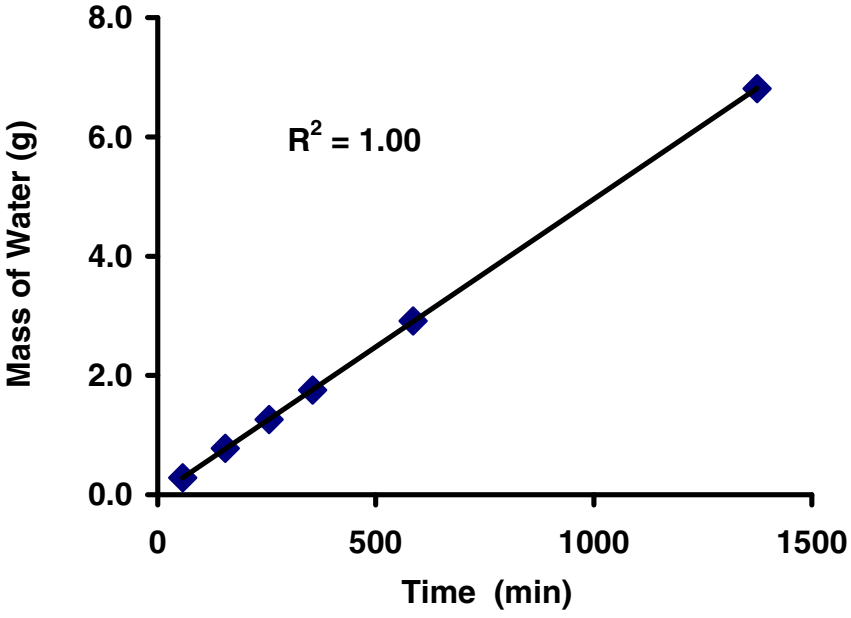

Figure 2.6. Mass of water pumped at ambient conditions with a set point of 50 µl/min

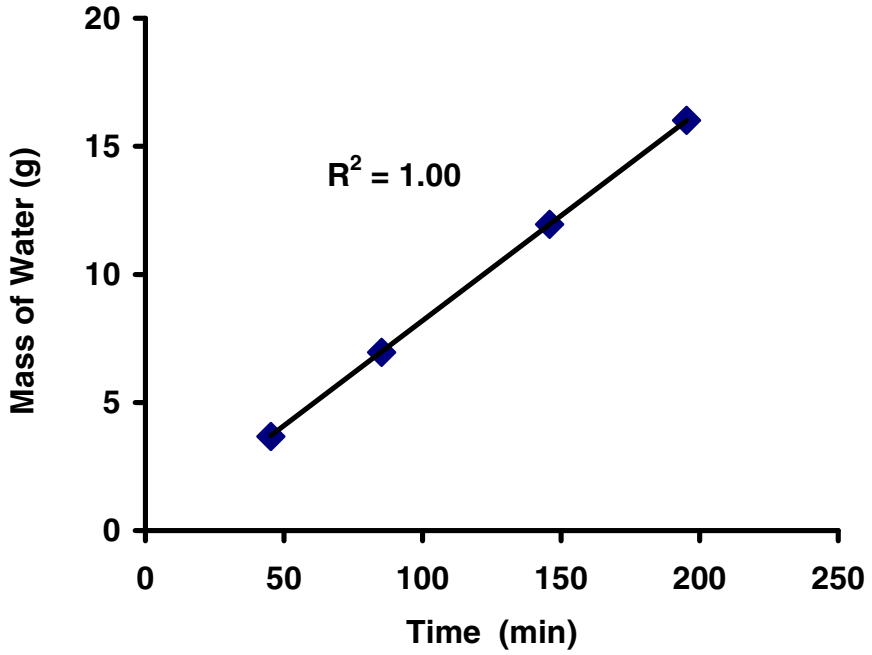

Figure 2.7. Mass of pumped water at 250 bar with a set point of 80 µl/min

Furnace Design

The furnace was used to heat the reactants from room temperature, approximately 25°C, to 600°C - 750°C. A cut out view of the furnace is presented in Figure 2.8. The shell of the furnace was constructed from stainless steel sheet. Its dimensions are presented in Figure 2.9.

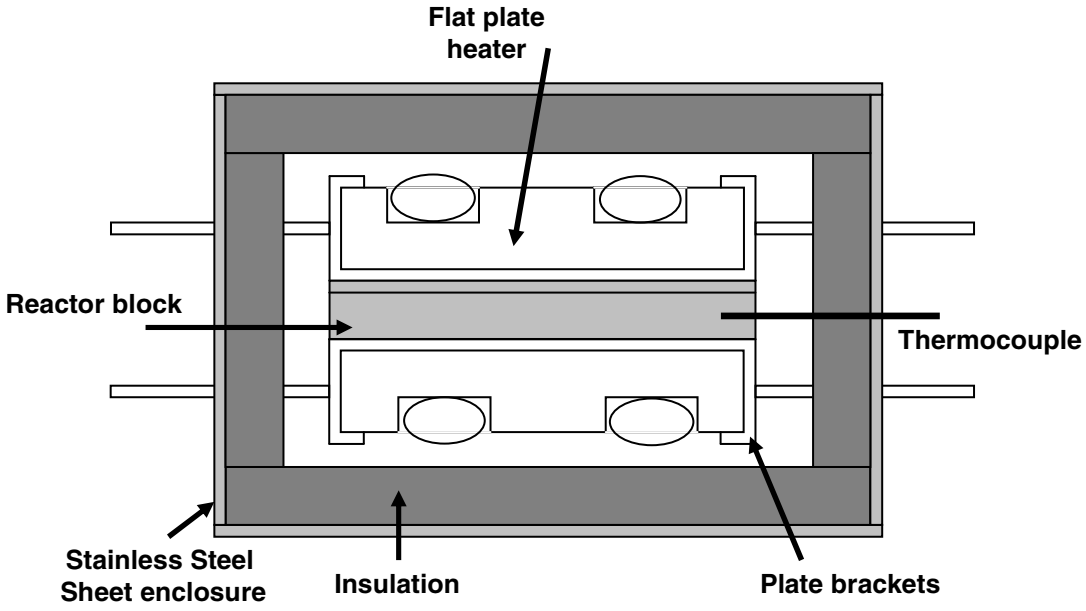

Figure 2.8. Cut out view of the reactor furnace design

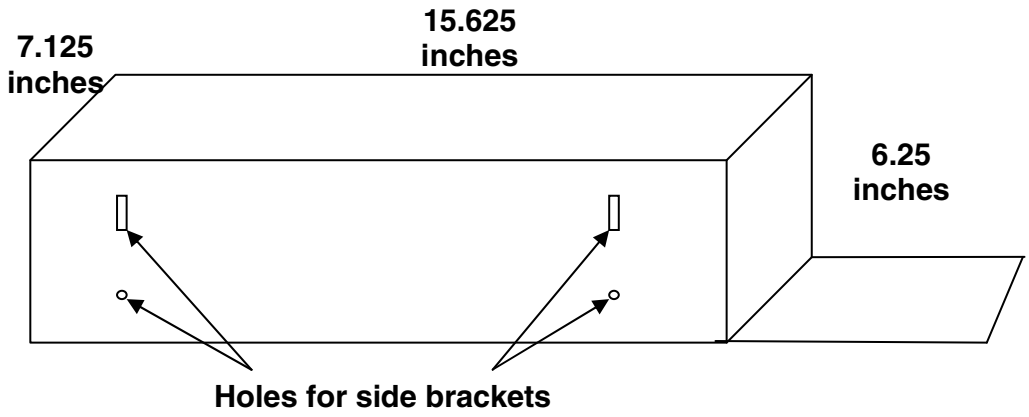

Figure 2.9. Reactor furnace enclosure dimensions

The furnace shell was insulated with 1.5 inch thick Fiberboard from Thermcraft Inc. The heater brackets, that held the heaters in place, were fabricated from stainless steel sheet and their dimensions are presented in Figure 2.10. The heaters were 11.6 inches by 3.1 inches PH ceramic flat plat heaters from Thermcraft Inc. They were constructed from 80-20 nickel-chrome wire helically wound and placed in a grooved ceramic holder. Each heater used 115 volts of AC, and 375 watts of power. The heaters were oriented parallel to each other with the reactor block in between them as presented in Figure 2.8. Conduction was the primary mode of heat transfer to the reactor block. The temperature of the reactor was controlled by an Omega Instruments CN9422-C2 1/16 DIN temperature controller with a P.I.D. control strategy connected to a 10 amp solid state relay. A 1/16 inch type J thermocouple was placed 1/2 inch into the reactor block and was used as the primary temperature reading for the controller. The wiring schematic used for the controller and relay is presented in Figure 2.11. A post tune heating profile with 80 µl/min of water flowing through the reactor is presented in Figures 2.12.

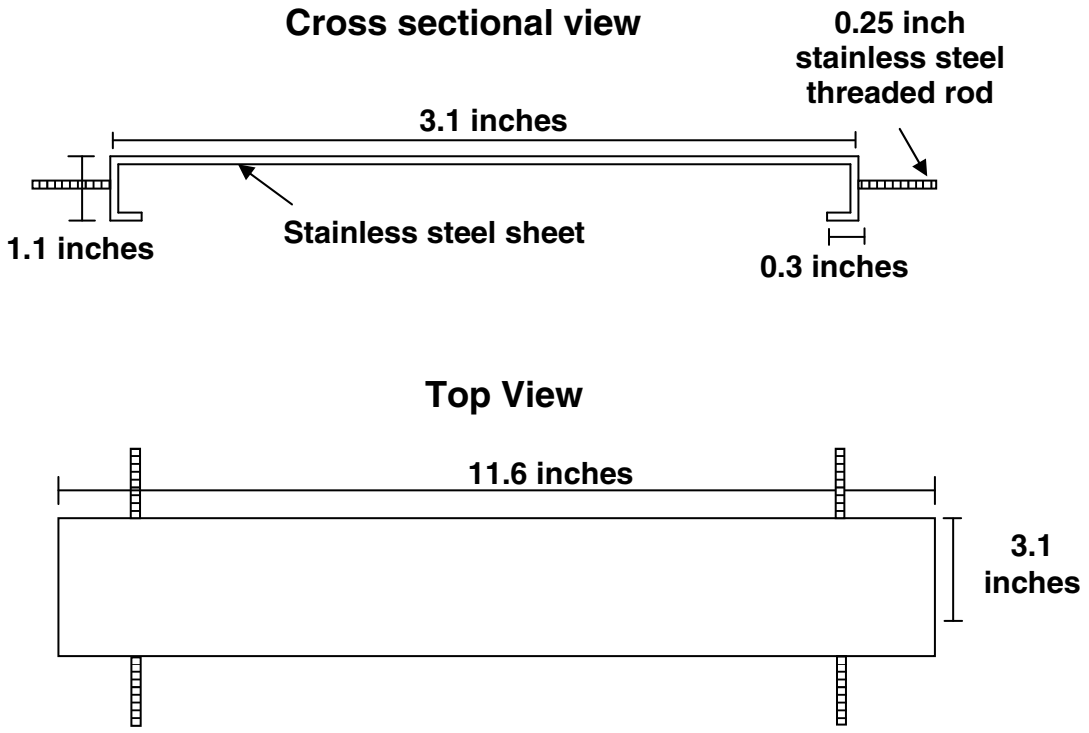

Figure 2.10. Ceramic flat plate heaters support design

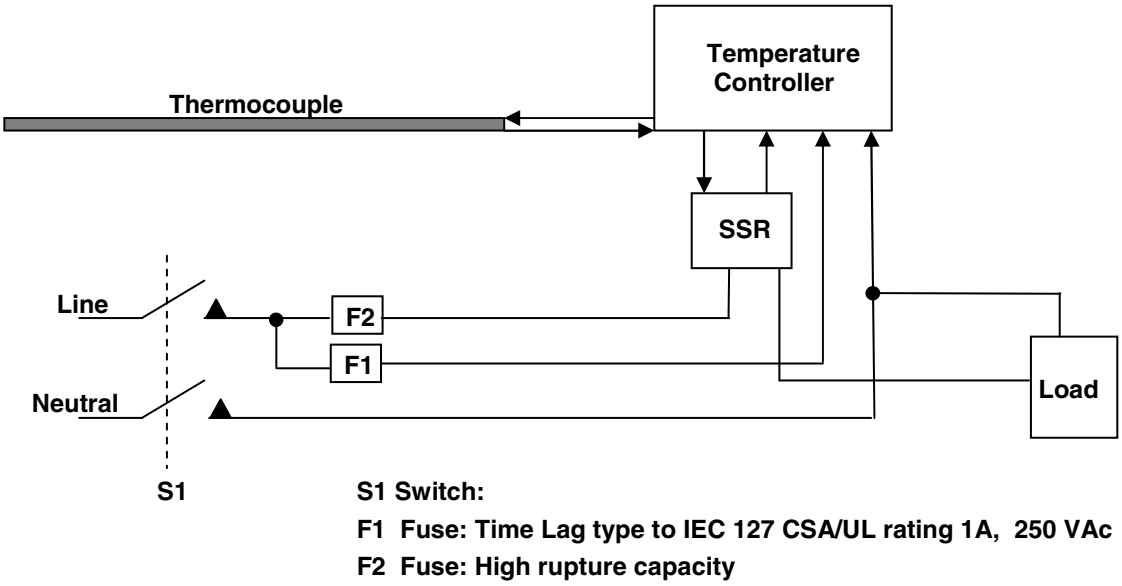

Figure 2.11. Wiring schematic for reactor furnace temperature controller and relay

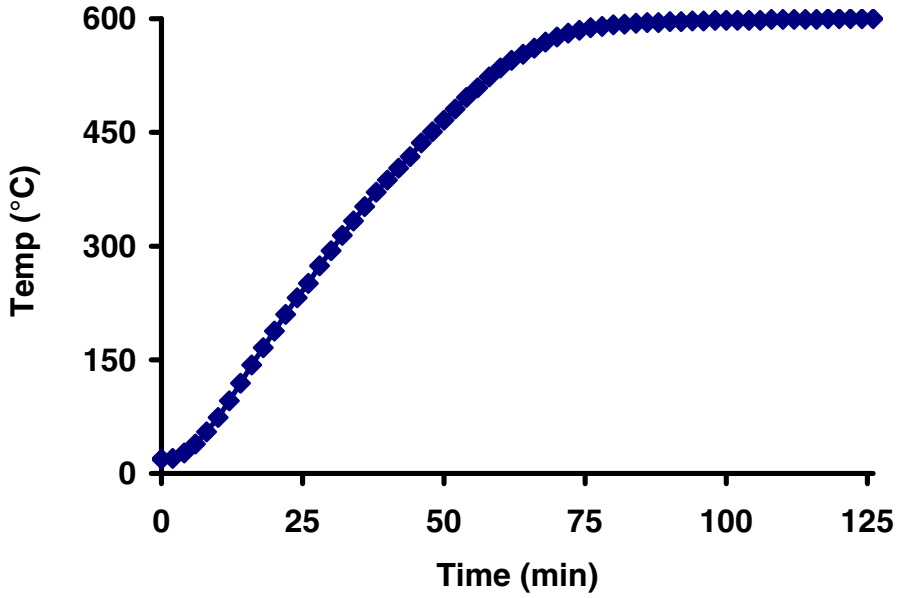

Figure 2.12. Heating profile of the reactor furnace with a flow rate of 80 µl/min of water through the reactor at ambient pressure

Single Tube Microchannel Reactor Block Design

The single tube reactor block was designed to switch in and out 2.0 meters of 1/16 inch outer diameter stainless steel HPLC tubing with 127 µm, 254 µm, and 508 µm inner diameters. The design parameters are presented in Table 2.1. The reactor block schematic is presented in Figure 2.13, and pictures are presented in Figure 2.14. The reactor was fabricated from a stainless steel block that had a square 1/16 inch channel cut into it by a computer numerical control machine (CNC). The HPLC tubing was then fitted into the grooves and a top plate was screwed into place.

Table 2.1. Design parameters for the single tube microchannel reactor

Design Parameter	Single Tube Microchannel Reactor		
Tube inner diameter	508 μm	254 μm	127 μm
Tube length	200 cm	200 cm	200 cm
Reactor volume	0.405 cm^3	0.101 cm^3	0.0253 cm^3
Reactor length	29.5 cm	29.5 cm	29.5 cm
Reactor width	7.87 cm	7.87 cm	7.87 cm
Reactor height	0.950 cm	0.950 cm	0.950 cm

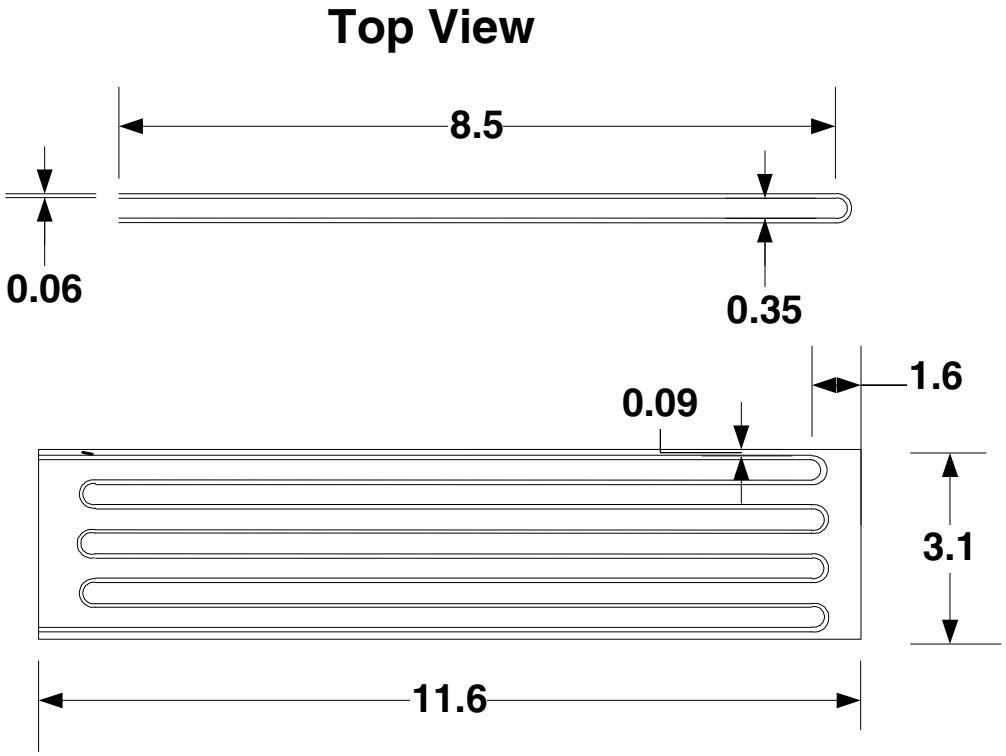

Figure 2.13. Single tube reactor block schematic; all measurements are in inches

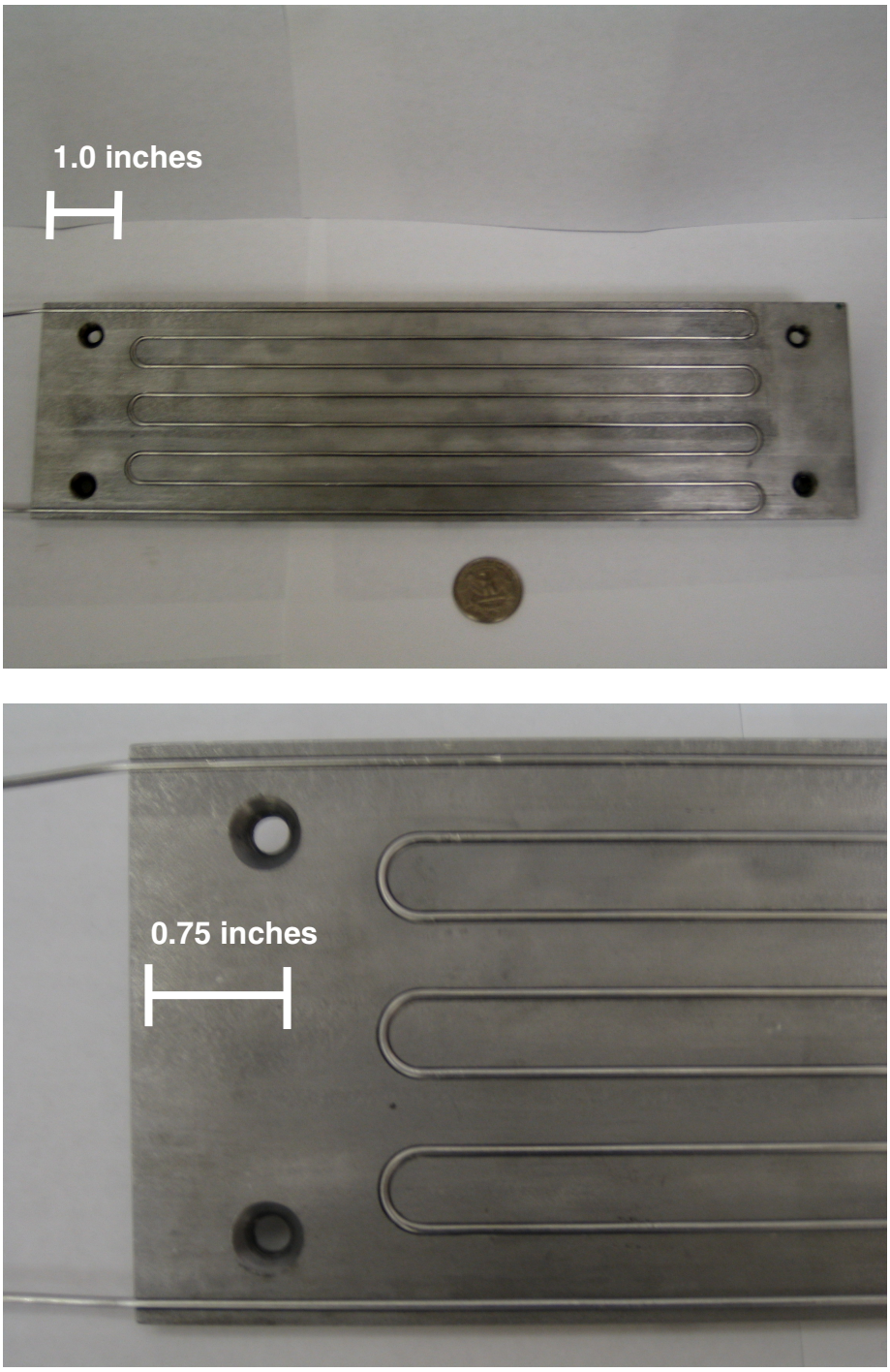

Figure 2.14. Single tube microchannel reactor block with tubing

The reactor was designed to achieve a 20 sec residence time in a 2.0 meter, 127 μm inner diameter HPLC tube. The residence time was calculated based on the volumetric flow rate at the reactor temperature and pressure

$$\tau = \frac{V_{Reactor}}{\nu_{Out}} \tag{2.1}$$

where $V_{Reactor}$ is the reactor volume and ν_{Out} is the volumetric flow rate of the reactants at the reactor temperature and pressure. The reactor volume is

$$V_{Reactor} = \frac{\pi}{4} d^2 L \tag{2.2}$$

where d is the diameter of the tubing and L is the length of the tubing. The volumetric flow rate is

$$\nu_{Out} = \frac{\rho_{In} \nu_{In}}{\rho_{Out}} \tag{2.3}$$

where ρ_{in} is the density of the reactants at ambient conditions, ρ_{out} is the density of the reactants at reactor conditions, and υ_{in} is the inlet volumetric flowrate. The density of the reactants was approximated by using the density of pure water at reactor temperature and pressure and was calculated by

$$\rho_{H_2O} = -4.9 * 10^{-7} T^3 + 1.6 * 10^{-3} T^2 - 1.8T + 743.6 \tag{2.4}$$

valid for $P = 250 \ \ Bar$ and $833 \le T(K) \le 1073$

The inlet tube of the reactor was fitted with braided ceramic high temperature insulation to minimize the amount the tube heated from radiation and conduction before it reached the reactor block.

Serpentine Microchannel Reactor

The serpentine microchannel reactor is similar to a traditional tubular reactor except the passage dimensions are rectangular and micron size. A picture of the device is presented in Figure 2.19. Cross sectional pictures from the first prototype built to determine process variables are presented in Figure 2.20. The prototype has 8 channels serpentined three times through the reactor. The final device is comprised of 21 channels that are serpentined 25 times through the reactor. The design parameters are presented in Table 2.2. Each serpentine layer is achieved by adding a set of two shims. A parallel array of 500 μm wide channels are through cut in the first shim, and the second shim acts as both the top plate for the first shim, and the bottom plate for the next channel shim. An example of the shim configuration is presented in Figure 2.21. A cross sectional view of the device is presented in Figure 2.22. The fluid is distributed to each of the channels through a header which is located at the start and end of each channel as presented in Figure 2.23. Each channel has the same path length in and out of the reactor to ensure even pressure and flow distribution between channels. The inlet and the outlet of the reactor are adapted HPLC unions. Stainless steel HPLC tubing can be connected to the inlet and outlet through these unions.

Table 2.2. Design parameters for the serpentine microchannel reactor

Design Parameter	Serpentine Microchannel Reactor
Channel width	500 μm
Channel height	75.0 μm
Channel length per shim	4.00 cm
Pitch X - direction	0.216 cm
Pitch Y - direction	0.015 cm
Number of shims	25
Total single channel length	100.2 cm
Total single channel volume	0.0376 cm^3
Channels per shim	21
Total channel volume	0.789 cm^3
Header length	4.50 cm
Header width	500 μm
Header height	250 μm
Header volume	0.00563 cm^3
Reactor volume	0.795 cm^3
Reactor length	4.80 cm
Reactor width	4.80 cm
Reactor height	1.40 cm

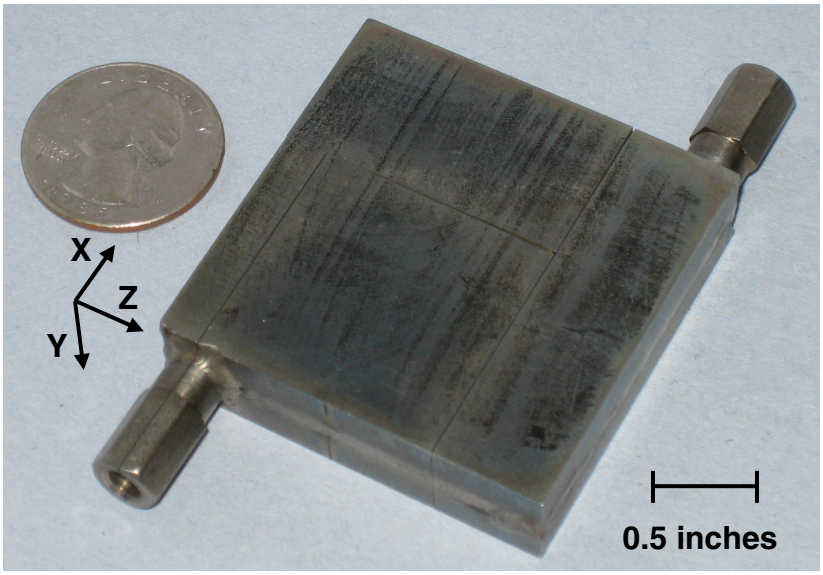

Figure 2.15. First prototype of the serpentine microchannel reactor

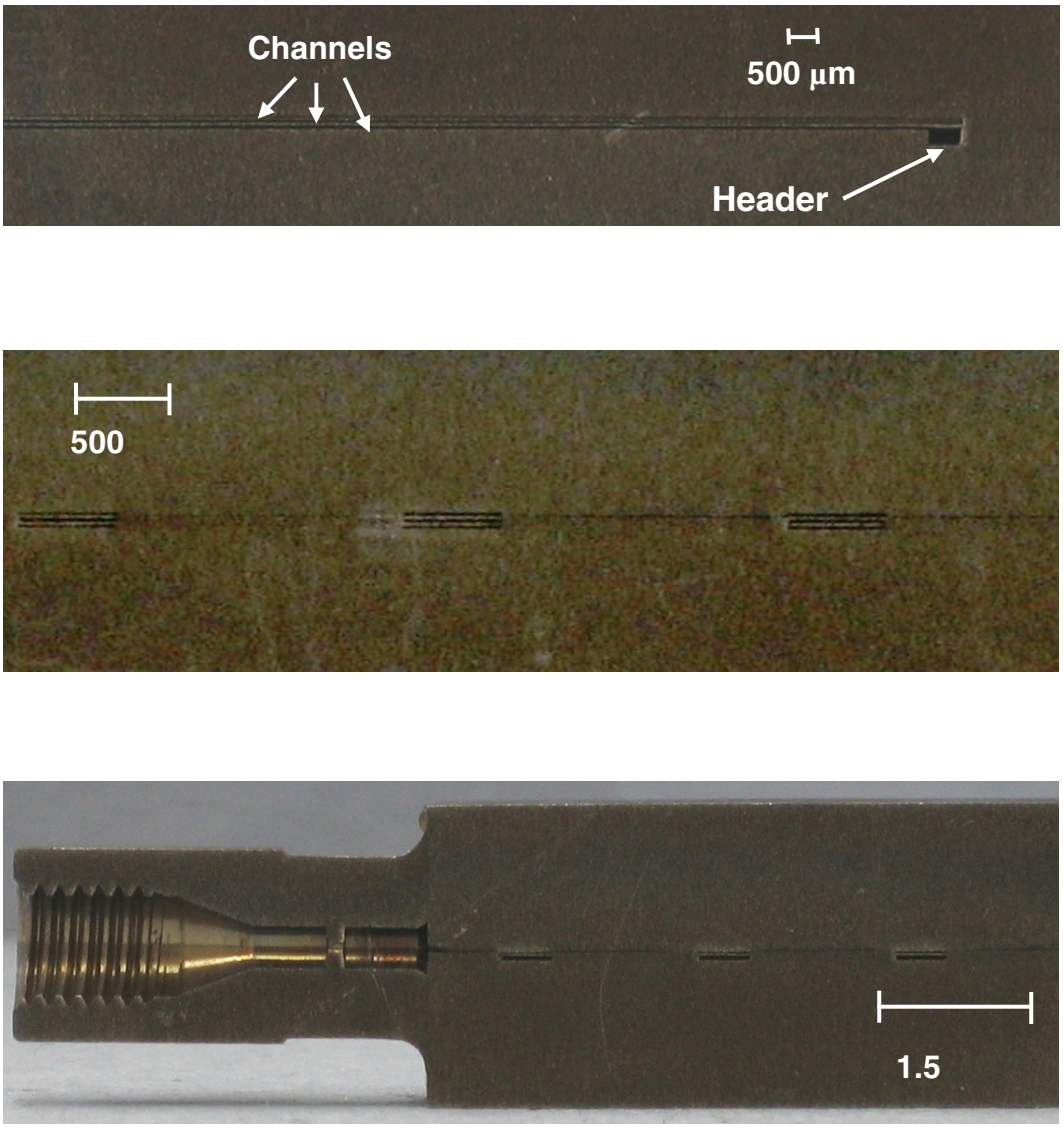

Figure 2.16. Transverse and longitudinal cross sectional views of the first prototype serpentine microchannel reactor

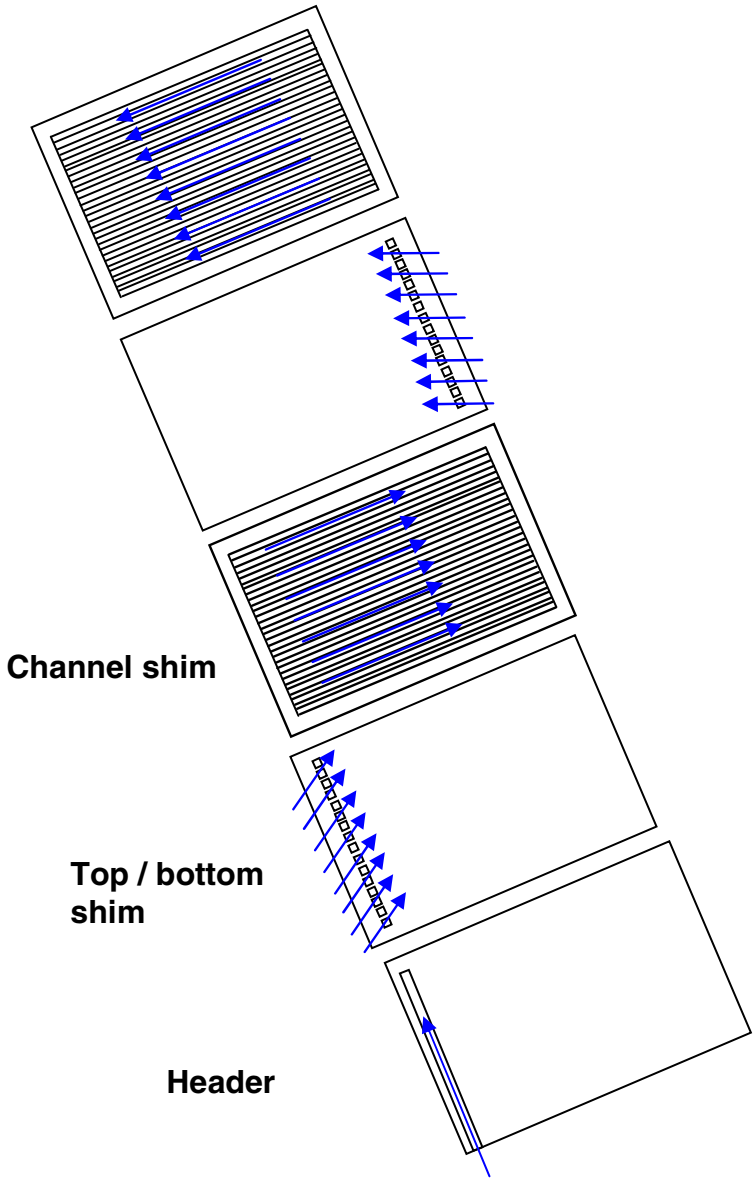

Figure 2.17. Expanded view of the serpentine microchannel reactor. The arrows represent the direction of flow (not to scale

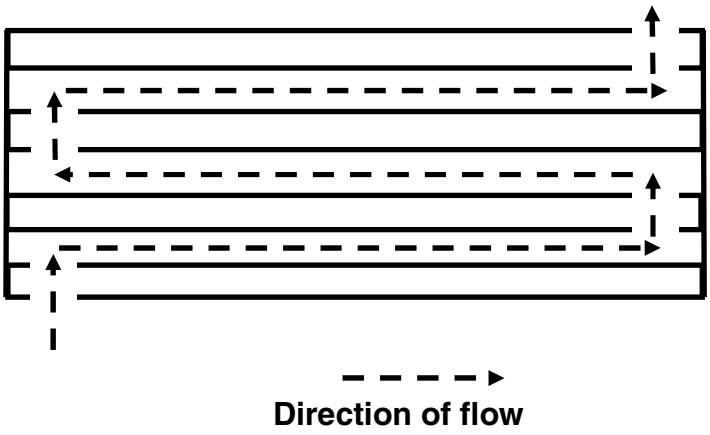

Figure 2.18. Cross-sectional view of the serpentine flow through the microchannel reactor

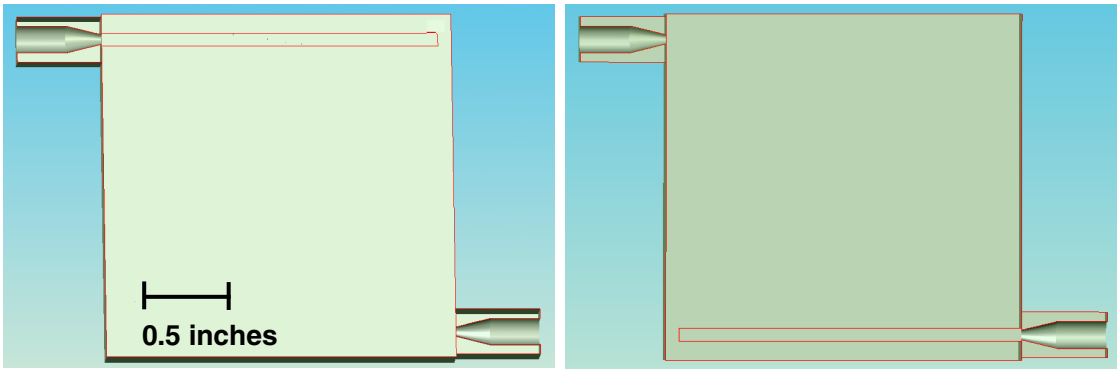

Figure 2.19. Serpentine microchannel reactor end plate design with inlet and outlet headers

The footprint of the reactor is 5.1 cm wide by 5.1 cm long. Each channel is 500 µm by 75 µm and has a total length of 100.2 cm. The total volume of the channels in the reactor is 0.79 cm^3. The headers are 500 µm by 250 µm and 4.5 cm long. They have a total volume of 0.011 cm^3. The total header volume accounts for 1.5 % of the total reactor volume, which is 0.80 cm^3.

The fabrication of the serpentine microchannel reactor was completed by the Industrial and Manufacturing Engineering department at Oregon State University. The microchannel reactor fabrication started with a piece of stainless steel bar stock that was cut into two plates with a fly cutter to produce a flat surface. The plates were cut to the dimensions of the reactor footprint and hand polished with fine abrasive paper to produce a flat finish. The two pieces made up the top and bottom plates of the microchannel reactor. A Toolcrafter CNC mill was used to cut the headers into each of these pieces. The shims used to create the channels were through cut by an ESI 5330 laser with a wavelength of 355 nm. A total of nine passes per channel at cutting speed of 150 mm/sec was used to cut each channel. After the shims were cut, each shim was hand polished with fine abrasive paper to achieve a smooth finish. Each piece of the microchannel reactor was then washed with acetone followed by methanol, and finally rinsed with deionized water. The pieces were then sprayed with nitrogen and placed into a mold to align all of the channels for bonding. The mold was placed into a Thermal Systems diffusion hot press, and pressed at 850°C, and 555 psi for 150 min. After bonding, the inlet and outlet ports were micro-tig welded onto the reactor. Finally, the perimeter of the reactor was tig welded to ensure the reactor was air tight under reactor pressures.

Condenser Design

After leaving the reactor, the reactor effluent was quenched and condensed in a counter current shell and tube heat exchanger. The schematic for the condenser is presented in Figure 2.15. The diameter of the tube was increased from 1/16 inch

HPLC tubing to1/8 inch stainless steel tubing before it entered the condenser to allow a greater surface area for the reactor effluent to condense. The outer tube diameter of the condenser was 3/8 inch. The length of the cooling section was determined to be 4 inches. The design equations to determine the length of the condenser cooling section are presented in appendix C.

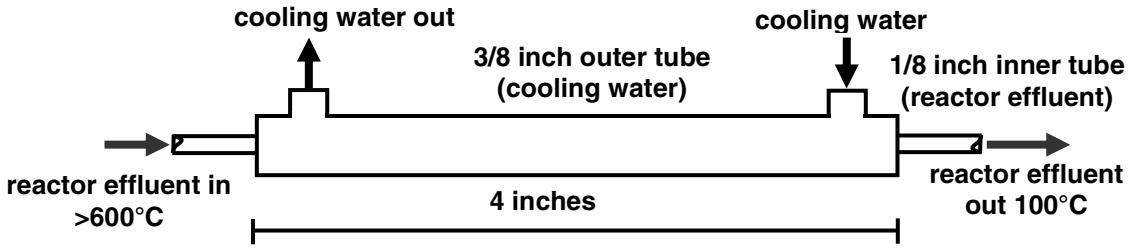

Figure 2.20. Shell and tube condenser schematic

In Line Filter and Back Pressure Regulator

After the temperature of the reactor effluent had been stepped down, it was passed through an in-line filter to remove any large particles. The filter was made up of several micron sized screens stacked in series and placed inside a Swagelok connector. A KHB series back pressure regulator from Swagelok was used to achieve pressures up to 250 bar.

Gas Liquid Separator

Once the temperature and pressure of the reactor effluent were at ambient conditions, it was passed through a gas liquid separator. The schematic for the gas liquid separator is presented in Figure 2.16. The liquid reservoir bottle was designed to hold a 250 ml

or 500 ml Kimax bottle. A gas tight sample line was connected to the gas liquid separator for liquid sampling.

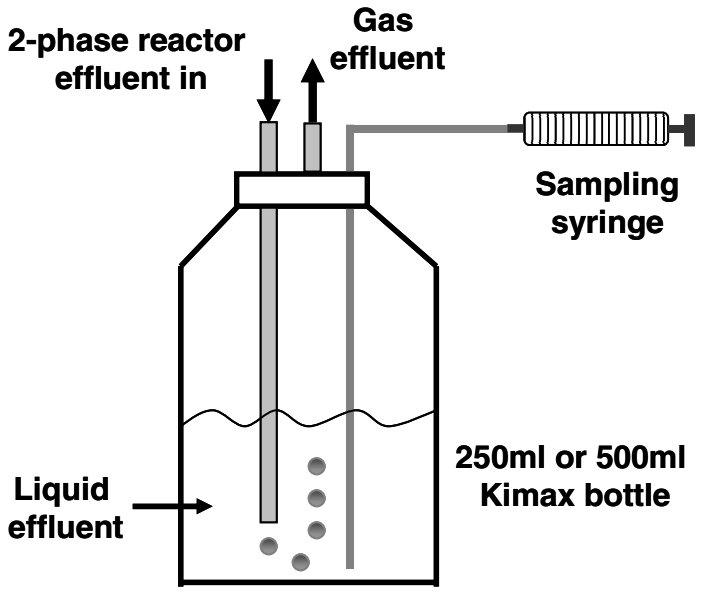

Figure 2.21. Gas liquid separator schematic

Drying Tube and Gas Mass Flow Meter

The gas was then passed through a 4 inch long, 0.38 inch inner diameter glass drying tube presented in Figure 2.17. The drying tube was filled with Drierite to eliminate residual water in the gas products.

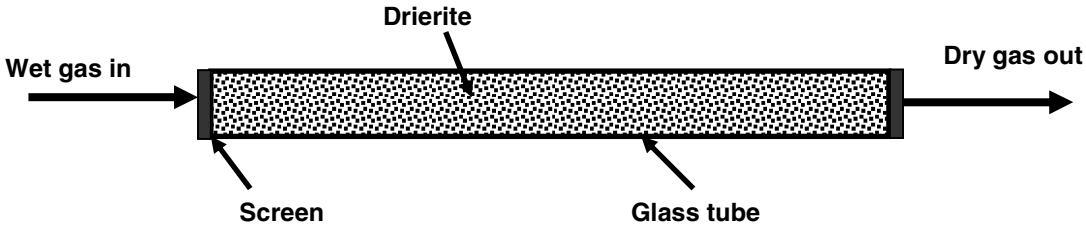

Figure 2.22. Drying tube schematic

The dried gas then passed through an Omega FMA 1800 0-20 SCCM gas mass flow meter. The flow meter uses a K-factor to relate the mass flow rate of an actual gas to the reference gas that the meter was calibrated for, in this case nitrogen. The K-factor is derived from gas density and heat capacity. K-factors used in this study are summarized in Table 2.3. The K-factor is related to the flow rates of the actual and reference gasses by

$$K_{Factor} = \frac{Q_a}{Q_r} \tag{2.5}$$

where Q_a is the mass flow rate of the actual gas and Q_r is the mass flow rate of the reference gas. Since the gas produced is comprised of four main species, an average K-factor is calculated based on the mole fraction of each gas in the stream

$$\overline{K}_{Factor} = \frac{1}{K_r} \sum_{y=1}^{i} y_i K_{Factor_i} \tag{2.6}$$

where K_r is the K-factor for the reference gas, and y_i is the mole fraction of the individual components. The actual gas flow rate is calculated by

$$Q_a = \overline{K}_{Factor} Q_r \tag{2.7}$$

The gas mass flow rate was integrated using an Omega FMA-Totalizer. The gas mass flow meter was also interfaced with an analogue to digital converter which used Peak Simple software to trace gas mass flow profiles of each experiment in real time. A 1 hertz sampling rate was used. The average gas flow rate was determined by integrating the analogue output from the flow meter over the time of the experiment. Numerical integration was performed by the trapezoid rule.

Table 2.3. K-factors for individual species which made up reactor gas effluent

Species	K-factor
CO_2	0.74
CH_4	0.72
CO	1.00
H_2	1.01

Gas Sampling

Integral gas sampling was used to determine steady state gas composition for each experiment. An experiment consisted of measuring gas composition and gas flow rate for one residence time. A 2.0 L Tedlar gas bag was used to collect steady state gas samples to account for deviations from steady state. When the gas bag was full or closed, the gas stream would proceed through a 0.3 psi check valve to the exhaust.

Pressure and Temperature Readings

Pressure gauges were monitored at three different locations in the reactor system. The locations of the pressure gauges are presented in Figure 2.1. The first pressure reading was taken by a pressure sensor located in the pump. The second pressure reading was taken after the condenser by a Swagelok stainless steel 0 – 413 bar pressure gauge. The third pressure reading was taken before the gas liquid separator by a Swagelok stainless steel 0 - 2 bar pressure gauge.

Temperature readings were taken after the condenser and before the gas liquid separator. The locations of the thermocouples are presented in Figure 2.1. An Omega temperature meter was used with type J thermocouples to measure the temperature of

the reactor effluent. The wiring schematic for the temperature meter is presented in Figure 2.18.

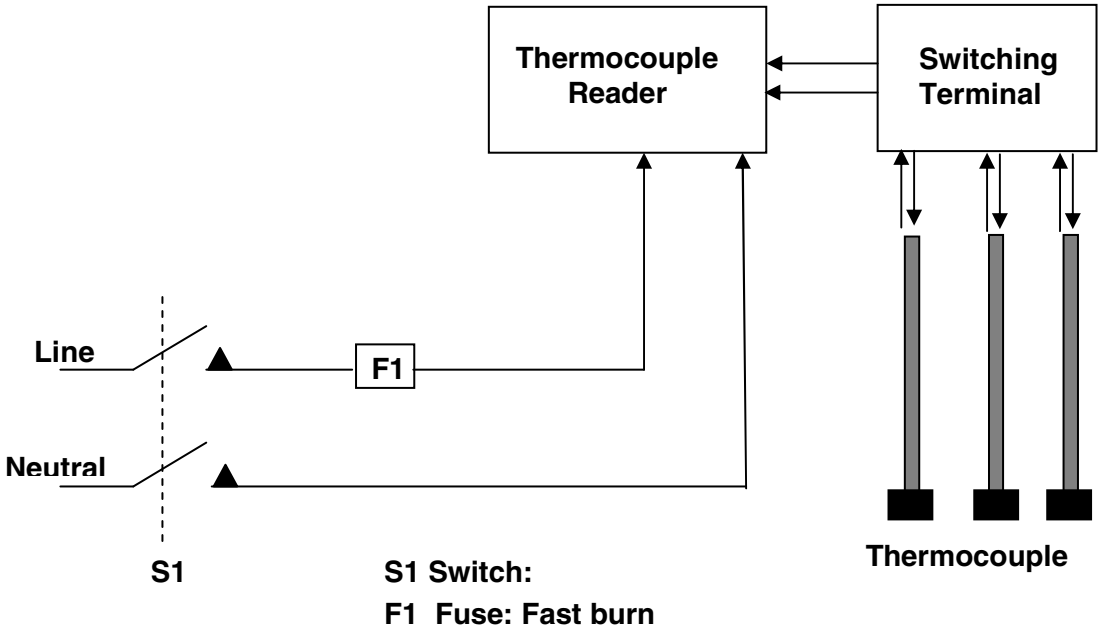

Figure 2.23. Wiring schematic for temperature meter

Experimental Methods

Reagents

Anhydrous α D-glucose was obtained from Mallinckrodt Chemicals (50-99-7). Water was de-ionized by a Barnstead D2 deionizer that was further purified by a Barnstead MP-3A Mega Pure System Distillation column. The mix gas standard containing CH_4, CO_2, and CO was obtained from Alltech (19792), and the hydrogen standard was obtained from Industrial Welding Supply Inc. grade 4.7 (>99.997% purity).

Reactor Operation

Reactor Start Up

The following procedure outlines the reactor start up for each experiment. Glucose solutions were degassed by sparging them with helium for 10 minutes at 5 psi. The reactor furnace was turned on and set to the desired temperature. Next the water for the heat exchanger was turned on, followed by the temperature meter. Once the furnace temperature had reached the set point, the pump was turned on. Water, at a flow rate of 0.5 ml/min, was allowed to flow through the system at atmospheric pressure. Once the water reached the gas liquid separator the backpressure regulator was adjusted to the desired pressure. The pressure gauge before the backpressure regulator and the pressure gauge at the pump were compared to determine if an obstruction was present in the channel. Once the reactor reached the desired pressure, a needle valve located after the drying tube was adjusted to close the system. The

reactor was sparged with helium to a pressure of 10 psi, and the system pressure was monitored for 5 minutes to determine if the reactor test loop was airtight. The pump was set to a flow rate of 0 ml/min and the water was switched to the reactants. The pump was then set to the desired experimental flow rate. Lastly, Peak Simple software was turned on and zeroed to track the flow profile.

Determination of steady state for the reactor and test loop was achieved by observing the gas mass flow profile. Once the gas mass flow profile had come to a steady gas flow the totalizer on the flow meter was zeroed. Time points from the totalizer were recorded throughout the run.

When the reactor test loop had been flushed with 2 L of gas from the glucose decomposition reaction the gasbag was opened. The gas bag was able to collect up to 2 L of gas over several hours.

Reactor Shut Down

At the end of each experiment the reactor was shut down by the following procedure. First the Peak Simple software collecting the gas flow profile was stopped, and the final data point off the totalizer was recorded. Secondly the gasbag was closed, and removed from the test loop for GC analysis. The flow rate on the pump was then set to 0 ml/min, and the reactants were switched to water. A 50 ml syringe was used to pull a liquid effluent sample from the gas liquid separator. The sample was tested for pH, residual glucose, and organic acids. A 20 ml aliquot of the sample was put into a scintillation vial and stored at -20°C. The system pressure was stepped down to

ambient pressure by adjusting the back pressure regulator. The pump was set to a flow rate of 0.1 ml/min and water was allowed to pump through the system for 4 hours. Finally the reactor furnace was turned off, and the reactor was allowed to cool with water running though the system.

Cleaning the Reactor

When the pressure drop through the reactor reached twice the original pressure drop of the tubing or microchannel device the reactor was cleaned. Typically the reactor was cleaned after each experiment. The cleaning processes for the single tube reactor started with disconnecting the reactor inlet and outlet tubing, and back flushing the reactor with water at a flow rate of 0.5 ml/min at 750°C and ambient pressure. The reactor was back flushed until the pressure drop of the reactor fell below 20 bar. The inlet and outlet fittings were re-connected and the system was forward flushed with water at a flow rate of 0.5 ml/min at 750°C and ambient pressure until the pressure drop of the reactor once again fell below 20 bar. After the reactor was flushed with water, an air line was attached to the inlet of the reactor, and air was allowed to flow through the reactor at 120 psi for one hour. The air was used to oxidize any residual char or tar that had accumulated on the wall of the reactor.

The cleaning process for the serpentine microchannel reactor was the same as the single tube microchannel reactor with one exception. Due to the fact that the microchannel device and the tubing connected to it had different geometries, char or coke would buildup at the interface between them. The reactor was disconnected from

the inlet and outlet tubing, and replaced with a HPLC union. The inlet and outlet sections of the tubing were flushed as previously described. The reactor was re-integrated into the system, and the previous process was repeated.

When the reactor inlet was fully plugged, or flushing the inlet and outlet tubing lines did not significantly reduce the pressure drop, the inlet and outlet lines were replaced.

Analytical Methods

Gas Composition Determination

The gas composition of the reactor effluent was determined by gas chromatography (GC). All gas samples were transferred with 500 µl and 250 µl gastight syringes. Gas chromatography was performed on a HP-5890II GC with a thermal conductivity detector. Two separate methods were used to identify the four main species in the gas products. The column used for both methods was a Alltech Carbosphere 80/100 6 foot by 1/8 inch by 0.85 inch stainless steel packed column. The first method was to detect and quantitate CO, CO_2, and CH_4. The method used helium as a carrier gas at a flow rate of 27.6 ml/min. The oven temperature was 80°C, the injector temperature was 120°C, and the detector temperature was 120°C. The method runtime was 8 minutes. The second method used was to detect and quantitate the amount of H_2 in the gas products. The method used nitrogen as the carrier gas at a flow rate of 34.0 ml/min. The oven temperature was 85°C, the injector temperature was 120°C, and the detector temperature was 120°C. The method runtime was 1 minute. Four different amounts of a gas mixture containing 4.0 mole % CH_4, 5.0 mole % CO_2, and 5.0 mole % CO, or a gas containing pure H_2 were injected to create standards curves for each of the species. Standards were injected three times for each concentration. A linear regression line was fit to the data, and a standard error analysis was applied. Standards curves for each species are presented in Figures 3.1 – 3.4. Standard response factors are presented in Table 3.1. Molar concentrations were calculated using the ideal gas law. Sample concentrations were calculated by

$$C_s = \frac{A_S}{R_{f,S}} \tag{3.1}$$

where C_s is the concentration of the species, A_S is the peak area, and $R_{f,S}$ is the response factor.

Table 3.1. Response factors for species quantified by GC

Species	Response Factor (counts·sec/mmol of species)	R^2
H_2	$3.30 \cdot 10^7 \pm 2.75 \cdot 10^5$	0.999
CO	$1.40 \cdot 10^9 \pm 3.82 \cdot 10^6$	0.999
CO_2	$1.59 \cdot 10^9 \pm 1.00 \cdot 10^7$	0.999
CH_4	$1.16 \cdot 10^9 \pm 2.49 \cdot 10^6$	0.999

Table 3.2. Response factors for species quantified by HPLC

Species	Response Factor (peak area/mmol of species)	R^2
Acetaldehyde	9370 ± 29.1	0.999
Acetic acid	6.03 ± 0.0215	0.999
Buytric acid	44.2 ± 0.126	0.999
Propenoic Acid	21.7 ± 0.194	0.999
Glucose	1.21 ± 0.0218	0.999

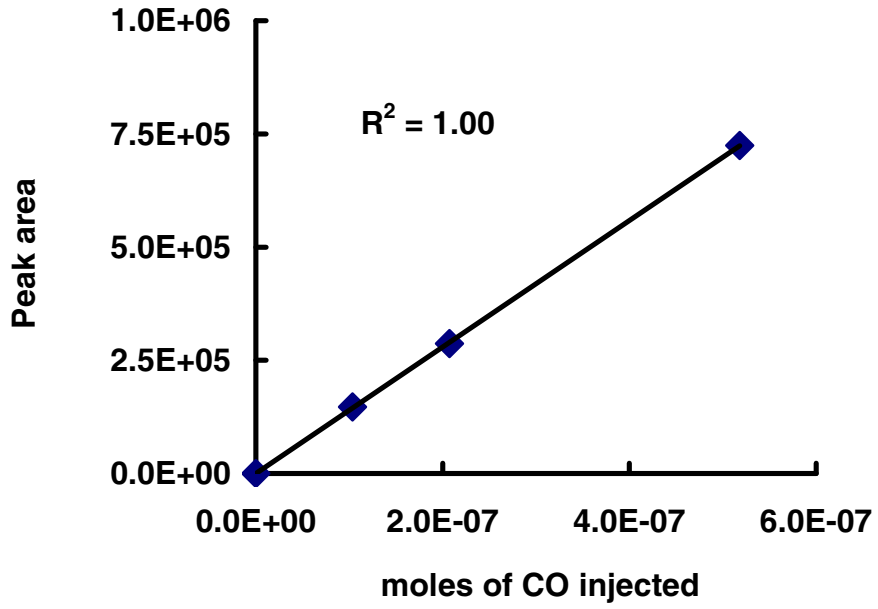

Figure 3.1. GC Calibration curve for the detection of CO by thermal conductivity

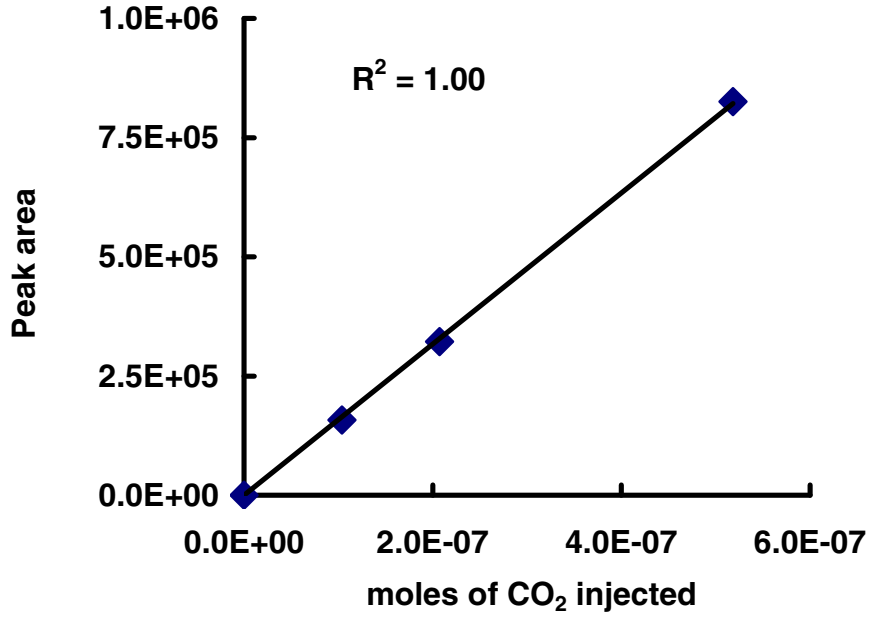

Figure 3.2. GC Calibration curve for the detection of CO_2 by thermal conductivity

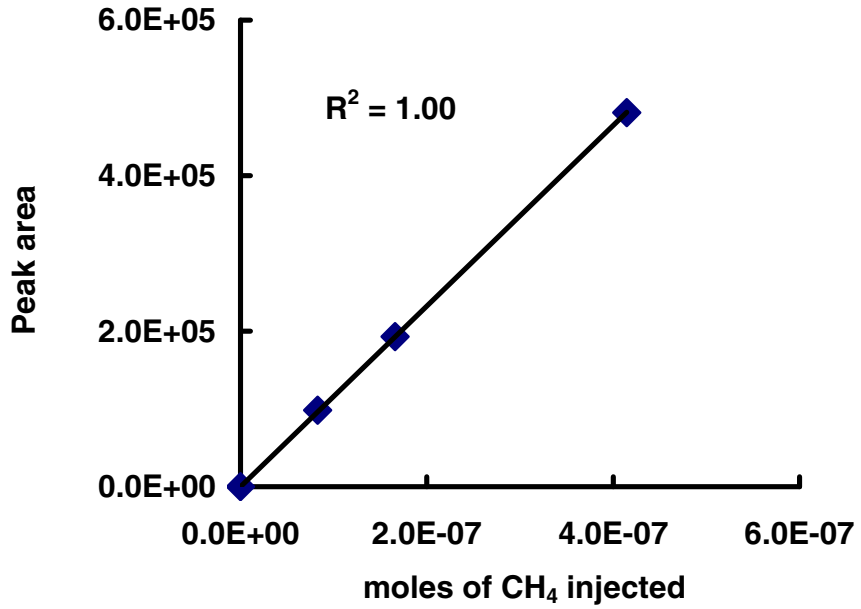

Figure 3.3. GC Calibration curve for the detection of CH_4 by thermal conductivity

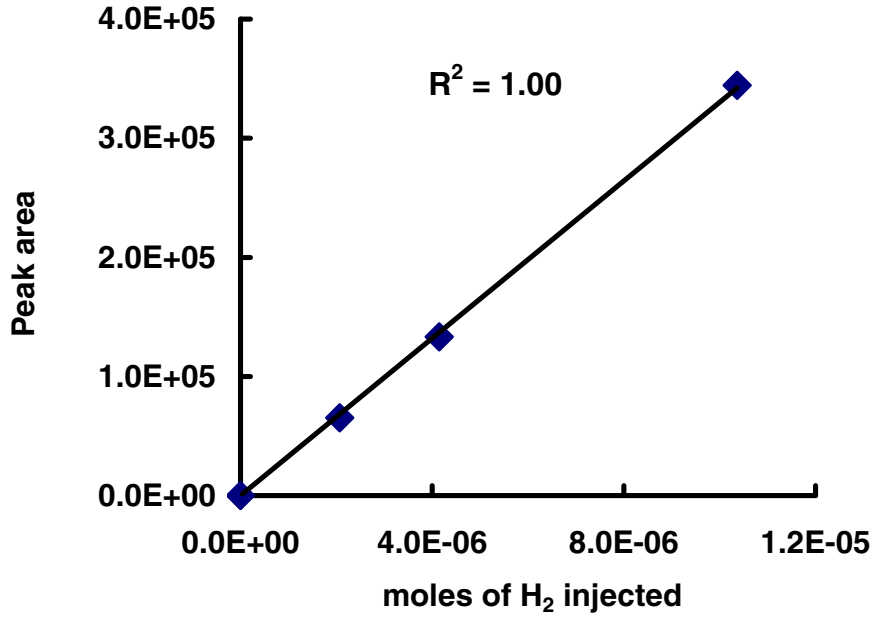

Figure 3.4. GC Calibration curve for the detection of H_2 by thermal conductivity

Glucose Analysis

Un-reacted glucose in the liquid effluent was determined by HPLC. The samples were filtered through a 0.45 µm nylon syringe filter before being injected onto a Bio-rad Aminex HPX-87P carbohydrate analysis column. The mobile phase was water, and the column was kept at 85°C. The flow rate was 0.6 ml/min, and runtimes were 25 minutes long. A HP-1037A refractive index detector was used to identify any residual glucose or other sugars. Standards were injected twice for each concentration and a linear regression line was fit to the data. A standard error analysis was applied. The glucose response factor is presented in Table 3.2, and the standards plot is presented in Figure 3.5. Sample concentrations were calculated as previously shown in Equation 3.1.

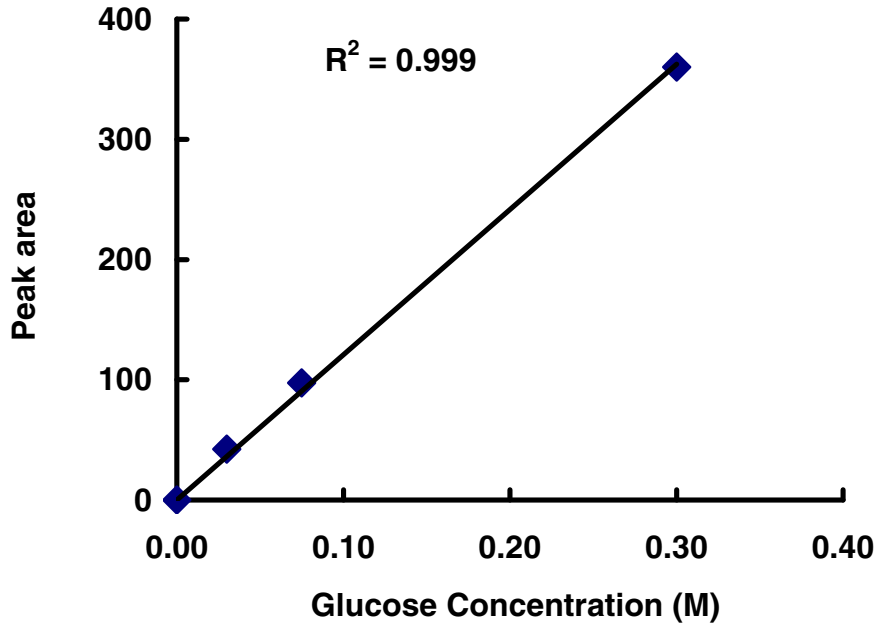

Figure 3.5. HPLC calibration curve for the detection of glucose by refractive index

Organic Acid Determination

Acetic acid, lactic acid, butyric acid, acetaldehyde, and propenoic acid are major intermediates of the low temperature reaction pathway. These compounds found in the liquid reactor effluent were analyzed by a HP-1090 HPLC with photodiode array detector. The organic acids were eluted on a Bio-Rad Aminex HPX-87H ion exchange column. The mobile phase was 5 mM sulfuric acid, and the column was kept at 65°C. The flow rate was 0.6 ml/min, and each run was 75 minutes long. The detection wavelengths were 210 nm and 290 nm. Standards were injected twice for each concentration and a linear regression line was fit to the data. A standard error analysis was applied. Response factors for acids detected in the liquid products are presented in Table 3.2. Standards curves are presented in Figures 3.6 – 3.9. Sample concentrations were calculated as previously shown in Equation 3.1.

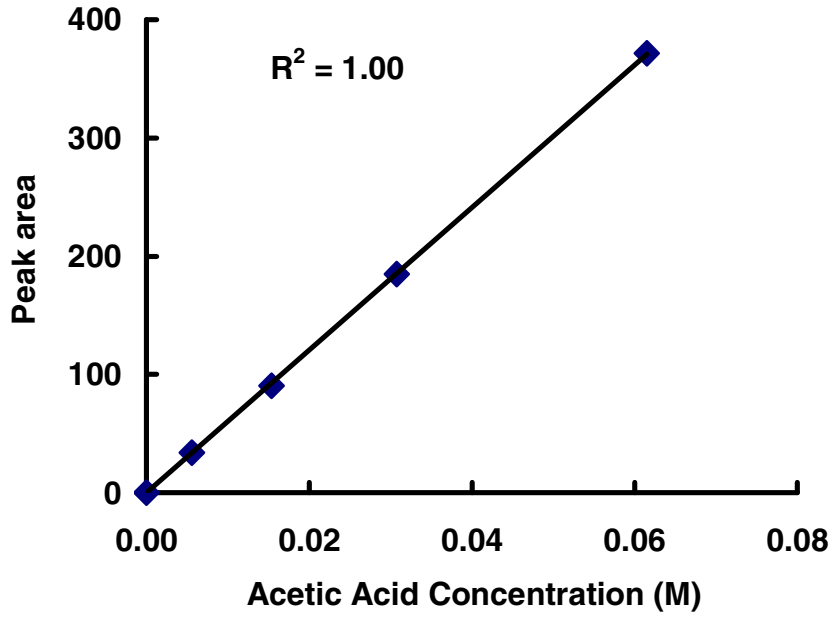

Figure 3.6. HPLC calibration curve for the detection of acetic acid at 210 nm

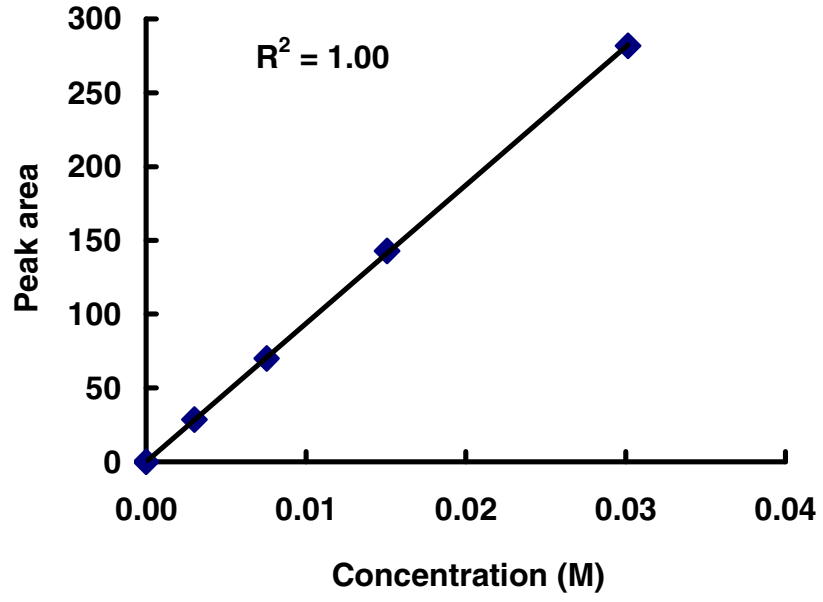

Figure 3.7. HPLC calibration curve for the detection of acetaldehyde at 290 nm

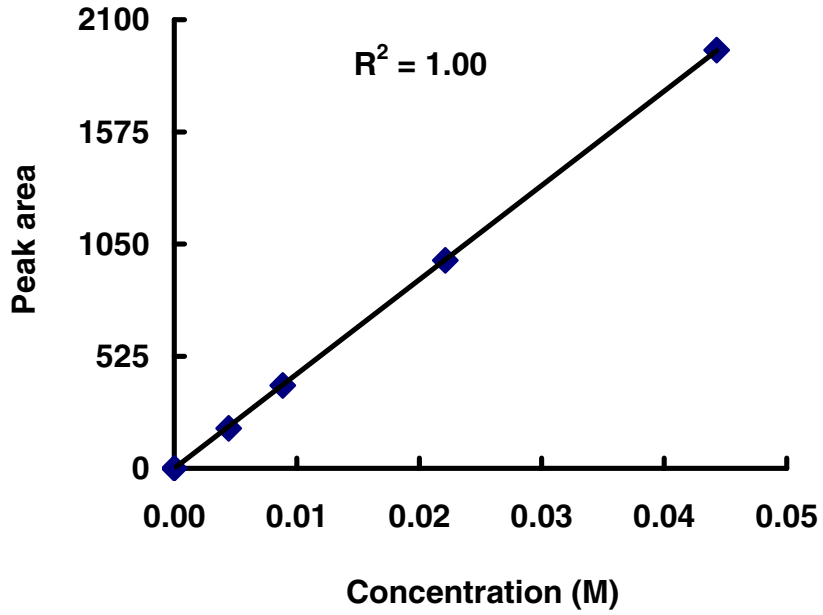

Figure 3.8. HPLC calibration curve for the detection of butyric acid at 210 nm

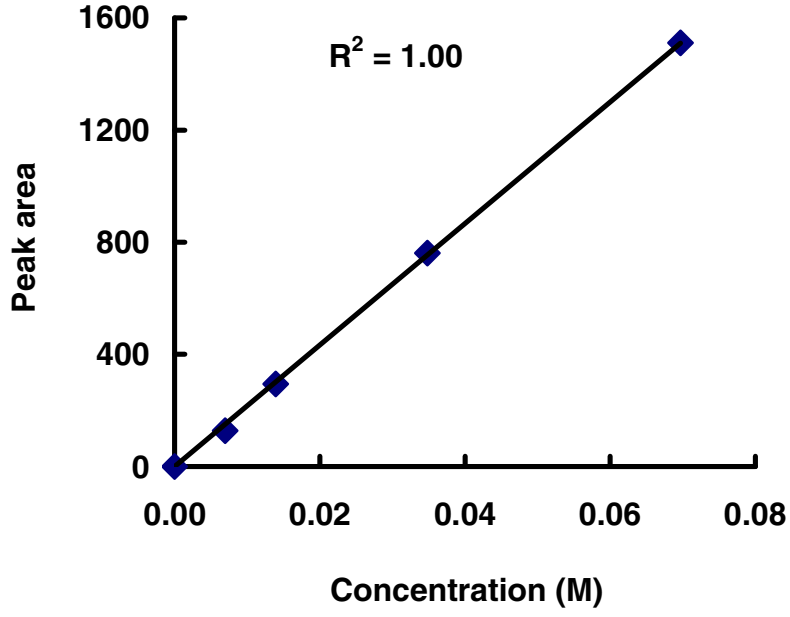

Figure 3.9. HPLC calibration curve for the detection of propenoic acid at 210 nm

Liquid Effluent pH

The pH of the liquid effluent was determined on a Beckman 340 pH / Temperature meter.

Results

Affect of Tubing Size on Gas and Liquid Products in the Single Tube Microchannel Reactor

The affect of reactor tube diameter on gas composition and gas production at 750°C, 250 bar, and 0.1 mol/L glucose was studied in the single tube microchannel reactor. The tubing diameters tested were 254 µm and 508 µm. The total gas flow per volume of reactor per hour is plotted against the inlet feed rate, and is presented in Figure 4.1. The total gas flow rate for each tubing diameter was linear and comparable.

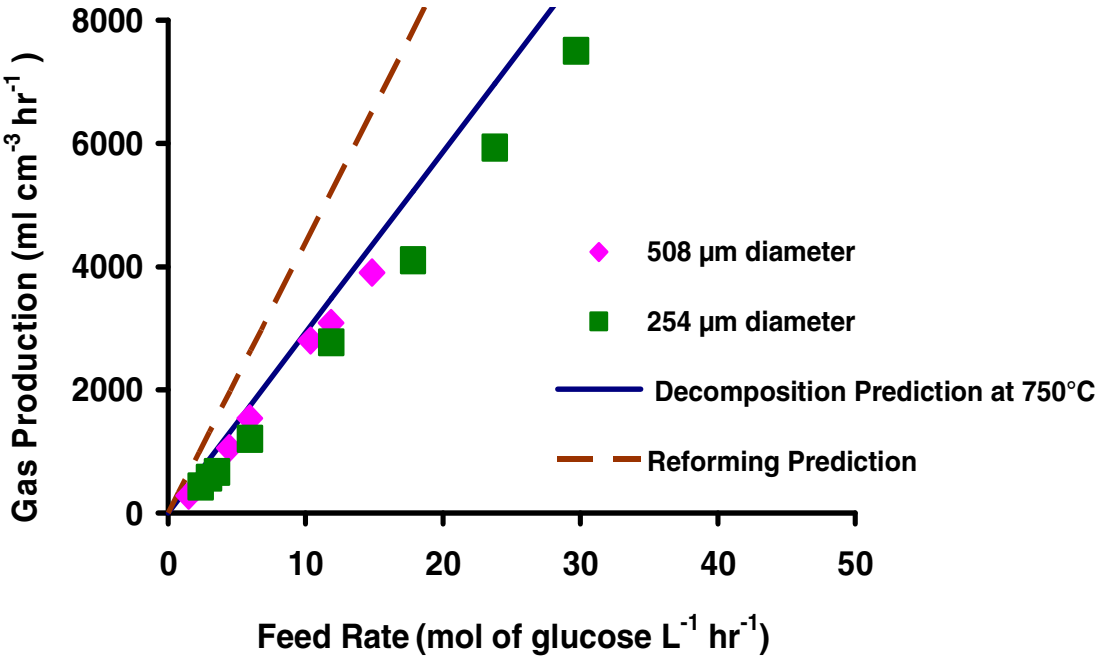

Figure 4.1. Normalized total gas production for 508 µm and 254 µm tubing diameters in the single tube microchannel reactor at 750°C, 250 bar, and 0.1 M glucose

The gas composition as a function of residence time for each tubing diameter was comprised of H_2, CO_2, CH_4, and CO, and is presented in Figures 4.2A - 4.2C.

Representative GC chromatograms are presented in Figures 4.3A – 4.3B. Figure 4.3A is an example chromatogram for the detection of H_2, and Figure 4.3B is an example chromatogram for the detection of CO_2, CO, and CH_4. The peak labeled 2 in Figure 4.3B was air and represented a small amount of residual air in the gas bag tube.

The average gas composition as a function of residence time in the 508 µm diameter tubing at 750°C, 250 bar, and 0.1 M glucose was 51 % H_2, 33 % CO_2, 12 % CH_4, and 0.7 % CO. The concentration of H_2, CO_2, and CH_4 were constant as a function of residence time ranging from 1.2 sec -12.3 sec. The concentration of CO was 0.37 % - 0.43 % for residence times greater than 4 sec, and increased at residence times less than 4 sec. The highest CO concentration was 1.8 mole % at a residence time of 1.2 sec. The concentration of CO as a function of residence time at 750°C is presented in Figure 4.2C.

The gas composition in the 254 µm diameter tubing was similar to the 508µm diameter tubing. The average gas composition was 50 % H_2, 35 % CO_2, 12 % CH_4, and 1.4 % CO. The CO concentration ranged from 0.4 % - 1.0 % for residence times ranging from 3.1 sec – 7.7 sec. An increase in the CO concentration, up to 3 mole %, was observed for residence times less than 3.1 sec. The concentration of CO as a function of residence time at 650°C is presented in Figure 4.2C.

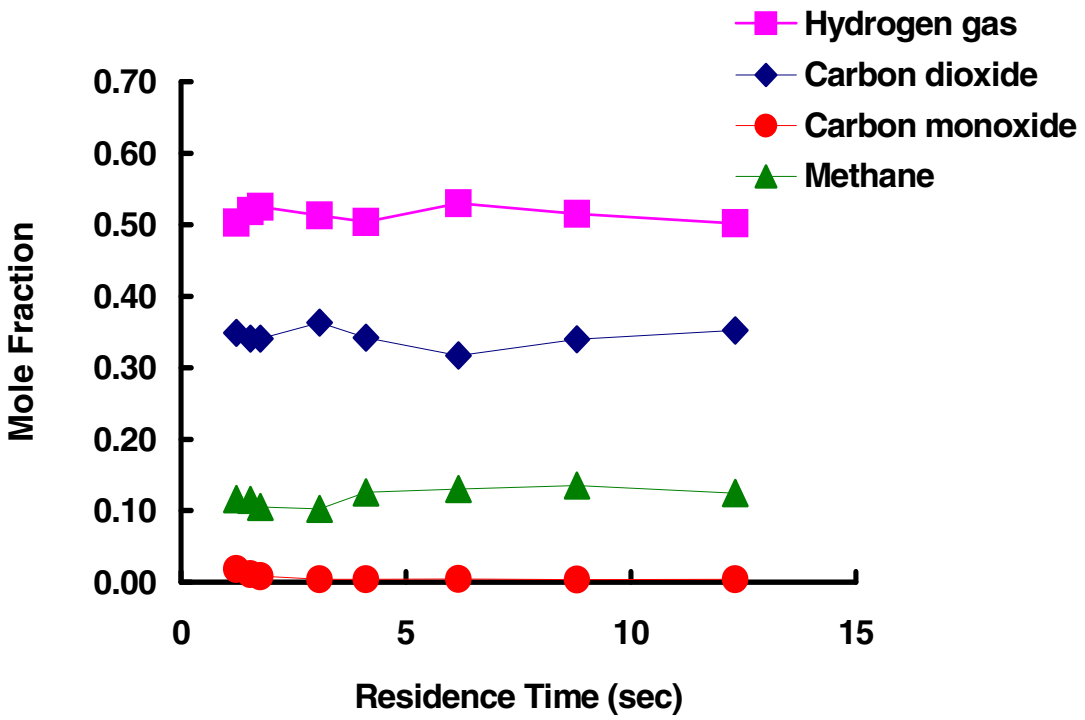

Figure 4.2A. Gas composition as a function of residence time in the 508 µm diameter single tube microchannel reactor at 750°C, 250 bar, and 0.1 M glucose

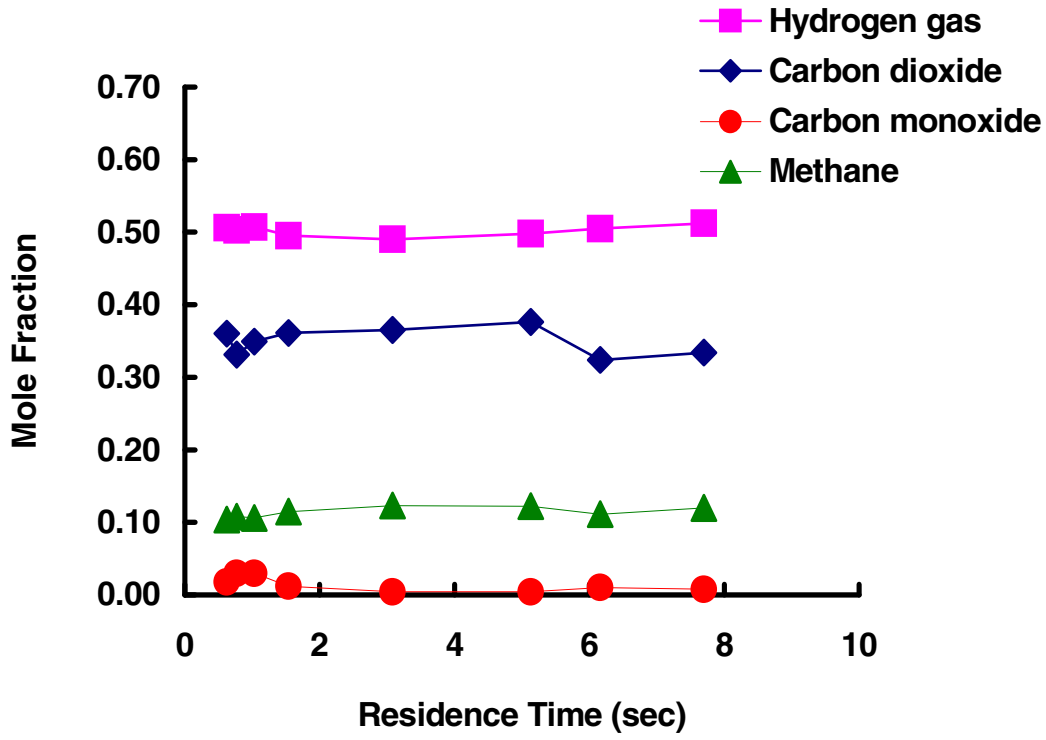

Figure 4.2B. Gas composition as a function of residence time in the 254 µm diameter single tube microchannel reactor at 750°C, 250 bar, and 0.1 M glucose

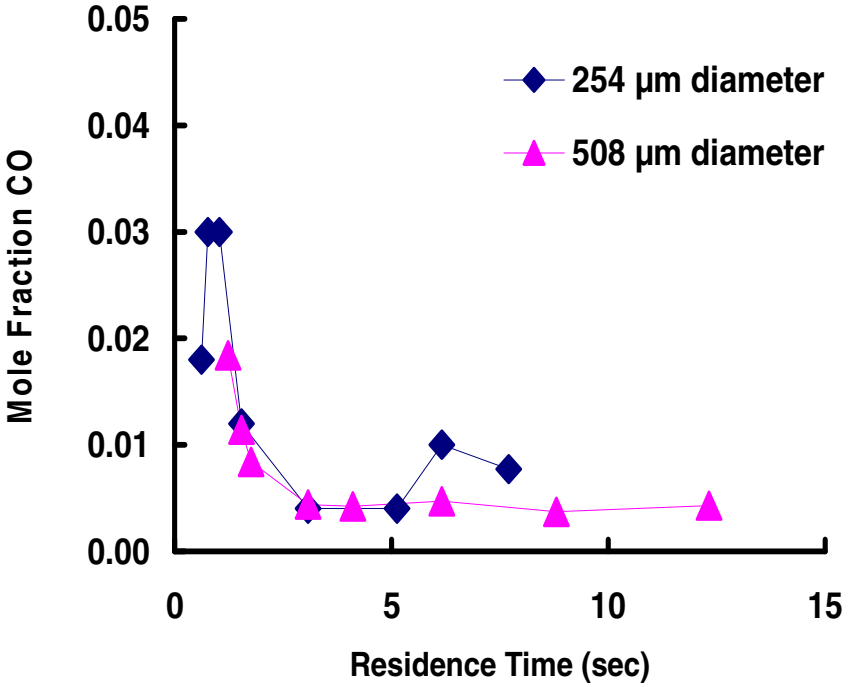

Figure 4.2C. CO concentrations for 508 µm and 254 µm tubing diameters as function of residence time in the single tube microchannel reactor at 750°C, 250 bar, and 0.1 M glucose

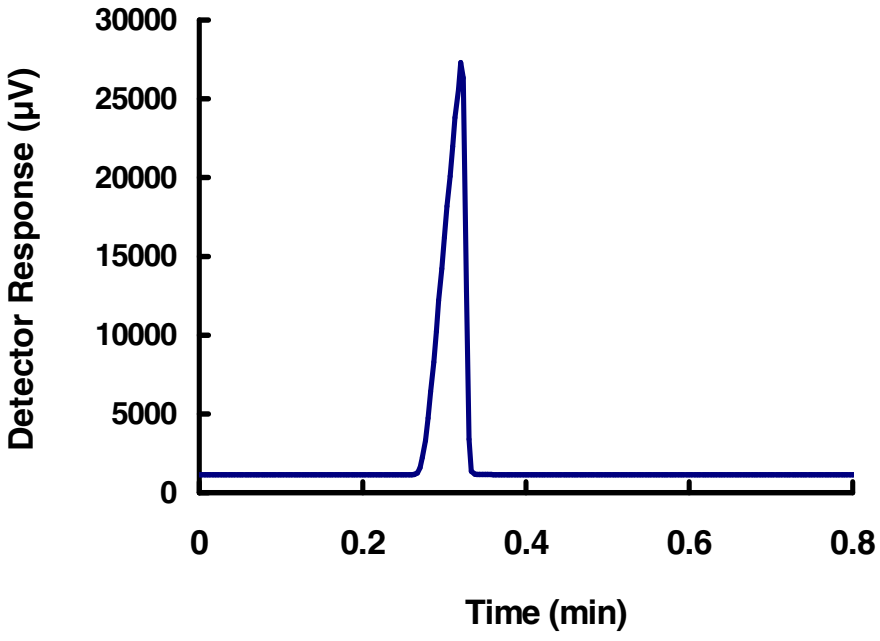

Figure 4.3A. Sample GC chromatogram of reactor gas effluent for the detection of H_2 in the serpentine microchannel reactor at 650°C, 250 bar, 0.1 M glucose, and 4.7 sec residence time

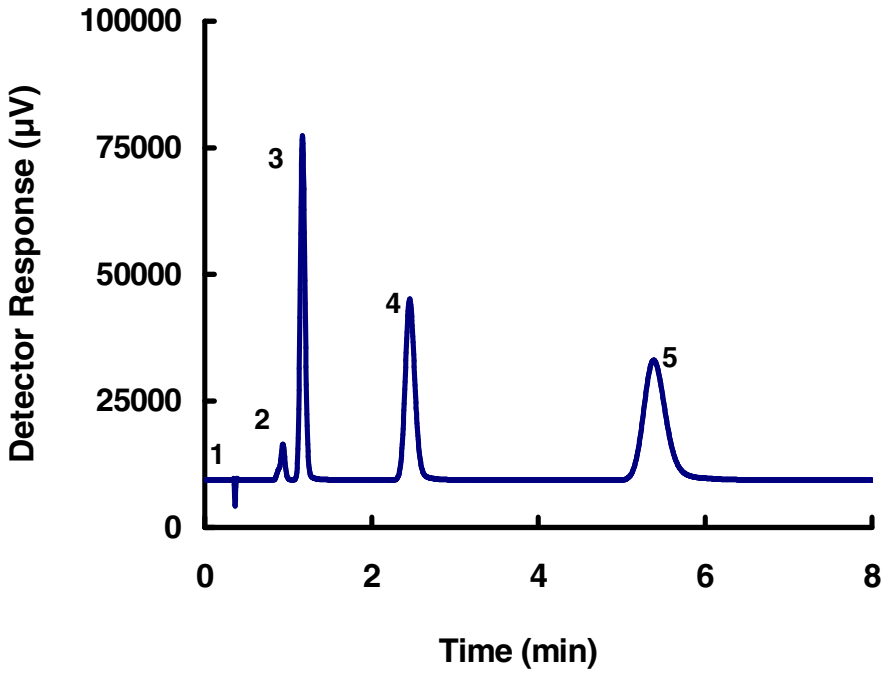

Figure 4.3B. Sample GC chromatogram of reactor gas effluent in the serpentine microchannel reactor at 650°C, 250 bar, 0.1 M glucose, and 4.7 sec residence time. Peaks (1) H_2; (2) air; (3) CO; (4) CH_4; (5) CO_2

Hydrogen Yield

The hydrogen yield, (Y_{H2}), is the moles of H_2 generated per mole of reacted glucose

$$Y_{H_2} = \frac{F_{H_2,o}}{F_{g,i} - F_{g,o}} \tag{4.1}$$

where $F_{H_2,o}$ is the outlet molar flow rate of H_2, $F_{g,i}$ is the inlet molar flow rate of glucose, and $F_{g,o}$ is the outlet molar flow rate of glucose. The inlet molar flow rate of glucose was determined by

$$F_{g,i} = C_{g,i} V \tag{4.2}$$

where $C_{g,i}$ is the inlet concentration of glucose, and V is the volumetric flow rate of the liquid feed at ambient temperature and pressure. $F_{g,o}$ was measured and determined

from the residual glucose analysis of the liquid reactor effluent. The H_2 gas flow rate was calculated by

$$F_{H_2,O} = F_{T,O}\ y_{H_2} \tag{4.3}$$

where y_{H_2} is the mole fraction of H_2 in the gas, and $F_{T,O}$ is the total molar gas flow rate calculated by

$$F_{T,O} = \frac{Q_a\ P_{sys}}{R\ T_{sys}} \tag{4.4}$$

where R is the gas constant (m^3 Pa mol^{-1} K^{-1}), P_{sys} is the total system pressure (Pa), T_{sys} is the system temperature (K), and Q_a is the volumetric gas flow rate (m^3 sec^{-1}).

Recovered Carbon in the Gas

Recovered carbon in the gas products, often referred to as gasification efficiency, is

$$\eta_c = 1 - \frac{F_{C,o}}{F_{C,i}} \tag{4.7}$$

where $F_{c,i}$ is the molar flow rate of carbon in the feed, and $F_{c,o}$ is the molar flow rate of carbon in the gas. $F_{c,o}$ is estimated by

$$F_{C,o} = (\nu_{CO_2}\ y_{CO_2} + \nu_{CO}\ y_{CO} + \nu_{CH_4}\ y_{CH_4})\ F_{T,O} \tag{4.5}$$

where ν_i is the number of moles of carbon per mole of species (mol mol^{-1}), y_i is the mole fraction of species i in the gas, and $F_{T,O}$ is the total molar flow rate of that gas (mol hr^{-1}). The moles of carbon in the feed ($F_{c,i}$) was calculated by

$$F_{C,i} = C_{g,i}\ V\ \nu_g \tag{4.6}$$

Hydrogen yield and recovered carbon in the 254 µm diameter tubing and the 508 µm tubing at 750°C, 250 bar, and 0.1 M glucose are presented in Figures 4.4A – 4.4D.

Figures 4.4A and 4.4C reveal a small linear decrease in hydrogen yield and recovered carbon as a function of increasing residence time. They also show an increase in hydrogen yield and recovered carbon in the 508 µm diameter tubing compared to the 254 µm diameter tubing. Figures 4.4B and 4.4D depict hydrogen yield and recovered carbon as a function of inlet flow rate rather than residence time. In Figures 4.4B and 4.4D there is no observed difference in the hydrogen yield and carbon recovery between the 508 µm and 254 µm tube diameters. However there is a small increase in the hydrogen yield and recovered carbon for both of the tube sizes as a function of increasing inlet flow rate.

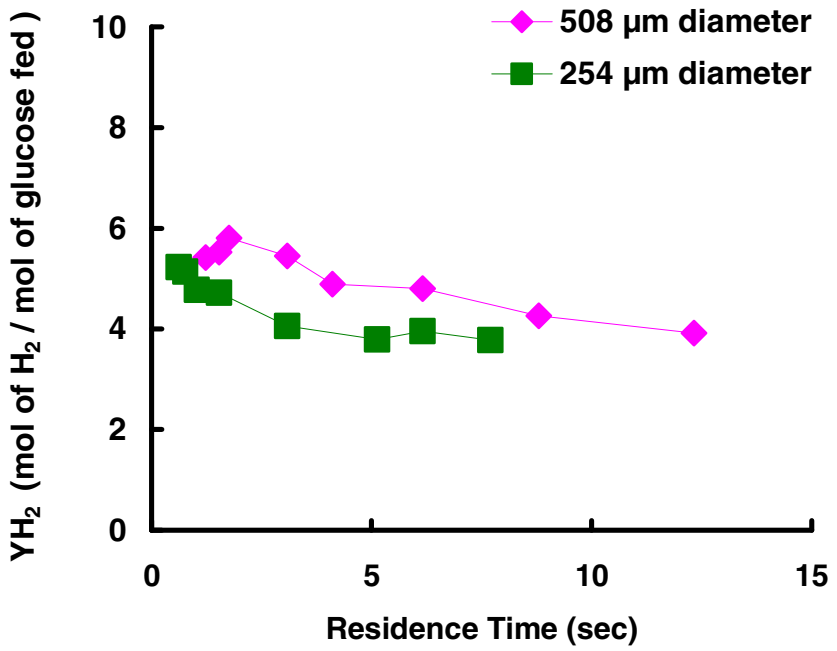

Figure 4.4A. Hydrogen yield as a function of residence time for 508 µm and 254 µm tubing diameters in the single tube microchannel reactor at 750°C, 250 bar, and 0.1 M glucose

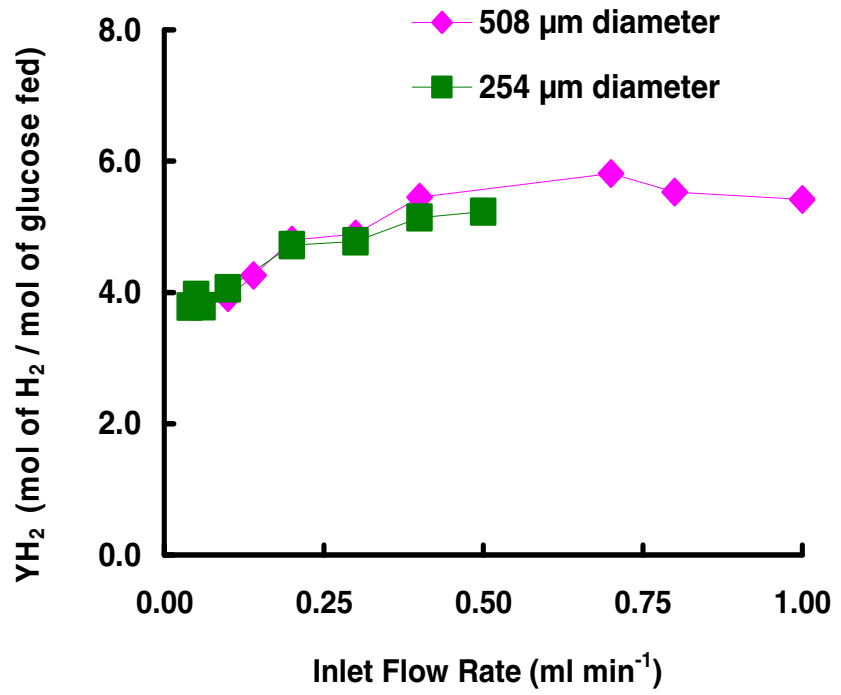

Figure 4.4B. Hydrogen yield as a function of inlet flow rate for 508 µm and 254 µm tubing diameters in the single tube microchannel reactor at 750°C, 250 bar, and 0.1 M glucose

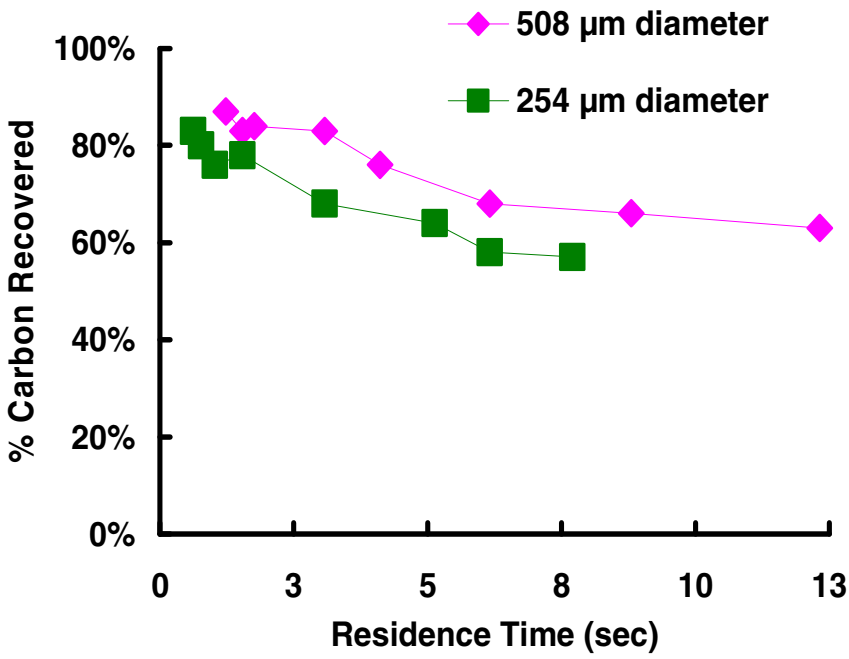

Figure 4.4C. Recovered carbon as a function of residence time for 508 µm and 254 µm tubing diameters in the single tube microchannel reactor at 750°C, 250 bar, and 0.1 M glucose

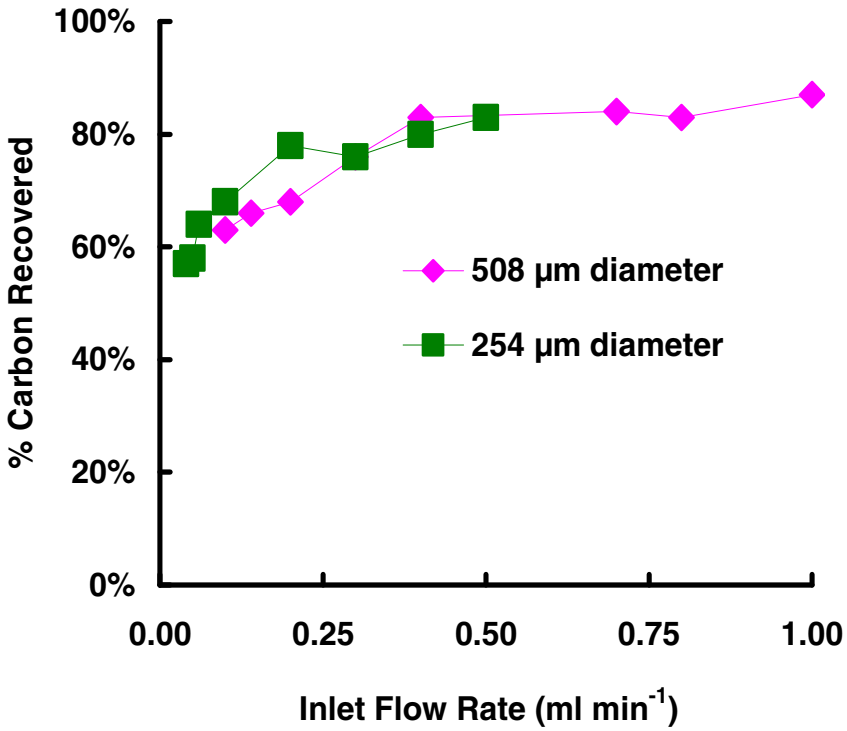

Figure 4.4D. Recovered carbon as a function of inlet flow rate for 508 µm and 254 µm tubing diameters in the single tube microchannel reactor at 750°C, 250 bar, and 0.1 M glucose

The pH of the liquid reactor effluent was measured for each residence time in the 508 µm diameter and 254 µm diameter tubing and is presented in Figure 4.5. In the 508 µm diameter tubing pH sharply increases as a function of residence time ranging from 1.2 sec to 1.8 sec. The pH remains constant at 4.2 for residence times greater than 1.8 sec. A similar trend in pH for the liquid products is observed in the 254µm diameter tubing. The pH of the liquid products sharply increases as a function of residence times ranging from 0.6 sec – 3.0 sec. The pH remains constant at 4.3 for residence times greater than 3 sec.

Single Tube Microchannel Reactor Organic Acids Analysis

The organic acids analysis of the liquid products completed for experiments in the 508 µm single tube reactor at 750°C, 250 bar, and 0.1 M glucose revealed small amounts of acetic acid in the liquid products at residence times less than 1.1 sec. The organic acids analysis completed for experiments in the 254 µm single tube reactor at 750°C, 250 bar, and 0.1 M glucose revealed small amounts of acetic acid in the liquid products for experiments at residence times less than 0.5 sec. The concentration of acetic acid in the liquid products for experiments run in the 508 µm and 254 µm diameter tubes at 750°C, 250 bar, and 0.1 M glucose are presented in Figure 4.6.

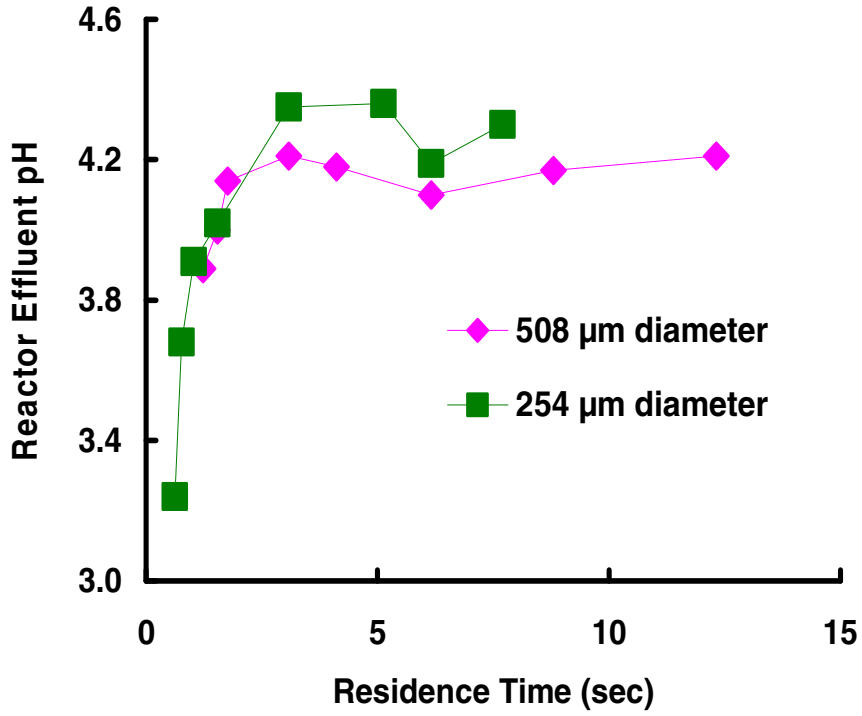

Figure 4.5. pH of liquid reactor effluent for 508 µm and 254 µm tubing diameters in the single tube microchannel reactor at 750°C, 250 bar, and 0.1 M glucose

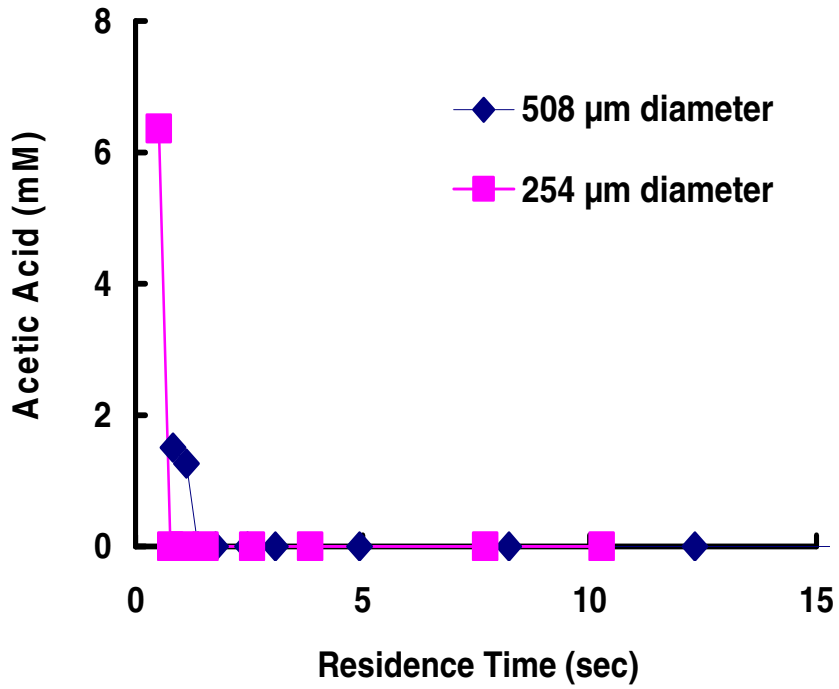

Figure 4.6. Acetic acid concentration in the liquid reactor effluent for 508 µm and 254 µm tubing diameters in the single tube microchannel reactor at 750°C, 250 bar, and 0.1 M glucose

Glucose Conversion

Residual glucose was determined by HPLC, and a sample chromatogram is presented in Figure 4.7. The reactor feed is compared to the liquid reactor effluent run at 650°C, 250 bar, 0.1 M glucose, and a 4.7 sec residence time. Glucose conversion as a function of residence time for the 254 µm diameter single tube microchannel reactor at 750°C, 0.1 M glucose, and 250 bar is presented in Figure 4.8A. Glucose conversion as a function of residence time in the 508 µm diameter single tube microchannel reactor at 650°C, 250 bar, and 0.1 M glucose is presented in Figure 4.8B. No residual glucose was detected in any of the liquid samples represented in Figures 4.8A and 4.8B.

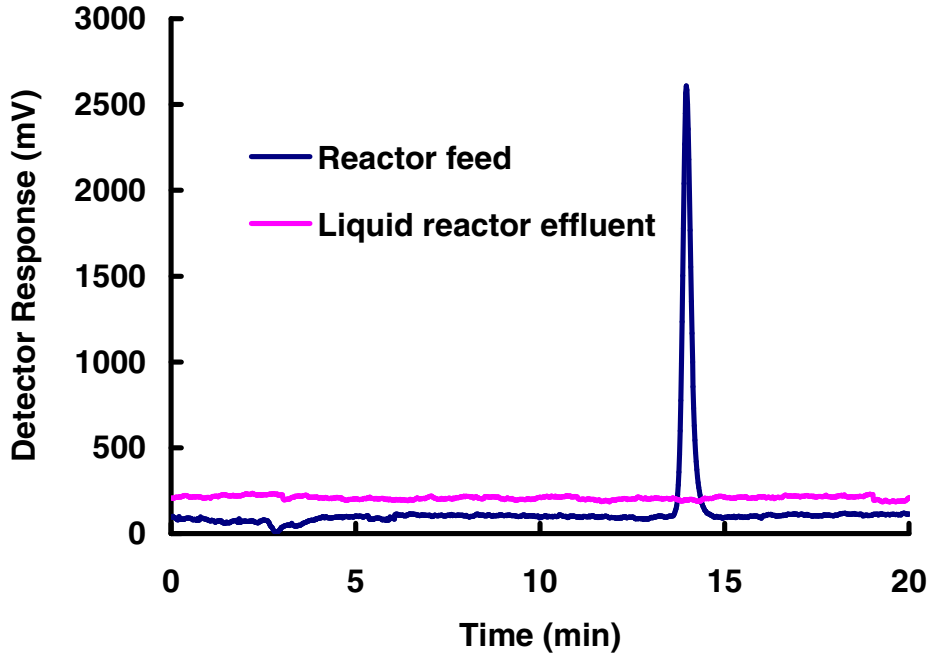

Figure 4.7. Sample HPLC chromatogram of liquid reactor effluent at 650°C, 250 bar, 0.1mol/L glucose, 4.7 sec residence time in the serpentine microchannel reactor

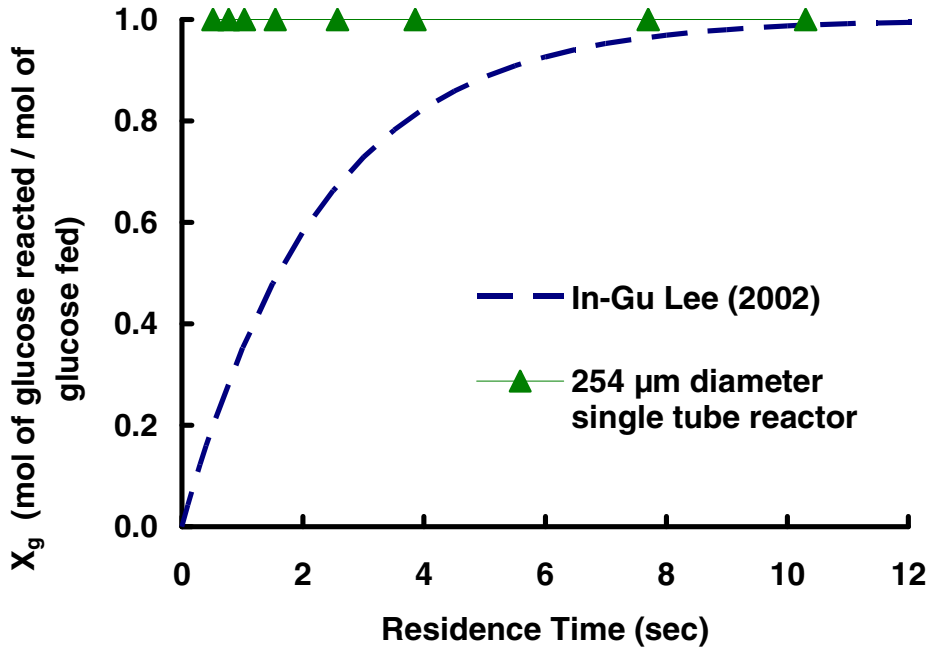

Figure 4.8A. Conversion of glucose as a function of residence time in the 254µm diameter single tube reactor at 750°C, 250 bar, and 0.1 M glucose

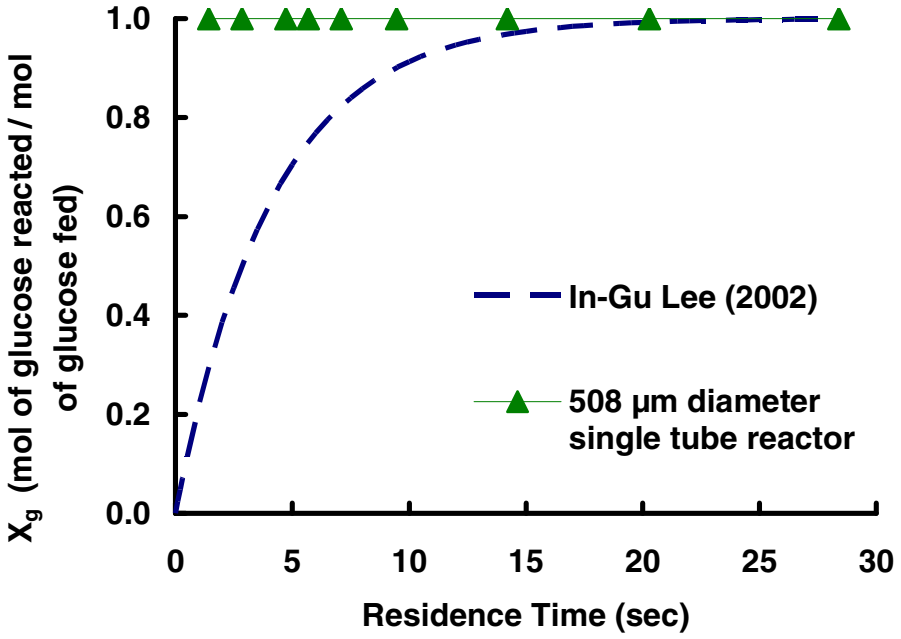

Figure 4.8B. Conversion of glucose as a function of residence time in the 508µm diameter single tube reactor at 650°C, 250 bar, and 0.1 M glucose

Affect of Temperature on Gas and Liquid Products in the Serpentine Microchannel Reactor

The affect of decreasing reactor temperature from 750°C to 650°C was investigated in the serpentine microchannel reactor at 250 bar and 0.1 mol/L glucose. The total gas flow rate per volume of reactor at 650°C and 750°C is plotted against the inlet feed rate, and is presented in Figure 4.9. The gas production for experiments conducted at 750°C as a function of the glucose feed rate was linear, and exhibited a significant increase in gas production compared to experiments conducted 650°C. The gas production for experiments run at 650°C started out linear as a function of feed rate, but approach an asymptote at higher feed rates.

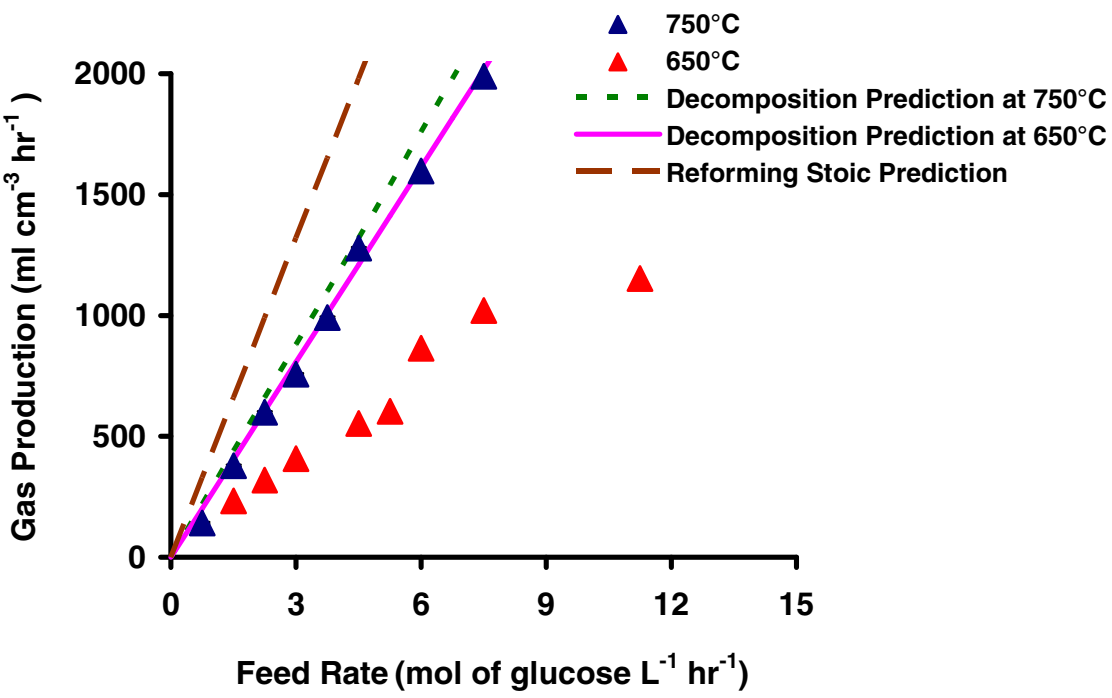

Figure 4.9. Normalized total gas production for the serpentine microchannel reactor at 650°C and 750°C, 250 bar, and 0.1 M glucose

Gas compositions for experiments conducted at 750°C, 250 bar, and 0.1 M glucose in the serpentine microchannel reactor were comprised of H_2, CO_2, CH_4, and CO, and are presented in Figure 4.10A. Gas composition was constant as a function of residence time, and ranged from 1.9 sec to 24.3 sec. Gas compositions in the serpentine microchannel reactor were similar to the single tube microchannel reactor at comparable conditions. The average gas composition at 750°C, 250 bar, 0.1 M glucose, and residence times ranging from 2.4 sec – 24 sec was 52.5 % H_2, 34.8 % CO_2, 10.3 % CH_4, and 0.5 % CO.

Gas compositions for experiments run at 650°C, 250 bar, and 0.1 M glucose in the serpentine microchannel reactor as a function of residence time are presented in Figure

4.10B. The gas was comprised of H_2, CO_2, CH_4, and CO. The concentration of H_2, CO_2, and CH_4 were constant with respect to residence time and had average mole fractions of 47.6 %, 35.1 %, and 7.8 %. The concentration of CO decreased as residence time increased. The concentration of CO was plotted vs. residence time and is presented in Figure 4.10C. The highest concentration was 11.7% at a residence time of 1.9 sec, and the lowest was 3.0 % at a 14.0 sec residence time.

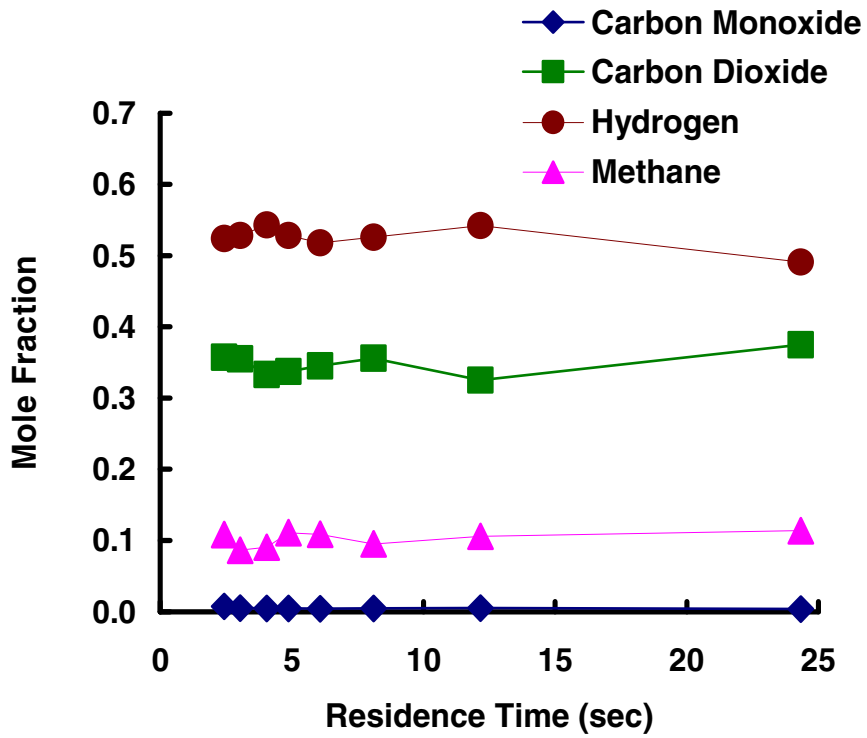

Figure 4.10A. Gas composition as a function of residence time in the serpentine microchannel reactor at 750°C, 250 bar, and 0.1 M glucose

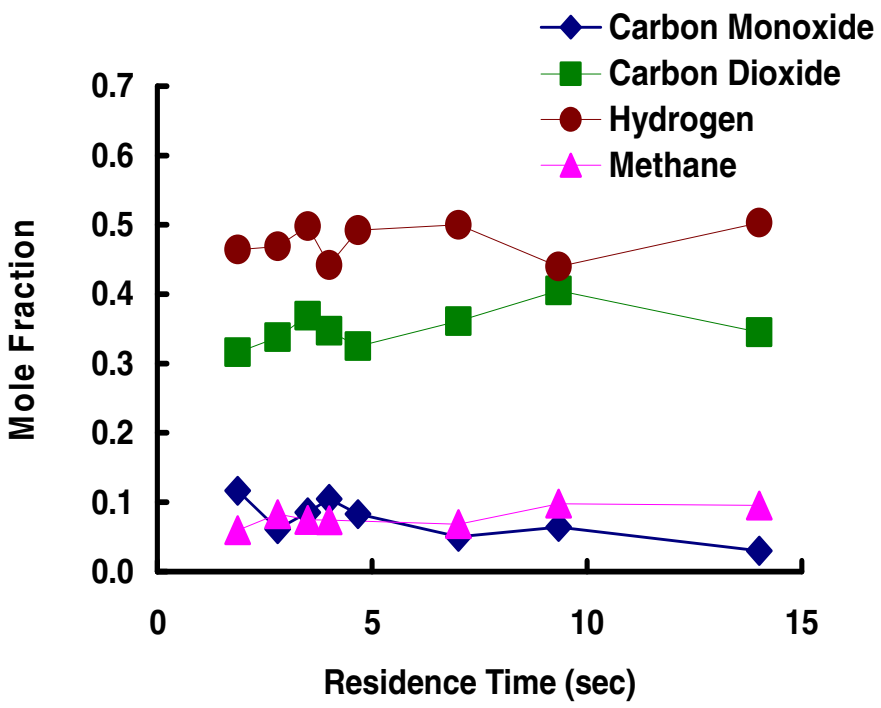

Figure 4.10B. Gas composition as a function of residence time in the serpentine microchannel reactor at 650°C, 250 bar, and 0.1 M glucose

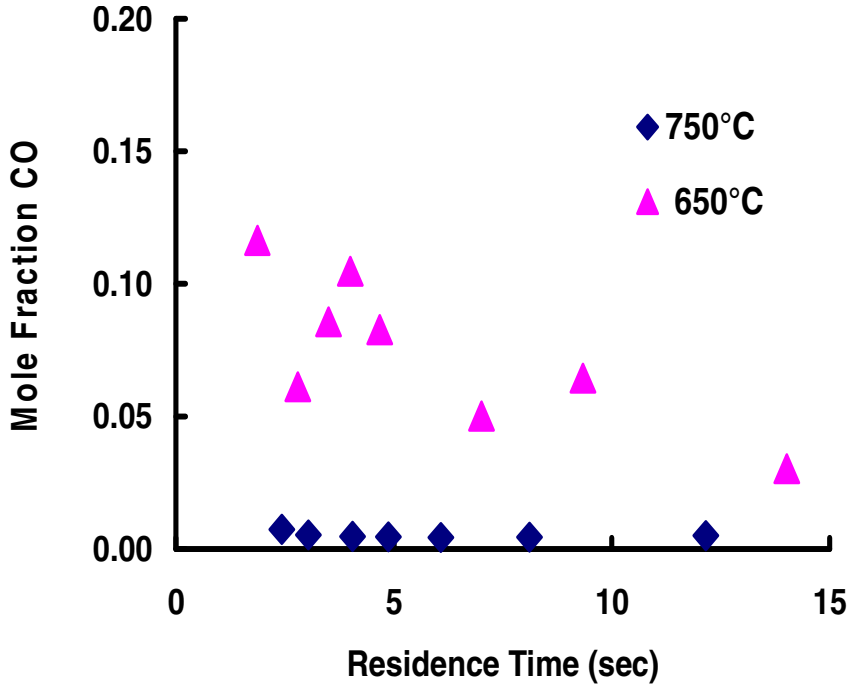

Figure 4.10C. CO concentration as a function of residence time in the serpentine microchannel reactor at 650°C and 750°C, 250 bar, and 0.1 M glucose

Hydrogen yield and recovered carbon as a function of residence time in the serpentine microchannel reactor 650°C and 750°C are presented in Figures 4.11A – 4.11B. At 750°C the hydrogen yield was constant as a function of residence time, and produced an average of 5.7 ±0.29 mol of hydrogen per mol of glucose fed. At 650°C the hydrogen yield was also constant as a function of residence time, and produced 2.6 ±0.44 mol of hydrogen per mol of glucose fed. Recovered carbon followed similar trends as the hydrogen yield. The recovered carbon at 750°C was constant with respect to residence time and averaged 79 % ± 6.9 %. At 650°C the recovered carbon was also constant with respect to residence time for residence times greater than 2.8 sec. The average recovered carbon for residence times ranging from 2.8 sec - 14 sec was 47 % ± 6.9 %, and decreased to 34 % at a residence time of 1.9 sec.

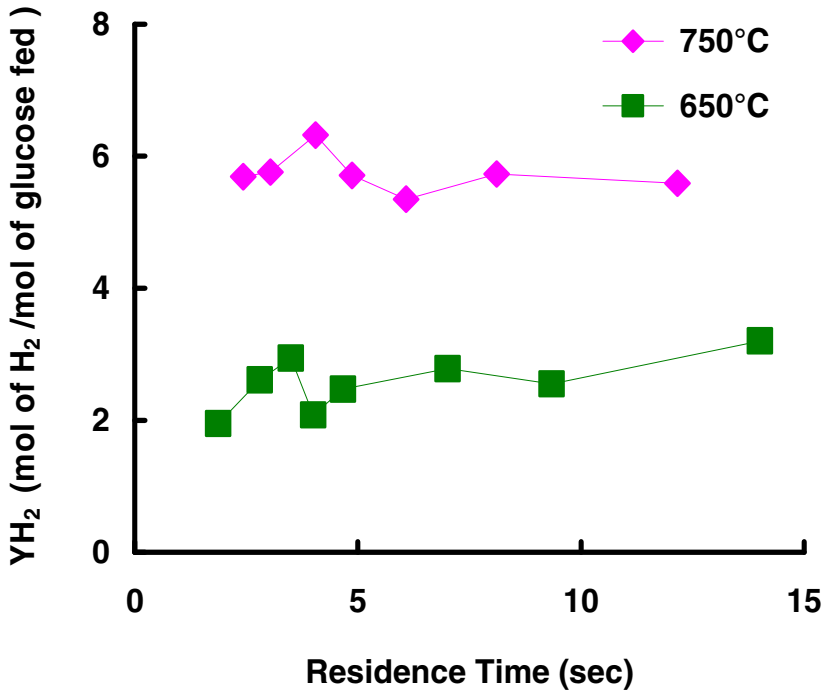

Figure 4.11A. Hydrogen yield for the serpentine microchannel reactor at 650°C and 750°C, 250 bar, and 0.1 M glucose

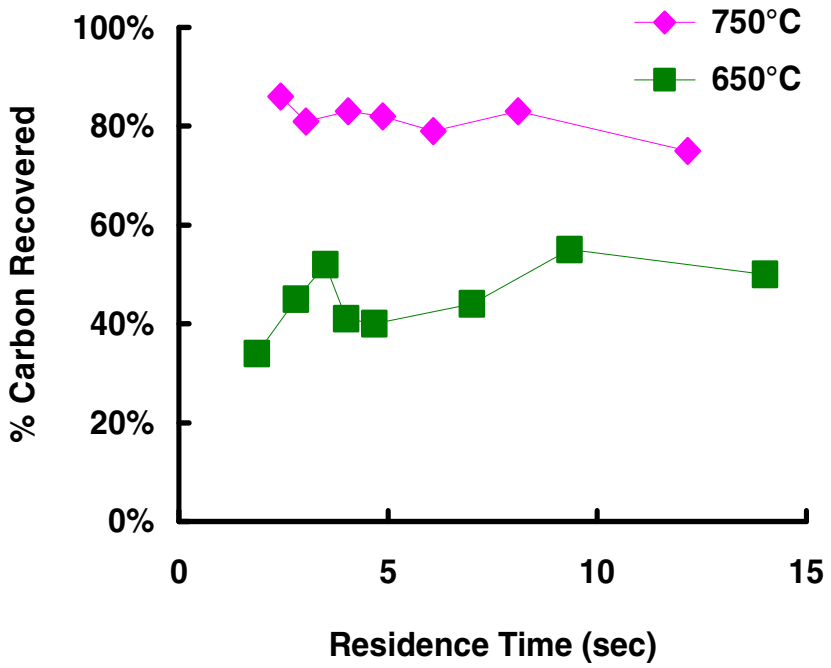

Figure 4.11B. Recovered carbon for the serpentine microchannel reactor at 650°C and 750°C, 250 bar, and 0.1 M glucose

Due to the unwanted formation of organic acids, the pH of the liquid products from the serpentine microchannel reactor at 650°C and 750°C was measured. pH as a function of residence time at 650°C and 750°C is presented in Figure 4.12. At 650°C the pH of the liquid reactor effluent was 3.2 as a function of residence time ranging from 1.9 sec – 4.7 sec. At residence times greater than 4.7 sec the pH increased linearly with increasing residence time. At 750°C the pH of the reactor effluent averaged 4.2 as a function of residence time ranging from 3 sec – 24.3 sec. At residence times less than 3 sec, the pH of the liquids products started to decrease.

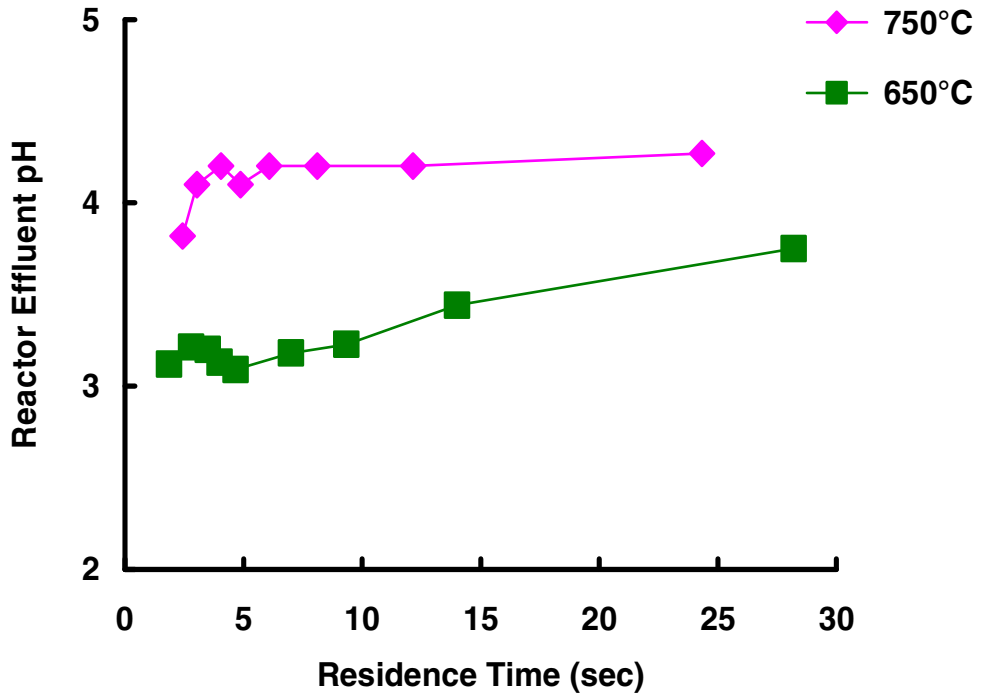

Figure 4.12. pH of liquid reactor effluent for the serpentine microchannel reactor at 650°C and 750°C, 250 bar, and 0.1 M glucose

Serpentine Microchannel Reactor Organic Acids Analysis

Organic acid determination in the liquid products for experiments run at 650°C and 750°C was completed by HPLC. Sample chromatograms are presented in Figures 4.13A – 4.13D. Figures 4.13A and 4.13B represents a reactor experiment at 750°C and a residence time of 4.9 sec. The HPLC chromatograms for this experiment contain no peaks at 210 nm and 290 nm. Figures 4.13C and 4.13D represent a reactor experiment at 650°C and a residence time of 4.7 sec. There are several distinct peaks at 210 nm and two small peaks at 290 nm. The organic acids identified in the reactor liquid effluent were acetic acid, acetaldehyde, propenoic acid, and butyric acid. Propenoic acid was present in the liquid products for experiments run at 650°C and residence

times less than 7.0 sec. However, the highest concentration was less than 3 mM, which was in the noise of the instrument, and thus was not quantified.

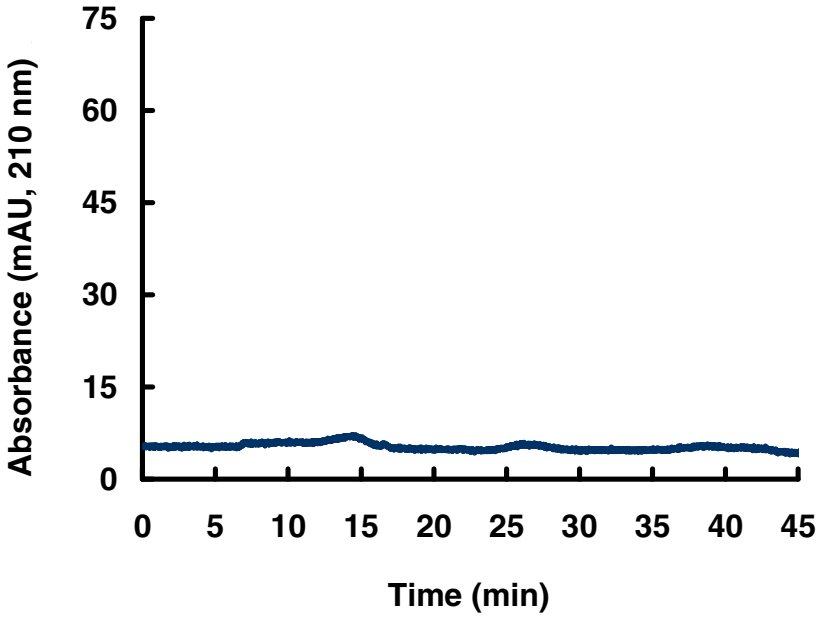

Figure 4.13A. Sample HPLC chromatogram of liquid reactor effluent at 750°C, 250 bar, 0.1 mol/L glucose, 4.9 sec residence time in the serpentine microchannel reactor detected at 210 nm

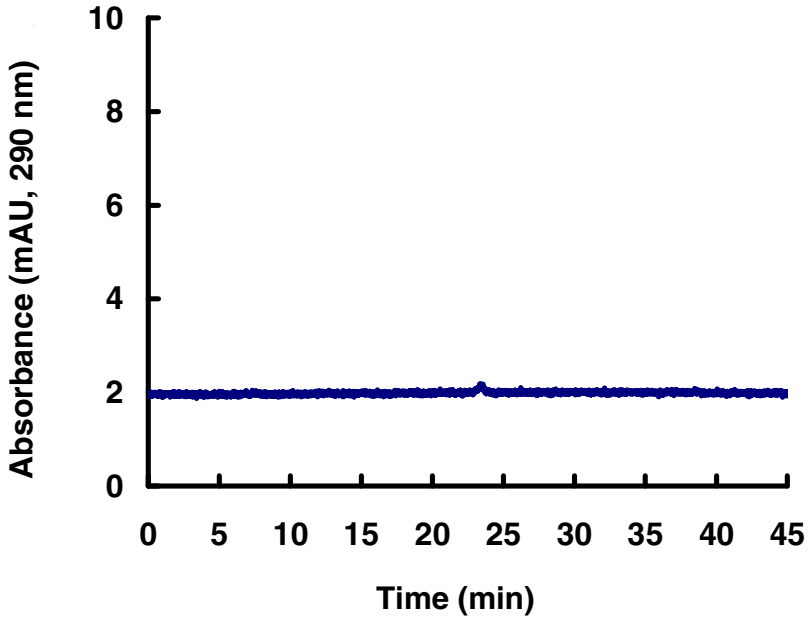

Figure 4.13B. Sample HPLC chromatogram of liquid reactor effluent at 750°C, 250 bar, 0.1 mol/L glucose, 4.9 sec residence time in the serpentine microchannel reactor detected at 290 nm

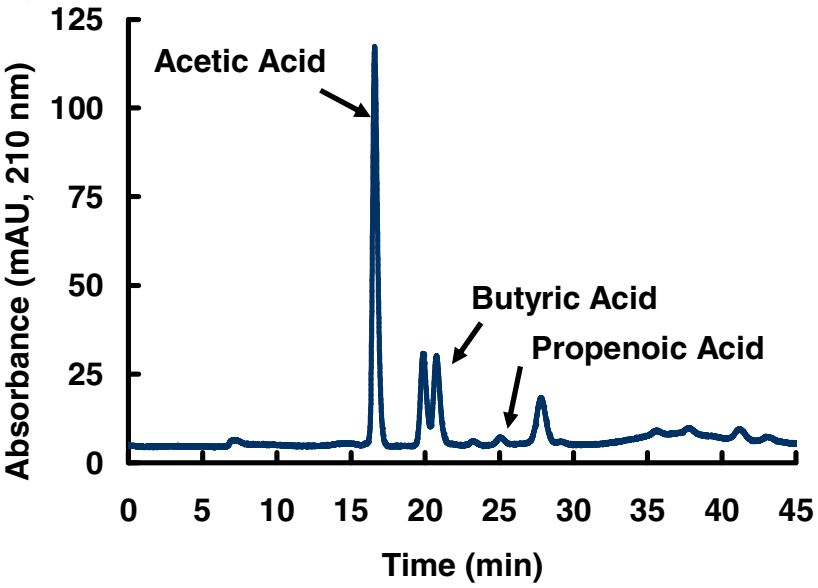

Figure 4.13C. Sample HPLC chromatogram of liquid reactor effluent at 650°C, 250 bar, 0.1 mol/L glucose, 4.7 sec residence time in the serpentine microchannel reactor detected at 210 nm

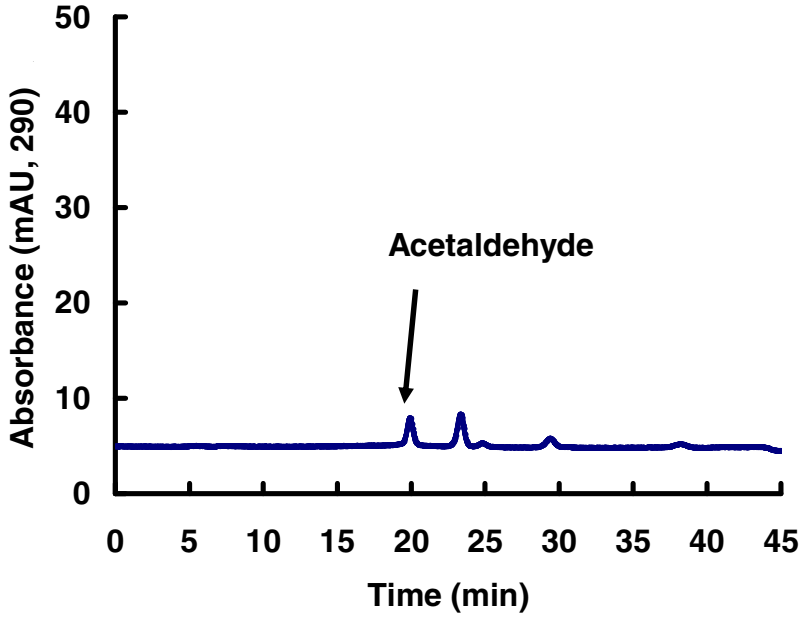

Figure 4.13C. Sample HPLC chromatogram of liquid reactor effluent at 650°C, 250 bar, 0.1 mol/L glucose, 4.7 sec residence time in the serpentine microchannel reactor detected at 290 nm

Quantification of the organic acids at 650°C and 750°C are presented in Figures 4.14A – 4.14C. The concentration of acetic acid in the liquid reactor effluent at 650°C and 750°C in the serpentine microchannel reactor is presented in Figure 14.4A. At 650°C and residence times greater than 4.7 sec there was a linear increase in the amount of acetic acid in the liquid products with respect to decreasing residence time. At residence times less than 4.7 sec. the concentration of acetic acid was constant at 55 mM. The concentration of butyric acid in the liquid products at 650°C and 750°C is presented in Figure 14.4B. There was no butyric acid in any of the samples run at 750°C. At 650°C the concentration of butyric acid decreases exponentially as a function of increasing residence time. The concentration of acetaldehyde in the liquid reactor effluent at 650°C and 750°C is presented in Figure 14.4C. There was no

acetaldehyde present in the samples run at 750°C. At 650°C the concentration of acetaldehyde exponentially decreased as a function of residence times ranging from 1.9 sec – 7 sec. No acetaldehyde was detected in the liquid products at residence times greater than 7 sec.

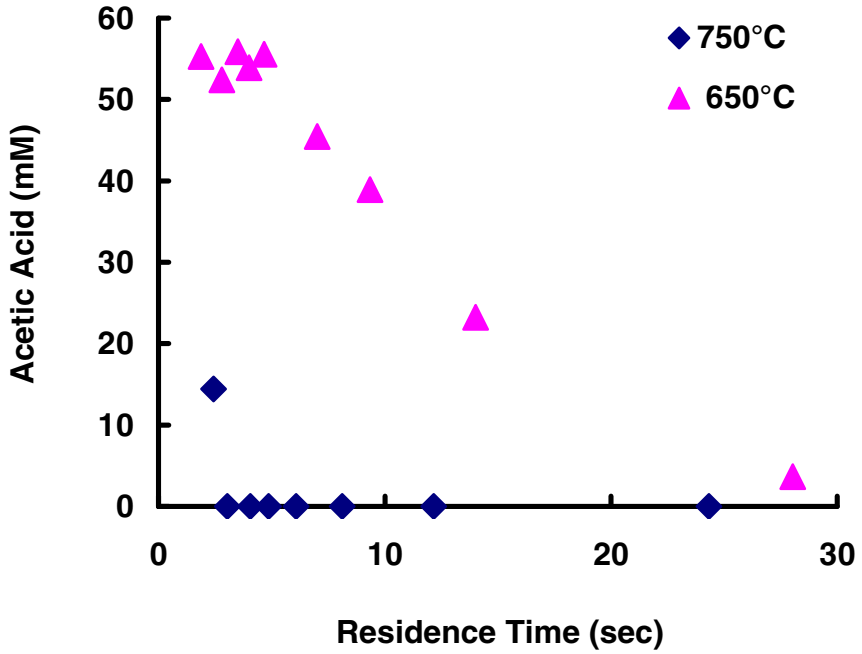

Figure 4.14A. Acetic acid concentration in the reactor liquid effluent for the serpentine microchannel reactor at 750°C, 250 bar 0.1 M glucose

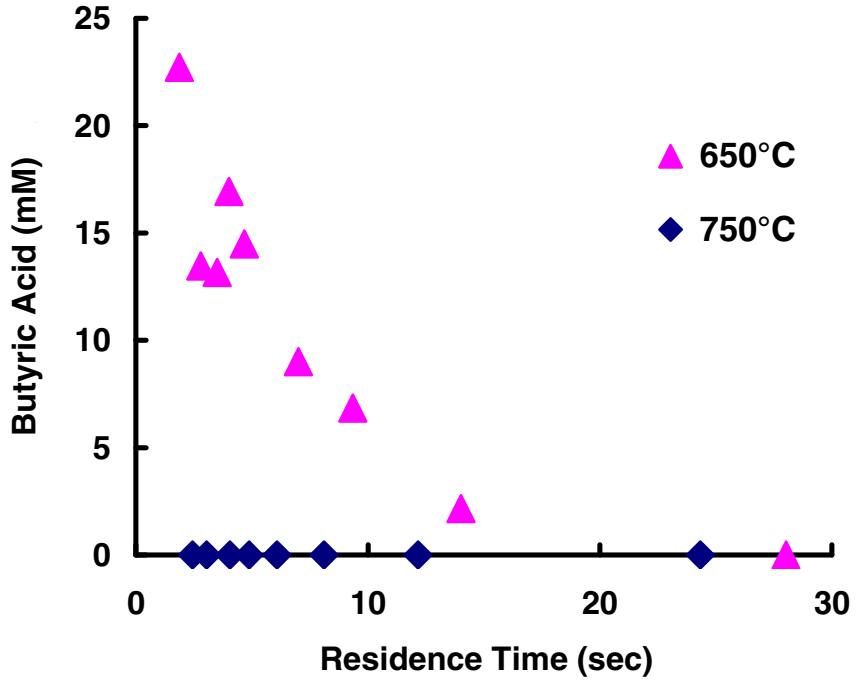

Figure 4.14B. Butyric acid concentration in the reactor liquid effluent for the serpentine microchannel reactor at 750°C, 250 bar 0.1 M glucose

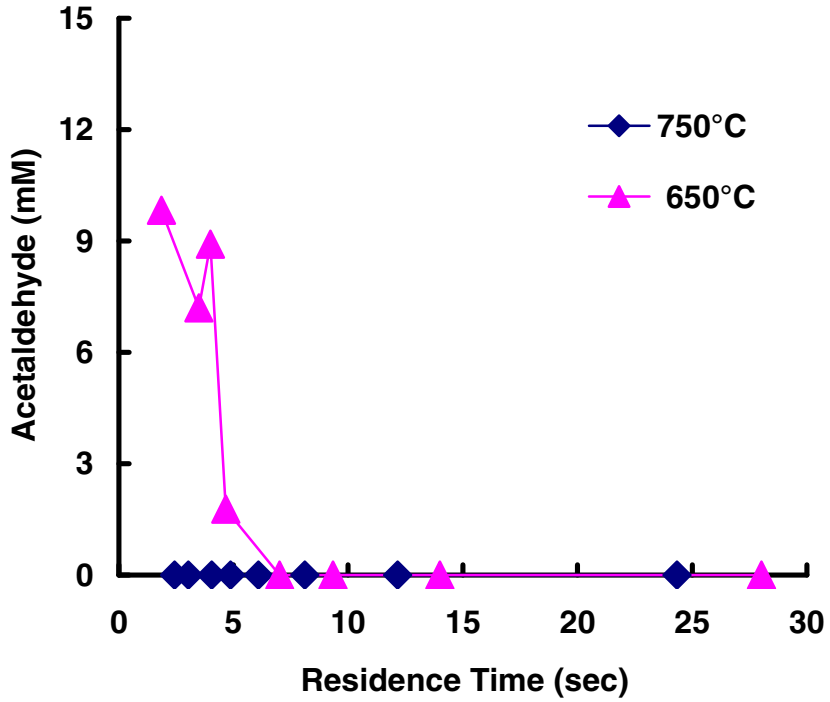

Figure 4.14C. Acetaldehyde concentration in the reactor liquid effluent for the serpentine microchannel reactor at 750°C, 250 bar 0.1 M glucose

Increased Glucose Feedstock Concentrations

Glucose feed concentrations were increased to 0.8 M and 0.4 M to determine the effect of the water glucose ratio on the gas and liquid products. Reactor conditions for the 254 μm single tube reactor were 650°C, 250 bar, and residence times ranging from 1.8 sec – 7.0 sec. Higher glucose concentrations in the feed resulted in reactor fouling before a steady state gas composition and flow rate could be measured at every condition tested. The formation of coke at the inlet eventually plugged the reactor. The liquid effluent had a clear pale yellow hue, and a pungent odor.

Process Repeatability

An experiment conducted at 650°C, 250 bar, 0.1 M glucose, and 4.7 sec residence time was repeated from a cold start to determine reactor experimental error, also called random error.

There are two types of error associated with measuring gas composition and gas flow rates. The first type is point error and the second type is experimental error. Point error comes from sampling and instrumentation, and is typically small compared to experimental error. The point error associated with gas composition is presented in Table 4.1. The point error associated with measuring the gas composition is calculated from the standard deviation of three separate GC runs. The point error from the gas mass flow meter was 0.25% or better and was determined by Omega Instruments at the time of calibration. Experimental error was determined from the standard deviation

of the average gas compositions and gas flow rates from two experiment runs at the same conditions from a cold start. These errors are presented in Table 4.2, and include point error.

Recovered carbon (Equation 4.7) and hydrogen yield (Equation 4.1) were calculated from gas composition and total gas flow rate. The experimental error of the calculated values is also a function of the point error associated with the measured quantities. Error associated with total gas flow rate included point errors from the gas mass flowmeter and GC, as well as error from numerical integration associated with average gas flow rate determination.

Table 4.1. Analytical error associated with gas composition

Species	Average Gas Composition (mole %)	Error (1 S.D.)
H_2	49.2%	0.724%
CO_2	32.5%	0.440%
CO	8.31%	0.126%
CH_4	6.82%	0.137%

Table 4.2. Reactor experimental error

Process Parameter	Average	Error (1 S.D.)
H_2 (mole %)	46.7%	3.60%
CO_2 (mole %)	34.1%	2.21%
CO (mole %)	7.1%	1.6%
CH_4 (mole %)	7.3%	0.7%
Total gas flow (ml/hr)	454.8	17.74
Recovered carbon	42%	2.8%
Y_{H2} (mole of H2 per mole of glucose fed)	2.4	0.091

Thermodynamic Equilibrium Calculation of Gas Composition

The equilibrium gas composition from the decomposition of glucose in supercritical water was predicted from thermodynamic calculations. Minimization of total Gibbs energy was used to determine the equilibrium values (Koretsky, 2004). The gasification of glucose was separated into three reactions; the reforming reaction (Equation 1.1), the water gas shift reaction, (Equation 1.3), and the methanation reaction, (Equation 1.5). The physical properties and reference state Gibbs energy of the species were tabulated from Chemcad 5.4 (Chemstations Inc.) and are presented in Table 4.3.

The coefficient matrix β_{ij} relates the *j* elements to *i* species in the system

$$\sum_{i=1}^{m} n_i \, \beta_{ij} = b_j \tag{4.8}$$

where n_i is the moles of species *i*, b_j is the number of one element present at the inlet concentration, and m is the total number of species in the system. For a 0.1 M glucose solution to decompose to CO_2, CO, CH_4, and H_2 the coefficient matrix is

$$(n_{H_2O}\ n_{CH_4}\ n_{H_2}\ n_{CO}\ n_{CO_2}\ n_{glucose}) \begin{bmatrix} 0 & 2 & 1 \\ 1 & 4 & 0 \\ 0 & 2 & 0 \\ 1 & 0 & 1 \\ 1 & 0 & 2 \\ 6 & 12 & 6 \end{bmatrix} = \begin{bmatrix} 6 & 1123 & 562 \end{bmatrix} \tag{4.9}$$

Equation 4.9 can be re-written as three coupled equations

$$n_{CH_4} + n_{CO} + n_{CO_2} + 6n_{glucose} = 6 \tag{4.10}$$

$$2n_{H_2O} + 4n_{CH_4} + 2n_{H_2} + 12n_{glucose} = 1123 \tag{4.11}$$

$$2n_{H_2O} + n_{CO} + n_{CO_2} + 6n_{glucose} = 562 \tag{4.12}$$

The total Gibbs energy of the system is

$$\begin{aligned} G = {} & n_{CO_2}\mu_{CO_2} + n_{CO}\ \mu_{CO}\ + n_{H_2}\mu_{H_2} \\ & + n_{CH_4}\mu_{CH_4} - n_{H_2O}\mu_{H_2O} - n_{glucose}\mu_{glucose} \end{aligned} \tag{4.13}$$

where n_i is the number of moles of a species, and μ_i is the chemical potential for that species. A new function is defined by the introduction of Lagrangian multipliers, λ_j, Koretsky (2004)

$$G' = \sum_{i=1}^{m} \mu_i n_i + \sum_{j=1}^{l} \lambda_j \left(\sum_{i=1}^{m} n_i \beta_{ij} - b_j\right) \tag{4.14}$$

Equation 4.14 is minimized by setting its derivative with respect to n_i equal to zero

$$\left(\frac{dG'}{n_i}\right)_{T,P,n_{j\neq i}} = 0 = \mu_i + \sum_{j=1}^{l} \lambda_i \beta_{ij} \tag{4.15}$$

The chemical potential, μ_i, can be written as

$$\mu_i = g_i^o + RT \ln \frac{\hat{f}_i}{\hat{f}_i^o} \tag{4.16}$$

where g_i^o is the Gibbs energy for the species at standard state, R is the gas constant, $\hat{f}_i^o$ is the fugacity of the species at the reference state, and $\hat{f}_i$ is the fugacity of the species at the system conditions. When Equation 4.16 is substituted into Equation 4.15, the expression becomes

$$0 = g_i^o + RT \ln \frac{\hat{f}_i}{\hat{f}_i^o} + \sum_{j=1}^{l} \lambda_i \beta_{ij} \tag{4.17}$$

The fugacity of the individual species $\hat{f}_i$ is defined by

$$\hat{f}_i = \hat{\varphi}_i y_i P_{sys} \tag{4.18}$$

where $\hat{\varphi}_i$ is the fugacity coefficient, P_{sys} is the system pressure, and y_i is the mole fraction which can be rewritten as

$$y_i = \frac{n_i}{n_{total}} \tag{4.19}$$

where n_{total} is the total moles in the system

$$n_{total} = n_{CH_4} + n_{CO_2} + n_{CO} + n_{H_2} + n_{glucose} + n_{H_2O} \tag{4.20}$$

The fugacity coefficients were solved for by using

$$\ln \hat{\varphi}_i = \int [z_i - 1] \frac{d\,\mathrm{P_r}}{\mathrm{P_r}} \tag{4.21}$$

where z_i is the compressibility factor which is a function of the acentric factor, ω, and the reduced variables T_r and P_r. The pressure was solved for by the Soave Redlich Kwong equation of state

$$P = \frac{RT}{v-b} - \frac{a\alpha}{v(v+b)} \tag{4.22}$$

where

$$a = \frac{0.42747\, R^2 T_c^{\,2}}{P_c} \tag{4.23}$$

$$b = \frac{0.08664 RT_c}{P_c} \tag{4.24}$$

$$\alpha = (1 + (0.48508 + 1.55171\omega - 0.15613\omega^2)(1 - T_r^{\,0.5}))^2 \tag{4.25}$$

Substituting Equation 4.18 in Equation 4.17, and setting the reference state to 1 bar gives the following six equations

$$\Delta g^{o}_{f,CH_4} + RT \ln \hat{\varphi}_{CH_4} \frac{n_{CH_4}}{n_{total}} P_{sys} + \lambda_c + 4\lambda_H = 0 \tag{4.26}$$

$$\Delta g^{o}_{f,CO_2} + RT \ln \hat{\varphi}_{CO_2} \frac{n_{CO_2}}{n_{total}} P_{sys} + \lambda_c + 2\lambda_O = 0 \tag{4.27}$$

$$\Delta g^{o}_{f,H_2O} + RT \ln \hat{\varphi}_{H_2O} \frac{n_{H_2O}}{n_{total}} P_{sys} + 2\lambda_H + \lambda_O = 0 \tag{4.28}$$

$$\Delta g^{o}_{f,H_2} + RT \ln \hat{\varphi}_{H_2} \frac{n_{H_2}}{n_{total}} P_{sys} + 2\lambda_H = 0 \tag{4.29}$$

$$\Delta g^{o}_{f,CO} + RT \ln \hat{\varphi}_{CO} \frac{n_{CO}}{n_{total}} P_{sys} + \lambda_c + \lambda_O = 0 \tag{4.30}$$

$$\Delta g^{o}_{f,glucose} + RT \ln \hat{\varphi}_{glucose} \frac{n_{glucose}}{n_{total}} P_{sys} + 6\lambda_c + 12\lambda_H + 6\lambda_O = 0 \tag{4.31}$$

Equations 4.26 – 4.31 combined with Equations 4.10 – 4.12 form a set of nine coupled equations that were solved using Chemcad 4.5.0. The calculation was solved for reactor conditions at 250 bar, 0.1 M glucose, and temperatures ranging from 500°C to 800°C. The results are presented in Figures 4.15A and 4.15B.

A comparison of the experimental and equilibrium values for the decomposition of 0.1 M glucose at 250 bar, 650°C and 750°C are presented in Figures 4.16A and 4.16B. At 750°C the experimental CO and CO_2 concentrations were similar to equilibrium values. The equilibrium CO concentration was 0.62 % compared to a measured value of 0.43 % at a 6.1 sec residence time. There was a 55–fold increase in the measured

CH_4 concentration compared to the equilibrium value. The predicted CH_4 concentration was 0.02 % compared to a measured value of 10.9 % at a 6.1 sec residence time. The presence of CH_4 in the measured gas composition was accompanied by a decrease in the H_2 concentration. Equilibrium H_2 concentration was 66.4 % compared to a measured value of 51.8 % at a 6.1 sec residence time.

At a reactor temperature of 650°C there was a 12-fold increase in the experimental CO concentration. The predicated value was 0.42 % compared to a measured value of 5.0 % at a 7.0 sec residence time. There was also an increase in the measured CO_2 concentration and CH_4 concentration compared to equilibrium values. The predicted CH_4 concentration was 0.02 % compared to a measured value of 6.9 % at a 7.0 sec residence time. The measured H_2 concentration was 50.0 % at a 7.0 sec residence time compared to the equilibrium value of 66.2 %.

Table 4.3. Physical and thermodynamic properties used in equilibrium calculation of gas composition and heat of reaction calculation

								$Cp = A + B\,T + C\,T^2 + D\,T^{-2}$			
Species	T_c (K)	P_c (Bar)	V_c ($m^3\ kmol^{-1}$)	Mw ($g\ mol^{-1}$)	Acentric Factor	$H_f^{o\,(a)}$ ($kJ\ mol^{-1}$)	$g^{o\,(a)}$ ($kJ\ mol^{-1}$)	A	B	C	D
CH_4	191.1	45.8	0.099	16	0.013	-74.863	-50.820	12.440	0.076689	$-18004 \cdot 10^{-6}$	144800
H_2	33.30	13.0	0.064	2	0.00	0	0	27.012	0.0035081	0	8300.0
CO_2	304.2	73.9	0.094	44	0.420	-393.51	-394.41	42.388	0.015100	$-2.9080 \cdot 10^{-6}$	-889100
CO	133.0	35.0	0.093	28	0.041	-110.54	-137.16	25.694	0.0082930	$-1.4770 \cdot 10^{-6}$	101900
Glucose	1011	62.0	0.416	180	2.547	-1256.9	-909.40	176.67	0.40684	$-1.5154 \cdot 10^{-4}$	-5981800
H_2O	647.4	221	0.063	18	0.348	-241.83	-228.59	28.850	0.012055	0	100600

*Values were estimated from Tang and Kitagawa (2005) and Koretsky (2004)
(a) reference state was 298 K and 1 atm

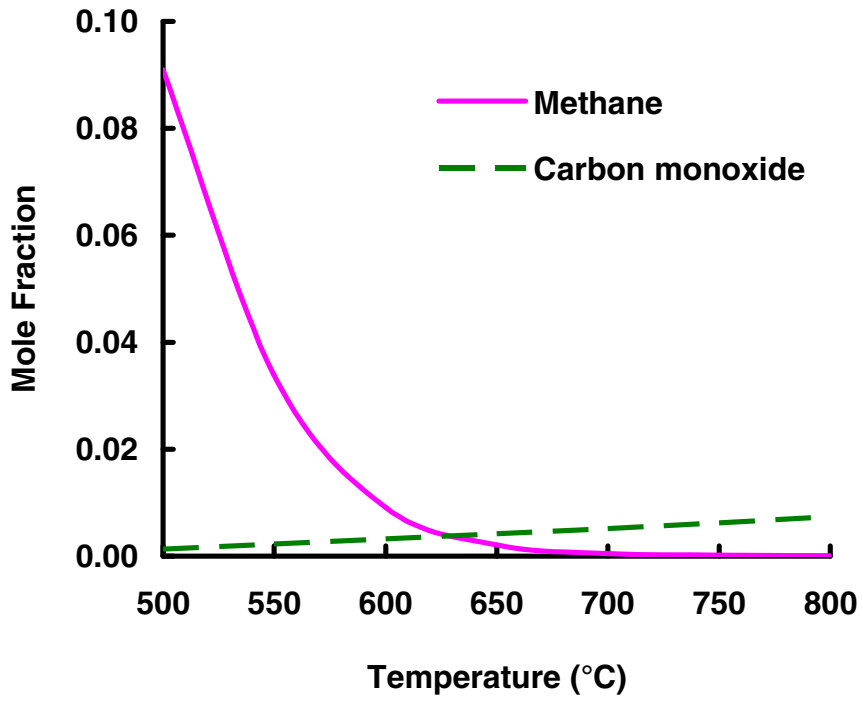

Figure 4.15A. Equilibrium gas compositions of CH_4 and CO for the decomposition of 0.1 M glucose at 250 bar

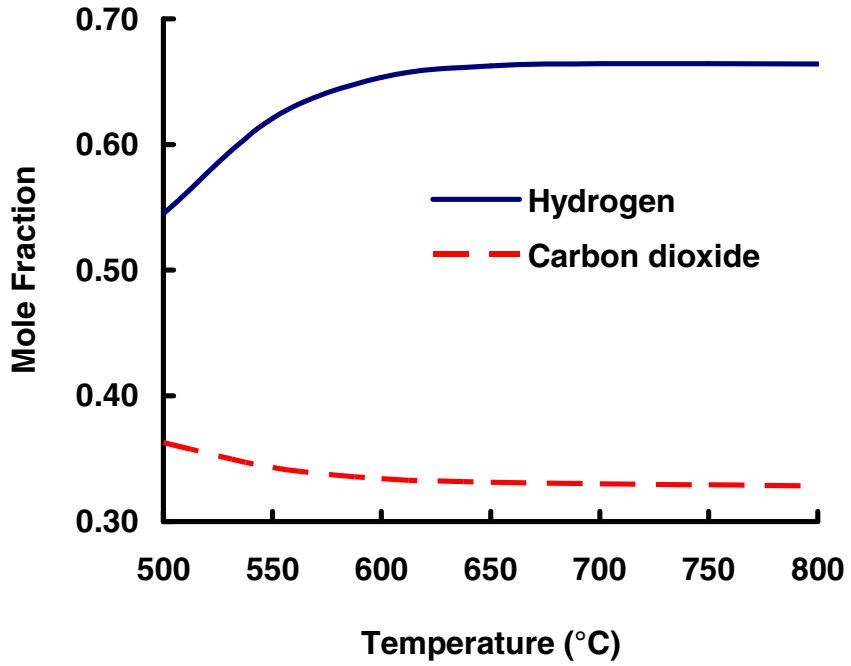

Figure 4.15B. Equilibrium gas compositions of CO_2 and H_2 for the decomposition of 0.1 M glucose at 250 bar

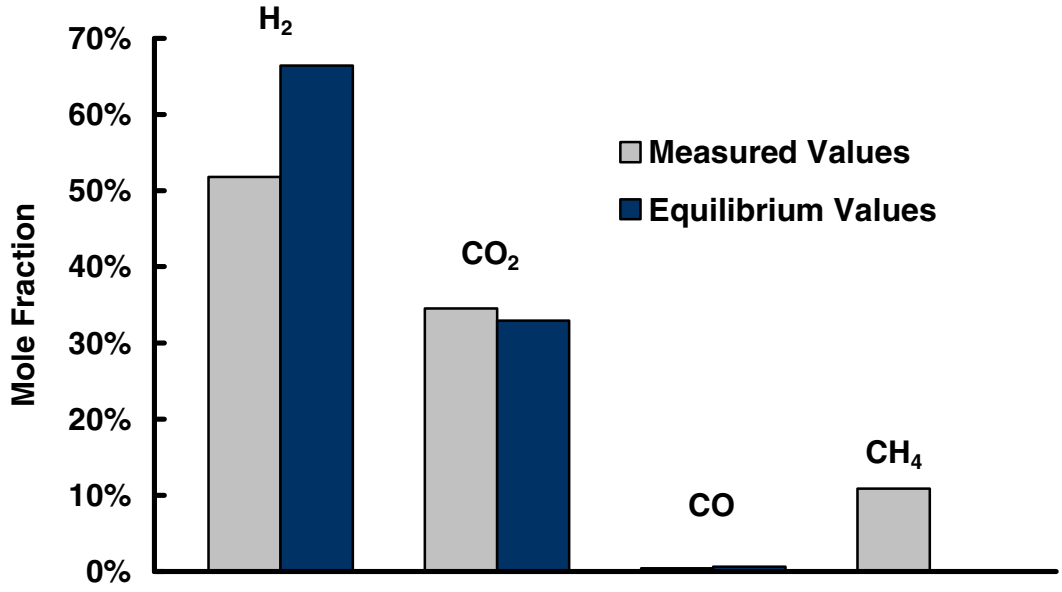

Figure 4.16A. Comparison of experimental and equilibrium gas compositions from the decomposition of 0.1 M glucose at 750°C, 250 bar, and a 6.1 sec residence time

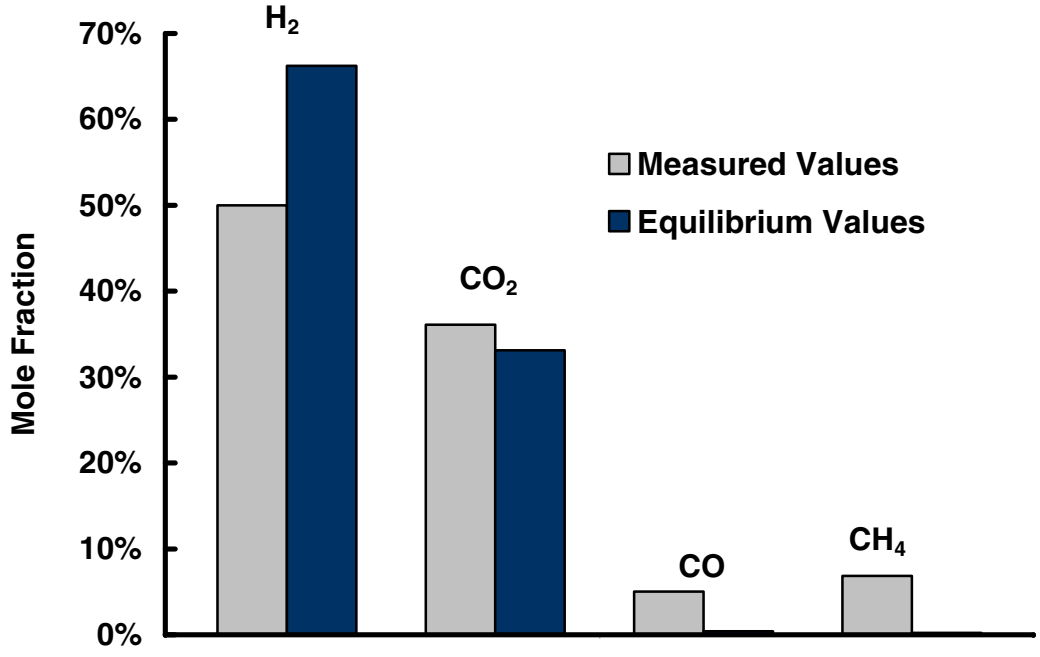

Figure 4.16B. Comparison of experimental and equilibrium gas compositions from the decomposition of 0.1 M glucose at 650°C, 250 bar, and a 7.0 sec residence time

Discussion

Reactor Performance

A process was developed to produce hydrogen gas from glucose solutions by supercritical water reforming in a microchannel reactor. At 750°C and 250 bar there was no difference in gas production and hydrogen yield as a function of residence time or reactor geometry. Gas production rates from the serpentine microchannel reactor, the 254 μm single tube reactor, and the 508 μm single tube reactor are presented in Figures 4.1 and 4.9. Gas production rates were linear as a function of feed rate in all three reactors, thus producing the same amount of gas per mole of feed. The gas production rate in the 254 μm single tube reactor was 258 liters of gas per mole of glucose fed compared to 275 liters of gas per mole of glucose fed in the 508 μm single tube reactor, and 267 liters of gas per mole of glucose fed in the 254 μm single tube reactor. The theoretical limit of gas production based on 100% glucose conversion in Equation 1.1 was 440 liters of gas per mole of glucose fed.

Average hydrogen yields for the decomposition of 0.1 M glucose are presented in Table 5.1. At 750°C and 250 bar, hydrogen yields averaged 4.6 ± 0.58 in the 254 μm single tube reactor, 5.2 ± 0.54 in the in the 508 μm single tube reactor, 5.5 ± 0.29 in the serpentine microchannel reactor. Hydrogen yields were relatively constant as a function of feed rate, and yields obtained were similar to hydrogen yields reported in the literature at similar reactor conditions. Lee et al. (2002) reported a hydrogen yield of 4.8 when a 0.6 M solution of glucose was gasified in a Hastelloy reactor at 750°C,

280 bar, and a 19 sec residence time. Antal et al. (2000) reported a hydrogen yield of 4.8 when they gasified a 1.25 M glucose solution in a carbon packed bed reactor at 745°C and 280 bar. The theoretical hydrogen yield based on 100% glucose conversion and the high temperature pathway in Equation 1.1 was 12 moles of H_2 per mole of glucose fed.

Yu et al. (1993) observed that, when glucose was gasified in reactors constructed of Inconel or corroded Hastelloy, hydrogen yields increased compared to reactors constructed from new Hastelloy. They concluded that Inconel strongly catalyzes the water gas shift reaction. Kersten et al. (2006) concluded Inconel, Hastelloy, and to a lesser extent stainless steel catalyze the gasification of glucose based on recovered carbon and the water gas shift reaction. The results of these catalytic activities are increased gas production, increased H_2 yield, and a decrease in CO concentration. For conclusions based on direct comparisons to reactors in the literature, a more complete understanding how the reactor material catalyzes the decomposition of glucose and water gas shift reaction are needed.

Gas compositions produced in the serpentine and single tube microchannel reactors at 750°C and 250 bar from a 0.1 M glucose solution were similar regardless of residence time and reactor geometry. Gas composition as a function of residence time in the serpentine microchannel reactor, 254 µm and 508 µm single tube microchannel reactors are presented in Figures 4.10A, 4.2B, and 4.2A. Given that gas compositions were constant as a function of residence time, average gas compositions from a range

of residence times were calculated and presented in Table 5.1. The gasification of glucose by supercritical water in a microchannel reactor was concluded to be moving toward equilibrium due to gas compositions independent of residence time and reactor geometry.

Table 5.1. Average gas compositions, hydrogen yield, and recovered carbon for the gasification of glucose by supercritical water based on reactor design

Reactor	Serpentine	Serpentine	254 µm Single Tube	508 µm Single Tube	Tubular Hastelloy Lee et al. (2002)	Carbon Packed Bed Antal et al. (2000)
Reactor channel geometry	Rectangular	Rectangular	Tube	Tube	Tube	Packed Bed
Glucose Concentration (mol L^{-1})	0.1	0.1	0.1	0.1	0.6	1.25
Pressure (bar)	250	250	250	250	280	280
Temperature (°C)	750	650	750	750	750	745
Residence Time (sec)	2.4 - 12.2	1.9 - 14.0	0.6 - 6.2	1.2 - 12.3	19	NR
H_2 Yield	5.7 ± 0.29	2.6 ± 0.42	4.6 ± 0.58	5.2 ± 0.54	4.8	4.8
Recovered Carbon in the Gas	81.3 ± 3.50	45.1 ± 6.94	74.8 ± 7.33	78.1 ± 8.32	99.7	92
Gas Composition (mole %)	(n = 7)	(n = 8)	(n = 7)	(n = 7)	(n = 1)	(n = 1)
H_2	52.9 ± 0.928	47.6 ± 2.59	50.1 ± 0.640	51.8 ± 1.03	46	46
CO_2	34.4 ± 1.27	35.1 ± 2.79	35.2 ± 1.88	34.2 ± 1.40	34.2	36
CH_4	10.1 ± 0.995	7.77 ± 1.35	11.3 ± 0.757	11.6 ± 1.25	12.2	13
CO	0.516 ± 0.108	7.45 ± 2.85	1.54 ± 1.11	0.59 ± 0.29	2.6	4
C_{2+}	0.0 ± 0.0	0.0 ± 0.0	0.0 ± 0.0	0.0 ± 0.0	4.5	NR

NR = not reported

Reactor performance based on gas composition in the serpentine microchannel reactor was compared to Lee et al. (2002) and Antal et al. (2000). The results are presented in Table 5.1. One significant difference between gas compositions reported in the literature and experimental gas compositions from the serpentine microchannel reactor is the presence of ethane and ethylene. There was no detectable ethane or ethylene in any of the serpentine microchannel reactor experiments. The concentration H_2 in the serpentine microchannel reactor was 8 mole % higher compared to gas compositions obtained by Lee et al. (2002) and Antal et al. (2000) at similar conditions. The concentration of CO in the serpentine microchannel was reduced by 5 fold compared to the Hastelloy reactor used by Lee et al. (2002), and 8 fold compared to the packed bed reactor used by Antal et al (2000). Kersten et al. (2006) concluded that metal reactors have a tendency to promote the water gas shift reaction. One possible explanation for the higher H_2 and lower CO concentrations in the serpentine microchannel reactor compared to reactors in the literature is the surface area to volume ratio, which would enhance the catalytic effect produced by the metal. The serpentine microchannel reactor has a surface area to volume ratio of 303.3 cm^{-1} as compared to 3.2 cm^{-1} in the Hastelloy reactor. Increased H_2 concentration, decreased CO concentration, and no ethane and ethylene present in the gas effluent are advantages of gasifying glucose in a microchannel reactor.

A rate constant for the gasification of glucose could not be derived because the glucose conversion was 100 % at all residence times tested. Conversion of glucose as a function of residence time at 650°C in the 508 µm single tube reactor, and 750°C in the 254 µm single tube reactor are presented in Figures 4.8A and 4.8B. The figures are compared to Lee et al. (2002) who measured residual glucose in a conventional 6.2 mm inner diameter Hastelloy tubular reactor. Lee et al. (2002) proposed that the decomposition of glucose was pseudo first order. The conversion of glucose in the single tube reactor for both diameters tested suggests that the decomposition of glucose was much faster in a microchannel reactor. The one notable difference was the initial reactor feed concentration. Whereas Lee et al. (2002) used a 0.6 M solution of glucose, a 0.1 M solution of glucose was used in this study. However, the initial concentration of glucose is independent of glucose conversion, assuming first order kinetics

$$X_g = 1 - e^{-\tau k_g} \tag{5.1}$$

where X_g is the residual glucose in the liquid products, τ is the residence time, and k_g is the rate constant for glucose. The rate constant for the decomposition of glucose in a tubular Hastelloy reactor determined by Lee et al. (2002) was 0.43 s^{-1} at 750°C and 0.18 s^{-1} at 650°C. Kersten et al. (2006) concluded that in a quartz reactor at 600°C a 1 wt % to 20 wt % glucose solution reached maximum glucose conversion at 40 sec residence time, and conversion was not dependant on feedstock concentration. In the single tube microchannel reactor the conversion of glucose was 100% at all residence times tested for the 254 µm and 508 µm diameter tubing. Although a rate constant was

not derived, this represents a significant enhancement in reaction kinetics compared to tubular reactors.

One reason for the kinetic enhancement in the microchannel reactor was the high heat flux, which is a result of an increased convective heat transfer coefficient that decreases with channel size (Lee et al. 2005). The higher heat flux decomposed the glucose faster leading to shorter residence times needed to reach 100 % glucose conversion.

Heat transfer in microchannels has been studied in a number of investigations for both liquids and gases in various geometries. Wu and Little (1983) measured Nusselt numbers higher than conventional correlations predicted for gasses in laminar and turbulent flow in rectangular microchannels. Choi et al. (1991) measured Nusselt numbers of nitrogen gas in microtubes. They observed that experimentally determined Nusselt numbers were higher than predicted by conventional correlations for turbulent flow, and Nusselt numbers exhibited a Reynolds number dependence for laminar flow. Lee et al. (2005) studied the heat transfer of water through rectangular microchannels for laminar flow and concluded that disagreement in boundary and inlet conditions between experimental results and conventional correlations rendered the correlations inaccurate. Lelea et al. (2004) studied heat transfer of water in stainless steel microtubes. They concluded that in laminar flow the classic correlations are applicable for heat transfer predictions. Heat transfer in micro geometries has been studied extensively for various flow regimes; however, there is a wide discrepancy between

published results. One general trend that emerges is measured Nusselt numbers and heat transfer coefficients higher than predicted values from classic correlations. A heat transfer study based on laminar flow of supercritical water in a rectangular microchannel is needed to determine if classic correlations are able to predict accurate Nusselt numbers.

Due to discrepancies in the literature about heat transfer correlations that accurately predict Nusselt numbers for laminar flow of supercritical fluids in microchannel geometries, conventional heat transfer correlations were used to analyze the serpentine and single tube microchannel reactors. A relationship between tube diameter and average convective heat transfer coefficient was derived from an average Nusselt number. Convective heat transfer coefficients of microreactors employed in the current study were compared to flow reactors used in the literature.

Convective heat transfer correlations for internal flow based on a constant surface temperature are presented in Table 5.2. Water was used to approximate the properties of the working fluid. Properties of water at reactor temperatures and 250 bar are presented in Table 5.3. Due to the rectangular geometry of the serpentine microchannel reactor, its hydraulic diameter was used

$$D_h = \frac{4\,A}{U_p} = \frac{4\,H\,W}{2\,(H+W)} \tag{5.2}$$

where A is the cross sectional area, U_p is the wetted perimeter, H is the height of the channel, and W is the width of the channel. Flow through the microchannel reactor was determined to be laminar at all conditions tested. The Reynolds number is

$$\mathrm{Re} = \frac{U\ D}{\nu} \tag{5.3}$$

where U is the velocity of the fluid, and ν is the kinematic viscosity of the fluid. Reynolds numbers ranged from 7 to 1500 in the serpentine and single tube microchannel reactors. In Laminar flow, the Renyolds number is less than 2100. The Graetz number, used to characterize laminar flow in a conduit, was determined to range from 0.001 – 0.4 for the single tube and serpentine microchannel reactors. Renyolds and Graetz numbers for the single tube and serpentine microchannel reactors are presented in Table 5.4. They were based on experimental runs at the fastest residence times tested.

Due to low Graetz numbers and Prandtl numbers less than 1 in the serpentine and single tube microchannel reactors, a Nusselt number of 3.66 down the length of the reactor was used to determine the relationship between the convective heat transfer coefficient and tubing diameter.

$$Nu = 3.66 \tag{5.4}$$

An average Nusselt number of 3.66 assumes fully devolved laminar flow, a uniform surface temperature, and a Prandlt number greater than 0.6. The Prandtl number is

$$\mathrm{Pr} = \frac{C_p\ \mu}{k} \tag{5.5}$$

where C_p is the heat capacity, μ is the dynamic viscosity, and k is the thermal conductivity of the fluid. Prandlt numbers for water at reactor temperatures and 250 bar are presented in Table 5.4. The Nusselt number is

$$Nu = \frac{h\,D}{k} \tag{5.6}$$

where h is the convective heat transfer coefficient. Nusselt numbers based on the appropriate correlation, and convective heat transfer coefficients for the single tube and serpentine microchannel reactors are presented in Table 5.4, and were based on experimental runs at the fastest residence time tested. A relationship between tube diameter and the convective heat transfer coefficient can be arrived at by substituting Equation 5.6 into Equation 5.4 and solving for h

$$h = \frac{3.66\,k}{D} \tag{5.7}$$

The convective heat transfer coefficient will vary with tubing diameter by

$$h \propto D^{-1} \tag{5.8}$$

The predicted heat transfer coefficient based on water at 750°C and 250 bar as function of tubing diameter is presented in Figure 5.1.

Table 5.2. Convection correlations for flow in a circular tube

Correlation	Conditions
$Nu = 5.21$	Laminar fully developed flow Uniform T_s Pr ≥ 0.6 Rectangular channel (width / height = 6.67)
$Nu = 3.66$	Laminar fully developed flow Uniform T_s Pr ≥ 0.6
$Nu = 3.66 + \dfrac{0.0668\left(\dfrac{D}{L}\right)\mathrm{Re\ Pr}}{1 + 0.04\left[\left(\dfrac{D}{L}\right)\mathrm{Re\ Pr}\right]^{2/3}}$	Laminar flow Pr >> 1 or an unheated starting length Uniform T_s
$Nu = 1.86\left(\dfrac{\mathrm{Re\ Pr}\ D}{L}\right)^{1/3}\left(\dfrac{\mu}{\mu_s}\right)^{0.14}$	$\left(\dfrac{\mathrm{Re\ Pr}\ D}{L}\right)^{1/3}\left(\dfrac{\mu}{\mu_s}\right)^{0.14} \geq 2$ Uniform Ts 0.48 < Pr < 16,700 $0.0044 < \left(\dfrac{\mu}{\mu_s}\right) < 9.75$
$Nu = 0.116\,(\mathrm{Re}^{2/3} - 125)\,\mathrm{Pr}^{1/3}\left[1 + \left(\dfrac{D}{L}\right)^{2/3}\right]\left(\dfrac{\mu}{\mu_s}\right)^{0.14}$	2300 < Re < 10,000

Table 5.3. Properties of water at reactor temperature and 250 bar

Temperature (°C)	Density (kg m^{-3})	Viscosity (Pa s)	Thermal conductivity (W m^{-1} °C^{-1})	Heat Capacity (J kg^{-1} °C^{-1})
650	64.8	$3.64 \cdot 10^{-5}$	0.109	2815
700	60.1	$3.83 \cdot 10^{-5}$	0.115	2726
750	56.2	$4.02 \cdot 10^{-5}$	0.120	2674

*Values estimated from ChemicaLogic SteamTab Companion Version 2.0

Table 5.4. Dimensionless heat transfer and fluid flow numbers based on water at reactor temperature and pressure

	Temperature (°C)	Reactor diameter (m)	Reactor length (m)	Residence time (sec)	Velocity (m sec^{-1})	Renyolds number	Graetz number	Nusselt number	Stanton number	Peclet number	Prandtl number	h (W m^{-2} °C^{-1})
Serpentine Microchannel Reactor	750	1.30E-04	1.0	1.9	0.54	97.66	0.011	3.7	0.042	87.21	0.893	3368
Single Tube Reactor	750	2.54E-04	2.0	0.62	3.2	1145	0.13	3.7	0.0036	1023	0.893	1729
Single Tube Reactor	750	5.08E-04	2.0	1.2	1.7	1184	0.27	3.7	0.0035	1057	0.893	864.6
Lee et al. (2002)	700	6.22E-03	0.67	10	0.067	653.8	5.53	3.7	0.0061	595.8	0.911	67.44
Serpentine Microchannel Reactor	650	1.30E-04	1.0	1.9	0.53	122.4	0.015	3.7	0.032	115.0	0.940	3062
254 Single Tube Reactor	650	2.54E-04	2.0	0.62	3.2	1459	0.17	3.7	0.0027	1371	0.940	1572
508 Single Tube Reactor	650	5.08E-04	2.0	1.2	1.7	1507	0.36	3.7	0.0026	1416	0.940	786.0
Lu et al. (2006)	650	6.00E-03	0.65	9.0	0.072	771.5	6.7	3.7	0.0051	725.0	0.940	66.55
Lu et al. (2006)	650	9.00E-03	0.65	9.0	0.072	1157	15	4.6	0.0042	1087	0.940	55.67
Holgate et al. (1995)	600	1.71E-03	4.71	5.1	0.92	3238	1.2	11	0.0034	3181	1.05	662.4

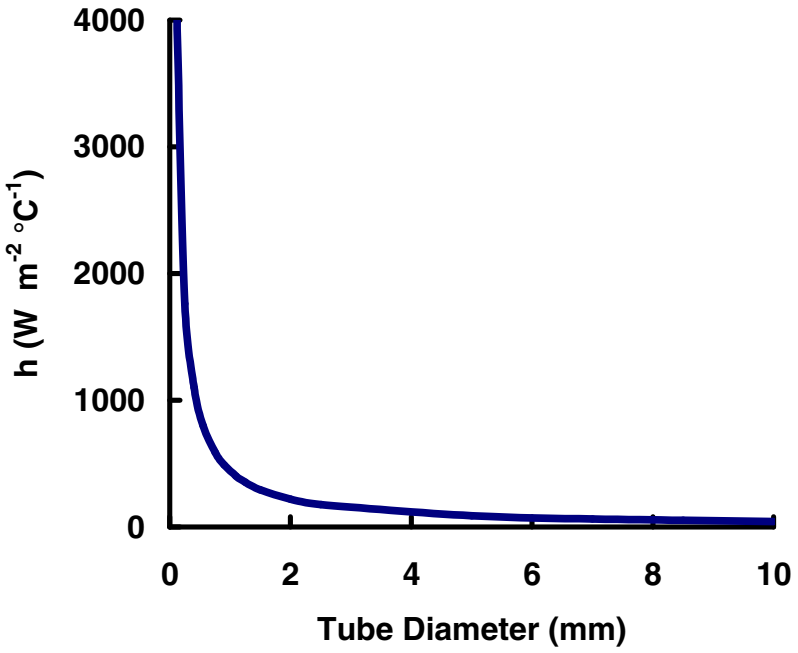

Figure 5.1. Predicted heat transfer coefficient based on water at 750°C, 250 bar, and a 3.0 sec residence time in the serpentine microchannel reactor as a function of tubing diameter

As the tubing diameter decreases the average convective heat transfer coefficient will increase. A higher convective heat transfer coefficient will ultimately lead to an increase in heat flux that will shorten residence times needed to gasify glucose solutions.

Convective heat transfer coefficients were calculated for reactors used by Lee et al. (2002), Lu et al. (2006), and Holgate et al. (1995), and were compared to convective heat transfer coefficients calculated for the single tube and serpentine microchannel reactors. Water, at reactor temperature and 250 bar, was used as the working fluid. A constant surface temperature was assumed. Variables used from the literature were

reactor dimensions, temperature, and residence time, and are presented in Table 5.4. Renyolds numbers and Graetz numbers were calculated for each reactor system, and used to determine the appropriate heat transfer correlation. Reynolds, Graetz, and Nusselt numbers for each reactor system at the fastest residence time tested are presented in Table 5.4. Convective heat transfer coefficients for each reactor system as a function residence time tested is presented in Figure 5.2. The convective heat transfer coefficients are plotted on a log scale.

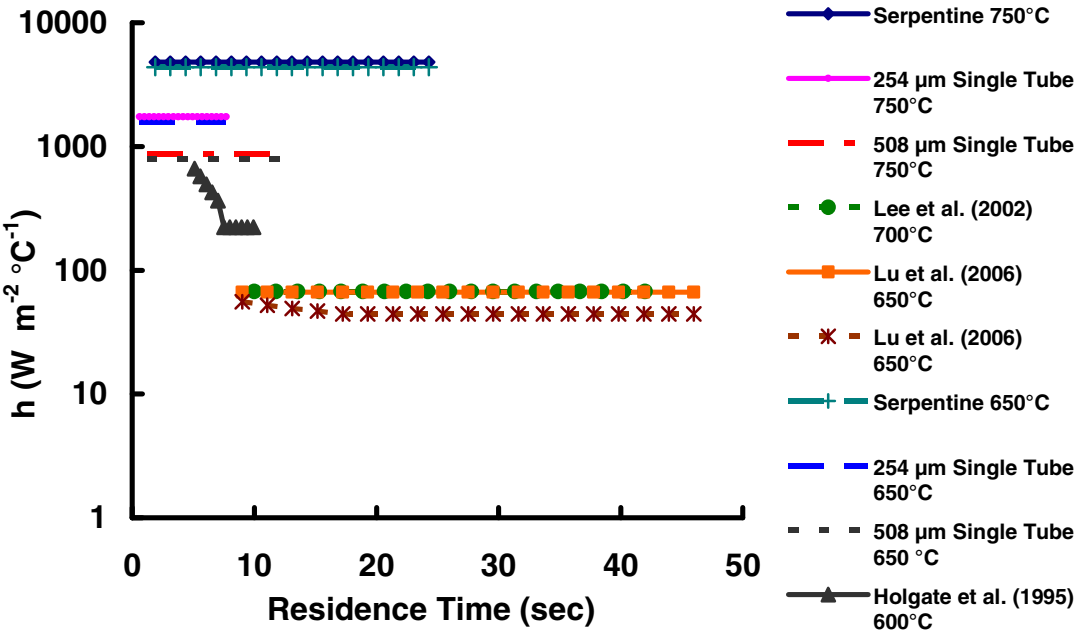

Figure 5.2. Convective heat transfer coefficient as a function of residence times tested for various reactor systems at the reactor temperature and 250 bar

The single tube and serpentine microchannel reactors at 650°C and 750°C represent a significant enhancement of the convective heat transfer coefficient compared to conventional flow reactors used by Lee et al. (2002) and Lu et al. (2006). The serpentine microchannel reactor at 650°C compared to the 9 mm inner diameter reactor used by Lu et al (2006) at 650°C, represented a 55 fold increase in the

convective heat transfer coefficient at the fastest residence times tested. An increase in the heat flux in the microchannel reactors, due to an enhanced convective heat transfer coefficient, shortened residence times necessary to completely gasify glucose in supercritical water.

Minimization of organic acids in the liquid products increases gasification efficiency and hydrogen yield. No organic acids were detected in the liquid effluent at 750°C, 250 bar, and residence times greater than 3.0 sec in the serpentine microchannel reactor; residence times greater than 1.8 sec in the 508 μm single tube reactor; and residence times greater than 0.8 sec in the 254 μm single tube reactor. A small amount of acetic acid was detected at shorter residence times. However, the concentration of acetic acid was minor and did not affect gas production or hydrogen yield. Concentration of acetic acid as a function of residence time at 750°C for all three reactors is presented in Figures 4.6 and 4.14A. The pH of the liquid effluent reached maximum values ranging from 4.1 to 4.3 for all three reactors. The feed pH ranged from 5.5 to 5.8. pH as a function of residence time for all three reactors are presented in Figures 4.5 and 4.12. The decrease in pH at low residence times was due to acetic acid present in the liquid. Absence of organic acids in the liquid products ensures greater gasification efficiencies and hydrogen yields from the decomposition of glucose.

Reaction Pathway

The reaction pathway proposed in the introduction has been validated from experimental data and equilibrium calculations. The reaction pathway is presented in Figure 1.1. Experimental data suggest that glucose was decomposed through acid intermediates rather than reformed by supercritical water.

The high temperature pathway in the reaction schematic, Equation 1.1, is a result of glucose reforming. An equilibrium calculation based on the minimization of Gibbs energy for the gasification of a 0.1 M glucose solution to H_2, CO, CO_2, and CH_4 is presented in Figures 4.15A and 4.15B. At 650°C equilibrium calculations predict 66.3 % H_2, 33.1 % CO_2, 0.4 % CO and 0.2% CH_4. The equilibrium calculations provide evidence that the reforming of glucose is thermodynamically favored at temperatures above 600°C due to the significant presence of H_2 and CO_2 in the gas products.

Organic acids identified in the liquid effluent were intermediates for the decomposition of glucose, and were further gasified as a function of residence time and temperature. The organic acids identified in the liquid were acetic acid, butyric acid, propenoic acid, and acetaldehyde. Chromatograms for the acid analysis are presented in Figures 4.3A and 4.3B. The chromatograms that correspond to experiments run at 650°C contain unidentified peaks that may reveal other acid intermediates, but were not identified. Organic acids quantified were acetic acid, butyric acid, and acetaldehyde. The concentrations of the acids in the liquid products are presented in Figures 4.14A – 4.14C. The concentration of the acids decreased as a

function of increasing residence time at 650°C, suggesting that the acid intermediates were being gasified at longer residence times. pH of the liquid products as a function residence time for experiments run at 650°C is presented in Figure 4.12. The pH of the liquid products increases as residence time increases, supporting the claim that the organic acids were being further gasified. At 750°C and residence times less than 3.0 sec there were small amounts of acetic acid present in the liquid products, indicating that the reaction was still proceeding through acid intermediates. However at residence times greater than 3.0 sec no organic acids were detected and were thought to be completely gasified. The absence of organic acids at 750°C, and the decrease of organic acids as a function of increasing residence time at 650°C suggest that further decomposition of organic acids to gas was temperature and residence time dependent.

Acetic acid had the highest concentration of any acid quantified, and was the major intermediate for the decomposition of glucose at the conditions tested. Assuming glucose was completely decomposed through an acetic acid intermediate the reaction at 650°C would be

$$C_6H_{12}O_6(s) \rightarrow 3\,C_2H_4O_2(g) + 2\,H_2O(g) \rightarrow 3.5\,CO_2(g) + 1.5\,CH_4(g) + 5\,H_2(g) + 1\,CO(g) \quad (5.9)$$

where 1 mole of glucose decomposes to 3 moles of acetic acid that further reacts with 2 moles of water to produce gas comprised of 45.4 % H_2, 31.8 % CO_2, 13.6 % CH_4, and 9.1 % CO. The decomposition of glucose through an acetic acid intermediate at 750°C would be

$$C_6H_{12}O_6(s) \rightarrow 3\,C_2H_4O_2(g) + 3\,H_2O(g) \rightarrow 4.5\,CO_2(g) + 1.5\,CH_4(g) + 6\,H_2(g)$$

(5.10)

where 1 mole of glucose decomposes to 3 moles of acetic acid that is further gasified to gas composed of 50 % H_2, 37 % CO_2, and 12.5 % CH_4. Heats of reaction for Equations 5.10, 5.11, and 1.1 are presented in Table 5.5. Thermodynamic data used to calculate the heat of reaction is presented in Table 4.3. The decomposition of glucose through acetic acid at 750°C theoretically yields 6 moles of hydrogen per mole of glucose fed. Experimental hydrogen yields for the serpentine microchannel reactor at 750°C are in close agreement with the predicted yield and range from 5.4 to 6.3 moles of H_2 per mole of glucose fed. Theoretical gas compositions based on the stoichiometry of Equations 5.10 and 5.11 were compared to observed gas compositions. Calculated equilibrium gas compositions and are presented in Figures 5.2 and 5.3. Equilibrium gas compositions were based on the minimization of Gibbs energy for the decomposition of a 0.1 M solution of glucose at 250 bar, 650°C and 750°C to produce H_2, CO_2, CO, and CH_4.

Table 5.5. Heats of reaction for the glucose reforming and glucose decomposition reactions

Reaction (equation)	$\Delta h_{rxn,298}$ (kJ mol^{-1})	$\Delta h_{rxn,650}$ (kJ mol^{-1})	$\Delta h_{rxn,750}$ (kJ mol^{-1})
1.1	346.8	380.9	386.1
5.10	140.5	148.7	147.6
5.11	99.37	122.7	126.4

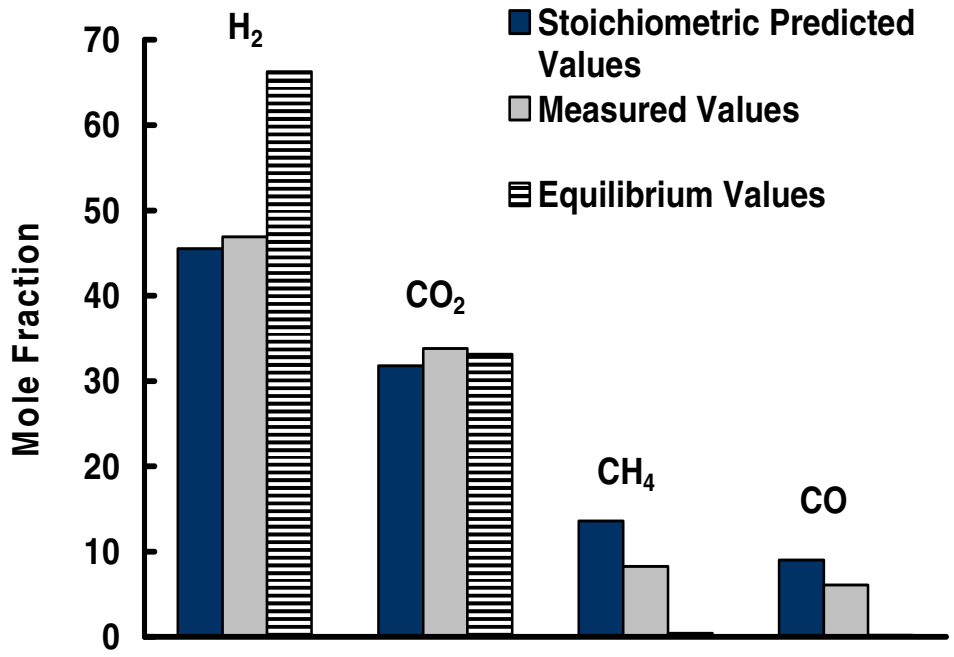

Figure 5.3. Stoichiometric predicted gas compositions from the decomposition of glucose through an acetic acid intermediate compared to equilibrium values for the decomposition of glucose obtained from the minimization of Gibbs energy at 650°C and 250 bar and measured values obtained in the serpentine microchannel reactor at 650°C, 250 bar, and a 2.8 sec residence time

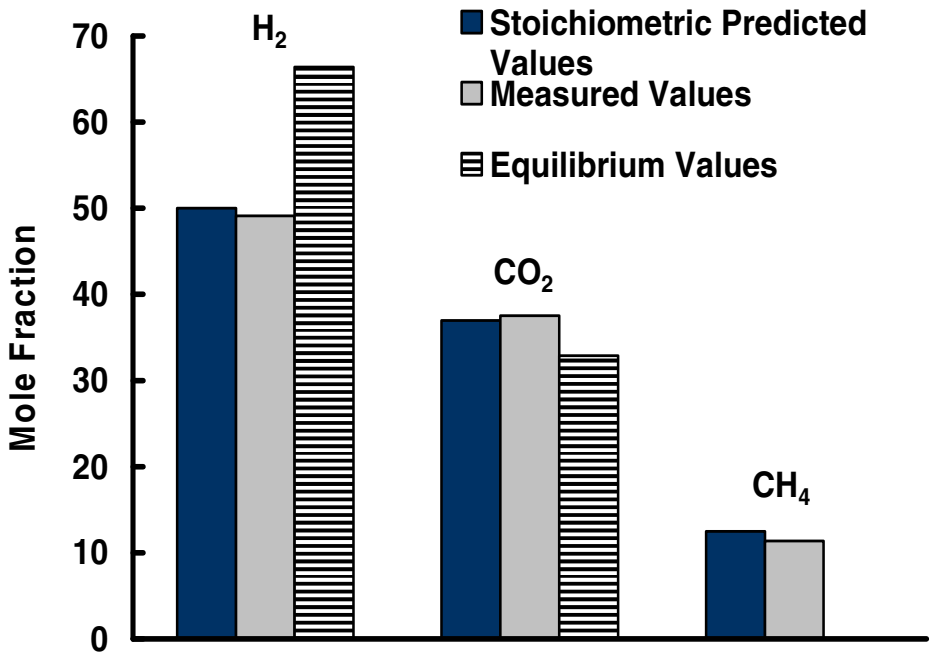

Figure 5.4. Stoichiometric predicted gas compositions from the decomposition of glucose through an acetic acid intermediate compared to equilibrium values for the decomposition of glucose obtained from the minimization of Gibbs energy at 750°C and 250 bar and measured values obtained in the serpentine microchannel reactor at 750°C, 250 bar, and a 24.3 sec residence time

At 650°C and 750°C the observed gas compositions are more comparable to the stoichiometric predicted gas compositions than the equilibrium values. The stoichiometric predicted values at 750°C are similar to the observed values. However the stoichiometric predicted composition for the decomposition of glucose at 650°C is slightly different than the observed composition. One possible explanation for this is organic acids in the liquid products that could affect the gas composition when further gasified. Another possible explanation is competing pathways that glucose is being decomposed through that become thermodynamically favored at lower temperatures. The competing pathways would produce several organic acids that when further reacted would change gas composition. A major intermediate for the decomposition of

glucose is acetic acid, which when reacted with water predicts gas compositions and H_2 yields similar to experimentally determined values.

Predicted gas production rates from reaction stoichiometry as a function of feed rate are compared to measured gas production rates, and are presented in Figures 4.1 and 4.9. Predicted gas production rates are based on the decomposition of glucose through an acetic acid intermediate and glucose reforming. Gas production rates predicted based on overall reaction stoichiometry assume complete glucose conversion to gas at 750°C and 650°C. The volume of gas per mole of glucose reacted was calculated using the ideal gas law at 25°C and 1.0 atm. Measured gas production rates are in good agreement with predicted gas production rates based on the decomposition of glucose at 650°C and 750°C for the single tube and serpentine microchannel reactors.

Previous work supports the hypothesis that glucose is decomposed through acid intermediates as precursors of the gaseous compounds. Holgate et al. (1995) studied the gasification of glucose in supercritical water and identified major acid intermediates including acetic acid, acetaldehyde, and propenoic acid. They also identified furfural, 5-methylfurfural, and 5-hydroxymethylfurfural in the liquid products. Dinjus and Kruse (2004) suggest that glucose is decomposed to furfurals and acids in parallel when gasified in supercritical water. The furfurals further react to acids and phenols in parallel. The phenols react to form acids, which are further reacted to gas products. A simple reaction pathway proposed by Dinjus Kruse (2004) is presented in Figure 5.4.

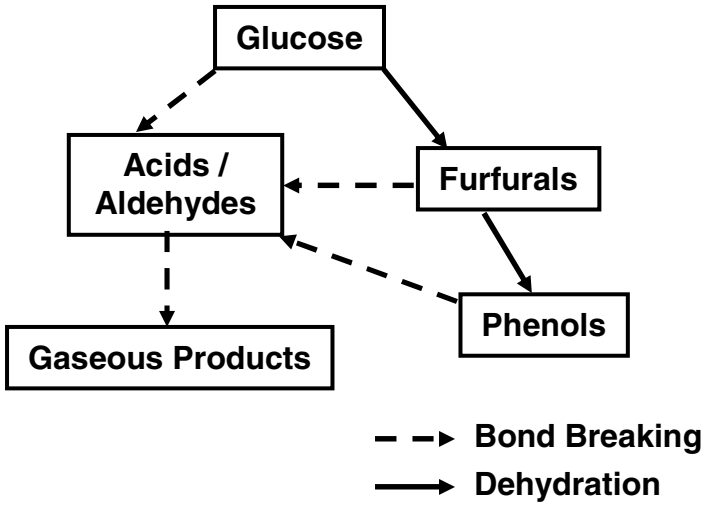

Figure 5.5. Reaction pathway for the decomposition of glucose proposed by Dinjus and Kruse (2004)

The liquid products produced in the serpentine microchannel reactor contained some of the same acids reported by Holgate et al. (1995), however no furfurals or phenols were observed in the liquid products of the microchannel reactors. The absence of furfurals and phenols in the liquid products can be attributed to the high heat flux microchannel reactor. Lu et al. (2006) concluded that furfural and phenol formation was favored at ionic conditions, ($T < 374°C$), and led to reactor fouling. Acid formation was favored at free radical conditions ($T > 374°C$). The high heat flux in the microchannel reactor minimizes the time necessary for the reactants to reach temperatures greater than 374°C. When higher concentrations of glucose solutions, greater than 0.4 M, were reacted in the microchannel reactor the liquid products had a yellow hue and eventually plugged indicating possible furfural and phenol formation. Organic acid intermediate formation from the decomposition of glucose in supercritical water was confirmed by previous work.

The presence of CH_4 in the gas products at all conditions tested supports the conclusion that glucose was being decomposed through acid intermediates. The equilibrium calculation for the decomposition of glucose at 650°C and 750°C contains no CH_4 in the product gas, and is representative of the high temperature or reforming pathway. Acetic acid, thought to be the major acid intermediate, was gasified at 600°C 345 bar and a 34 sec residence time by Yu et al. (1993) in Inconel and Hastelloy tubular reactors. The resulting gas products contained 35 % to 45 % CH_4 indicating that it is a direct product of the gasification of acetic acid. Lu et al. (2006) suggest that CH_4 was mainly formed by free radical reactions as glucose is decomposed to gas through acid intermediates.

Conclusion

A 0.1 M solution of glucose was gasified in supercritical water within a microchannel reactor at 750°C and 250 bar to yield H_2 rich gas with a low concentration of CO. In the serpentine microchannel reactor hydrogen yields averaged 5.7 ± 0.29 and peaked at 6.3 moles of H_2 produced per mole of glucose fed. Typical gas compositions at 750°C and 250 bar were 52.5 % H_2, 35.0 % CO_2, 12.1 % CH_4, and 0.4 % CO. Gas composition and H_2 yield were not dependent on residence time, indicating that the gas products were moving toward equilibrium. Processing times for the decomposition of glucose were decreased compared to values reported in the literature. Decreased processing times for complete glucose conversion were due to an increased heat flux resulting from the microchannel reactor geometry. Complete glucose conversion was

obtained in less than a 1.0 sec residence time, and minimal organic acids were detected in the liquid products. Glucose was determined to be decomposed rather than reformed at 750°C and 250 bar in the serpentine microchannel reactor. Acetic acid was the major intermediate in the reaction pathway. Stoichiometric hydrogen yield and gas composition from decomposition of glucose through an acetic acid intermediate was similar to measured hydrogen yields and gas compositions. Acetic acid present in the liquid products and CH_4 present in the gas products confirms that glucose was decomposed to organic acids that were further gasified to H_2, CO_2, CH_4, and CO.

Bibliography

Antal, J.A.J., Allen, S.G., Schulman, D., Xu, X. (2000). Biomass Gasification in Supercritical Water. Ind. Eng. Chem. Res., 39:4040-4053.

Berg, J.M., Tymoczko J.L., Stryer, L. (2002). Biochemistry. New York, W.H. Freeman and Co.

Choi, S.B., Barron, R.F., Warrington, R.O. (1991). Fluid Flow and Heat Transfer in Microtubes. Micromechanical Sensors, Actuators, and Systems, 32:123-134.

Cortright, R.D., Davda, R.R., Dumesic, J.A. (2002). Hydrogen from Catalytic Reforming of Biomass-Derived Hydrocarbons in Liquid Water. Nature, 418:964-967.

Dinjus, E., Kruse A. (2004) Hot Compressed Water-A Suitable and Sustainable Solvent and Reaction Medium. J. Phys.: Condens. Matter, 16: S1161-S1169.

Divilio, R.J. (1998). Modeling of Biomass to Hydrogen Via the Supercritical Water Pyrolysis Process. Proceedings from the 1998 DOE Hydrogen Program Review.

Divilio, R.J. (1999). Modeling of the Supercritical Water Pyrolysis Process. Proceedings from the 1999 DOE Hydrogen Program Review.

Ehara, K., Saka, S. (2002). A Comparative Study on Chemical Conversion of Cellulose Between the Batch Type and Flow Type Systems in Supercritical Water. Cellulose, 9:301-311.

Fushimi, C., Araki, K., Yamaguchi, Y., Tsutsumi, A. (2003). Effect of Heating Rate on Steam Gasification of Biomass. 2. Thermogravimetric-Mass Spectrometric (TG-MS) Analysis of Gas Evolution. Ind. Eng. Chem. Res., 42:3929-3936.

Guo, Z.Y., Wu, X.B. (1997). Compressibility effect on the Gas Flow and Heat Transfer in a Microtube. International Journal of Heat and Mass Transfer, 40(13):3251-3254.

Hao, X.H., Guo, L.J., Mao, X., Zhang, X.M., Chen, X.J. (2003). Hydrogen Production From Glucose Used as a Model Compound of Biomass Gasified in Supercritical Water. International Journal of Hydrogen Energy, 28:55-64.

Holgate R.H., Tester, J.W. (1994). Oxidation of Hydrogen and Carbon Monoxide in Sub- and Supercritical Water: Reaction Kinetics, Pathways, and Water Density Effects. 2. Elementary Reaction Modeling. J. Phys. Chem., 98:810-822.

Holgate, R.H., Meyer, J.C., Tester, J.W. (1995). Glucose Hydrolysis and Oxidation in Supercritical Water. AICHE Journal, 41(3):637-647.

Holladay, J., Wang, Y., Jones, E. (2004). Review of Portable Hydrogen Production Using Microreactor Technology. Chem. Rev., 104: 4767-4790.

Huber, G.W., Dumesic, J.A. (2006). An Overview of Aqueous-Phase Catalytic Processes for Production of Hydrogen and Alkanes in a Biorefinery. Catalysis Today, 111:119-132.

Huber, G.W., Shabaker, J.W., Dumesic, J.A. (2003) Raney Ni-Sn Catalyst for H_2 Production from Biomass-Derived Hydrocarbons. Science, 300:2075-2077.

Jensen, K.F. (2005) Silicon-Based Microreactors. Microreactor Technology and Process Intensification. Washington D.C., American Chemical Society, 2, 2-22.

Johanson, N.W., Spritzer, M.H., Hong, G.T., Rickman, W.S. (2001). Supercritical Water Partial Oxidation. Proceedings from the 2001 DOE Hydrogen Program Review.

Kersten, S. R. A., Potic, B., Prins, W., Van Swaaij, W.P.M. (2006). Gasification of Model Compounds and Wood in Hot Compressed Water. Ind. Eng. Chem. Res., 45: 4169-4177.

King, D.L., Brooks, K., Fischer, C., Pederson, L., Rawlings, G., Stenkamp, V.S., TeGrotenhuis, W., Wegeng, R., Whyatt, G. (2005) Fuel Reformation: Catalyst Requirements in Microchannel Architectures. Microreactor Technology and Process Intensification. Washington D.C., American Chemical Society, 7, 119-128.

Koretsky, M. (2004). Engineering and Chemical Thermodynamics. Hoboken, NJ, John Wiley & Sons.

Lee, I.G., Kim, M.S. Ihm, S.K., (2002). Gasification of Glucose in Supercritical Water. Ind. Eng. Chem. Res., 41:1182-1188.

Lee, P.S., GarimellaS.V., Liu, D. (2005). Investigation of Heat Transfer in Rectangular Microchannels. International Journal of Heat and Mass Transfer, 48:1688-1704.

Lelea, D., Nishio, S., Takano, K. (2004). The Experimental Research on Microtube Heat Transfer and Fluid Flow of Distilled Water. International Journal of Heat and Mass Transfer, 47:2817-2830.

Lu, Y.J., Guo, L.J., Ji, C.M., Zhang, X.M., Hao, X.H., Yan, Q.H. (2006). Hydrogen Production by Biomass Gasification in Supercritical Water: A Parametric Study. International Journal of Hydrogen Energy, 31:822-831.

McKendry, P. (2002). Energy Production from Biomass (Part 1): Overview of Biomass. Bioresource Technology, 83:37-46.

McKendry, P. (2002). Energy Production from Biomass (Part 2): Conversion Technologies. Bioresource Technology, 83:47-54.

McKendry, P. (2002). Energy Production from Biomass (Part 1): Gasification Technologies. Bioresource Technology, 83:55-63.

Milne, T.A., Elam, E.E., Evans, R.J. (2003). Hydrogen from Biomass: State of the Art Research and Challenges. A Report for the International Energy Agency Agreement on the Production and Utilization of HydrogenTask 16, Hydrogen From Carbon Containing Materials.

Norton, D.G., Deshmukh, S.R., Wetzel, E.D., Vlachos, D.G. (2005) Downsizing Chemical Processes for Portable Hydrogen Production. Microreactor Technology and Process Intensification. Washington D.C., American Chemical Society, 11, 179-193.

Penninger, J.M.L., Rep, M. (2005). Hydrogen Rich Fuel Gas From Wet Biomass by Gasification in Supercritical Water. Proceedings from International Hydrogen Energy Congress and Exhibition, 13-15.

Picha, D., H. (1985). Organic Acid Determination in Sweet Potatoes by HPLC. J. Agric. Food Chem, 33:743-745.

Potic, B., Kersten, S.R.A., Ye, M., van der Hoef, M.A., Kuipers, J.A.M., van Swaaij, W.P.M. (2005). Fluidization with Hot Compressed Water in Micro-Reactors. Chemical Engineering Science, 60:5982-5990.

Sabry, M.N. (2000). Scale Effects on Fluid Flow and Heat Transfer in Microchannels. IEEE Transactions on Components and Packaging Technologies, 23(3):562-567.

Shah, K., Ouyang, X., Besser, R.S. (2005) Microreaction for Microfuel Processing: Challenges and Prospects. Chem. Eng. Technol., 28:303-313.

Sutton, D., Kelleher, B., Doyle, A., Ross, J.R.H. (2001). Investigation of Nickel Supported Catalyst for the Upgrading of Brown Peat Derived Gasification Products. Bioresource Technology, 80:111-116.

Tang, H., Kitagawa, K. (2005). Supercritical Water Gasification of Biomass: Thermodynamic Analysis with Direct Gibbs Free Energy Minimization. Chemical Engineering Journal, 106:261-267.

Wang, Y., Holladay, J. D. (2005). Microreactor Technology and Process Intensification. Washington D.C., American Chemical Society.

Watanabe, M., Aizawa, Y., Iida, T., Levy, C., Aida, T.M., Inomata, H. (2005). Glucose Reactions Within the Heating Period and the Effect of Heating Rate on the Reactions in Hot Compressed Water. Carbohydrate Research, 340:1931-1939.

Watanabe, M., Aizawa, Y., Iida, T., Nishimura, R., Inomata, H. (2005). Catalytic Glucose and Fructose Conversions with TiO_2 and ZrO_2 in Water at 473 K: Relationship Between Reactivity and Acid-Base Property Determined by TPD Measurement. Applied Catalysis, 295:150-156.

Williams, P., T., Onwudili, J. (2005). Composition of Products From the Supercritical Water Gasification of Glucose: A Model Biomass Compound. Ind. Eng. Chem. Res., 44:8739-8749.

Williams, P.T., Onwudili, J. (2006). Subcritical and Supercritical Water Gasification of Cellulose, Starch, Glucose, and Biomass Waste. Energy and Fuels, 20:1259-1265.

Wu, P., Little, W.A. (1983). Measurement of Friction Factors for the Flow of Gassesin Very Fine Channels Used for Microminiature Refrigerators. Cryogenics, 24: 273-277.

Xu, X., Matsumura, Y., Stenberg, J., Antal, J.A.J. (1996). Carbon-Catalyzed Gasification of Organic Feedstocks in Supercritical Water. Ind. Eng. Chem. Res., 35:2522-2530.

Yoshida, T., Oshima, Y. (2004). Partial Oxidative and Catalytic Biomass Gasification in Supercritical Water: A Promising Flow Reactor System. Ind. Eng. Chem. Res., 43:4097-4104.

Yu, D., Aihara M., Antal, J.A.J. (1993). Hydrogen Production by Steam Reforming Glucose in Supercritical Water. Energy and Fuels, 7: 574-577.

Zeppa, G., Conterno, L., Gerbi, V. (2001). Determination of Organic Acids, Sugars, Diacetyl and Acetonin in Cheese by High Performance Liquid Chromatography. J. Agric. Food Chem, 49:2722-2726.

Appendix A. Experimental Data

Table A1. Reactor effluent gas composition for experiments in the single tube and the serpentine microchannel reactors at 250 bar, 0.1 M glucose, 650°C and 750°C

Flow Rate in (ml/min)	Temperature (°C)	Reactor	Residence Time (sec)	H_2 Mole Fraction	stdev	CO_2 Mole Fraction	stdev	CO Mole Fraction	stdev	CH_4 Mole Fraction	stdev
0.10	750	Microchannel	24.3	49.1%	0.8%	37.5%	0.6%	0.4%	0.0%	11.4%	0.1%
0.20	750	Microchannel	12.2	54.2%	0.9%	32.5%	0.4%	0.5%	0.0%	10.6%	0.1%
0.30	750	Microchannel	8.1	52.6%	0.3%	35.6%	0.1%	0.5%	0.0%	9.5%	0.1%
0.40	750	Microchannel	6.1	51.8%	0.1%	34.5%	0.2%	0.4%	0.0%	10.9%	0.1%
0.50	750	Microchannel	4.9	52.8%	1.2%	33.7%	0.2%	0.5%	0.0%	11.1%	0.0%
0.60	750	Microchannel	4.1	54.3%	0.4%	33.3%	0.3%	0.5%	0.0%	9.1%	0.1%
0.80	750	Microchannel	3.0	52.8%	0.5%	35.5%	0.4%	0.5%	0.0%	8.7%	0.1%
1.00	750	Microchannel	2.4	52.4%	0.1%	35.7%	0.1%	0.8%	0.0%	10.8%	0.1%
0.10	750	Single Tube ; 508 µm	12.3	50.2%	1.3%	35.2%	0.3%	0.4%	0.0%	12.5%	0.1%
0.14	750	Single Tube ; 508 µm	8.8	51.5%	1.4%	34.0%	0.3%	0.4%	0.0%	13.5%	0.1%
0.20	750	Single Tube ; 508 µm	6.2	53.0%	0.1%	31.7%	0.5%	0.5%	0.0%	13.0%	0.2%
0.30	750	Single Tube ; 508 µm	4.1	50.4%	0.1%	34.2%	0.4%	0.4%	0.0%	12.6%	0.1%
0.40	750	Single Tube ; 508 µm	3.1	51.3%	0.4%	36.3%	0.3%	0.4%	0.0%	10.3%	0.0%
0.70	750	Single Tube ; 508 µm	1.8	52.5%	0.1%	34.1%	0.4%	0.8%	0.0%	10.5%	0.1%
0.80	750	Single Tube ; 508 µm	1.5	51.9%	0.2%	34.1%	0.5%	1.1%	0.0%	11.5%	0.1%
1.00	750	Single Tube ; 508 µm	1.2	50.3%	0.2%	34.9%	0.9%	1.8%	0.0%	11.7%	0.2%
0.04	750	Single Tube ; 254 µm	7.7	51.2%	1.1%	33.4%	1.0%	0.8%	0.0%	12.0%	0.2%
0.05	750	Single Tube ; 254 µm	6.2	50.5%	1.0%	32.4%	0.5%	1.0%	0.0%	11.1%	0.2%
0.06	750	Single Tube ; 254 µm	5.1	49.8%	0.3%	37.6%	0.7%	0.4%	0.0%	12.2%	0.2%
0.10	750	Single Tube ; 254 µm	3.1	49.0%	0.6%	36.5%	0.5%	0.4%	0.0%	12.3%	0.2%
0.20	750	Single Tube ; 254 µm	1.5	49.5%	0.8%	36.1%	0.4%	1.2%	0.0%	11.5%	0.1%
0.30	750	Single Tube ; 254 µm	1.0	50.7%	0.4%	34.9%	0.2%	3.0%	0.0%	10.6%	0.0%
0.40	750	Single Tube ; 254 µm	0.8	50.3%	1.5%	33.1%	0.5%	3.0%	0.0%	10.8%	0.2%
0.50	750	Single Tube ; 254 µm	0.6	50.6%	0.2%	36.0%	0.3%	1.8%	0.0%	10.4%	0.1%
0.20	650	Microchannel	14.0	50.3%	0.5%	34.5%	1.1%	3.0%	0.1%	9.5%	0.2%

0.30	650	Microchannel	9.3	44.0%	0.9%	40.5%	0.5%	6.5%	0.2%	9.8%	0.3%
0.40	650	Microchannel	7.0	50.0%	0.8%	36.1%	0.2%	5.0%	0.0%	6.9%	0.0%
0.60	650	Microchannel	4.7	49.2%	0.7%	32.5%	0.4%	8.3%	0.1%	6.8%	0.1%
0.70	650	Microchannel	4.0	44.2%	0.2%	34.7%	0.3%	10.5%	0.1%	7.4%	0.1%
0.80	650	Microchannel	3.5	49.8%	0.9%	36.9%	0.9%	8.6%	0.1%	7.5%	0.1%
1.00	650	Microchannel	2.8	46.9%	0.3%	33.8%	0.3%	6.1%	0.1%	8.3%	0.1%
1.50	650	Microchannel	1.9	46.4%	1.0%	31.6%	1.2%	11.7%	0.6%	6.0%	0.3%

Table A2. Gas flow rate, hydrogen yield and, percent recovered carbon for experiments in the single tube and the serpentine microchannel reactors at 250 bar, 0.1 M glucose, 650°C and 750°C

Flow Rate in (ml/min)	Temperature (°C)	Reactor	Residence Time (sec)	YH_2 (mol of H2 formed per mol of glucose reacted)	Total Gas Flow (ml/hr)	Recovered Carbon in Gas
0.10	750	Microchannel	24.3	3.8	113.6	64%
0.20	750	Microchannel	12.2	5.6	302.6	75%
0.30	750	Microchannel	8.1	5.7	479.2	83%
0.40	750	Microchannel	6.1	5.4	605.8	79%
0.50	750	Microchannel	4.9	5.7	792.9	82%
0.60	750	Microchannel	4.1	6.3	1022.9	83%
0.80	750	Microchannel	3.0	5.8	1278.6	81%
1.00	750	Microchannel	2.4	5.7	1592.0	86%
0.10	750	Single Tube ; 508 µm	12.3	3.9	114.4	63%
0.14	750	Single Tube ; 508 µm	8.8	4.3	169.8	66%
0.20	750	Single Tube ; 508 µm	6.2	4.8	265.4	68%
0.30	750	Single Tube ; 508 µm	4.1	4.9	426.1	76%
0.40	750	Single Tube ; 508 µm	3.1	5.5	623.4	83%
0.70	750	Single Tube ; 508 µm	1.8	5.8	1134.8	84%
0.80	750	Single Tube ; 508 µm	1.5	5.5	1249.5	83%
1.00	750	Single Tube ; 508 µm	1.2	5.4	1582.0	87%
0.04	750	Single Tube ; 254 µm	7.7	3.8	43.2	57%
0.05	750	Single Tube ; 254 µm	6.2	4.0	57.5	58%
0.06	750	Single Tube ; 254 µm	5.1	3.8	66.9	64%
0.10	750	Single Tube ; 254 µm	3.1	4.1	121.6	68%
0.20	750	Single Tube ; 254 µm	1.5	4.7	279.5	78%
0.30	750	Single Tube ; 254 µm	1.0	4.8	414.5	76%
0.40	750	Single Tube ; 254 µm	0.8	5.1	599.2	80%
0.50	750	Single Tube ; 254 µm	0.6	5.2	757.5	83%
0.20	650	Microchannel	14.0	3.2	186.3	50%
0.30	650	Microchannel	9.3	2.6	254.7	55%

0.40	650	Microchannel	7.0	2.8	325.8	44%
0.60	650	Microchannel	4.7	2.5	442.2	40%
0.70	650	Microchannel	4.0	2.1	482.8	41%
0.80	650	Microchannel	3.5	2.9	691.1	52%
1.00	650	Microchannel	2.8	2.6	816.2	45%
1.50	650	Microchannel	1.9	2.0	922.8	34%

Table A 3. Organic acids analysis for experiments in the single tube and the serpentine microchannel reactors at 250 bar, 0.1 M glucose, 650°C and 750°C

Temperature (°C)	Reactor	Residence Time (sec)	Acetic acid (mmol/L)	Propenoic acid (mmol/L)	butyric acid (mmol/L)	Acetaldehyde (mmol/L)
750	Microchannel	24.3	0.0	0.0	0.0	0.0
750	Microchannel	12.2	0.0	0.0	0.0	0.0
750	Microchannel	8.1	0.0	0.0	0.0	0.0
750	Microchannel	6.1	0.0	0.0	0.0	0.0
750	Microchannel	4.9	0.0	0.0	0.0	0.0
750	Microchannel	4.1	0.0	0.0	0.0	0.0
750	Microchannel	3.0	0.0	0.0	0.0	0.0
750	Microchannel	2.4	14.4	0.0	0.0	0.0
650	Single Tube ; 508 µm	1.4	25.0	0.0	26.0	N/T
650	Single Tube ; 508 µm	2.8	35.0	0.0	24.1	N/T
650	Single Tube ; 508 µm	4.7	18.6	0.0	7.1	N/T
650	Single Tube ; 508 µm	7.1	14.8	0.0	0.0	N/T
650	Single Tube ; 508 µm	9.5	10.5	0.0	0.0	N/T
650	Single Tube ; 508 µm	14.2	3.0	0.0	0.0	N/T
650	Single Tube ; 508 µm	20.3	1.2	0.0	0.0	N/T
650	Single Tube ; 508 µm	28.4	0.0	0.0	0.0	N/T
750	Single Tube ; 508 µm	0.8	1.5	0.0	0.0	0.0
750	Single Tube ; 508 µm	1.1	1.3	0.0	0.0	0.0
750	Single Tube ; 508 µm	1.4	0.0	0.0	0.0	0.0
750	Single Tube ; 508 µm	1.8	0.0	0.0	0.0	0.0
750	Single Tube ; 508 µm	2.5	0.0	0.0	0.0	0.0
750	Single Tube ; 508 µm	3.1	0.0	0.0	0.0	0.0
750	Single Tube ; 508 µm	4.9	0.0	0.0	0.0	0.0
750	Single Tube ; 508 µm	8.2	0.0	0.0	0.0	0.0
750	Single Tube ; 508 µm	12.3	0.0	0.0	0.0	0.0
750	Single Tube ; 508 µm	20.5	0.0	0.0	0.0	0.0
750	Single Tube ; 254 µm	0.513	6.4	0.0	0.0	0.0

750	Single Tube ; 254 µm	0.77	0.0	0.0	0.0	0.0
750	Single Tube ; 254 µm	1.03	0.0	0.0	0.0	0.0
750	Single Tube ; 254 µm	1.54	0.0	0.0	0.0	0.0
750	Single Tube ; 254 µm	2.57	0.0	0.0	0.0	0.0
750	Single Tube ; 254 µm	3.85	0.0	0.0	0.0	0.0
750	Single Tube ; 254 µm	7.7	0.0	0.0	0.0	0.0
750	Single Tube ; 254 µm	10.3	0.0	0.0	0.0	0.0
650	Microchannel	1.87	55.3	2.6	22.7	9.8
650	Microchannel	3.5	55.9	1.1	13.2	7.2
650	Microchannel	4	53.9	1.6	16.9	8.9
650	Microchannel	4.67	55.6	1.3	14.5	1.8
650	Microchannel	7.01	45.4	0.0	6.8	0.0
650	Microchannel	9.34	38.9	0.0	2.2	0.0
651	Microchannel	14.0	23.2	0.0	9.0	0.0
652	Microchannel	28.0	3.7	0.0	0.0	0.0

N/T = Not tested

Appendix B. Reactor Block Temperature Modeling

Purpose

To model the temperature distribution of the single tube reactor block to determine if cold spots exist near the edge of the reactor block.

Conduction was the primary mode of heat transfer to the reactor block and is presented in Figure 2.8. Heat was conducted to the top and bottom of the reactor block, which made up 70% of the total surface area of the reactor block. The sides of the reactor block, which make up the remaining 30% of the total surface area, were exposed to air. Radiation was the primary mode of heat transfer to these surfaces. The temperature controller used to determine the reactor temperature was placed 1.2 cm into the side of the reactor block and is presented in Figure B1. The whole reactor was surrounded by 3.5 cm thick insulation to minimize heat loss to the surroundings. A thermocouple was used to measure the temperature at various places in the y-z, and x-z planes. The goal of modeling the temperature distribution in the reactor block was to determine if the sides of the reactor are below the set temperature of the temperature controller.

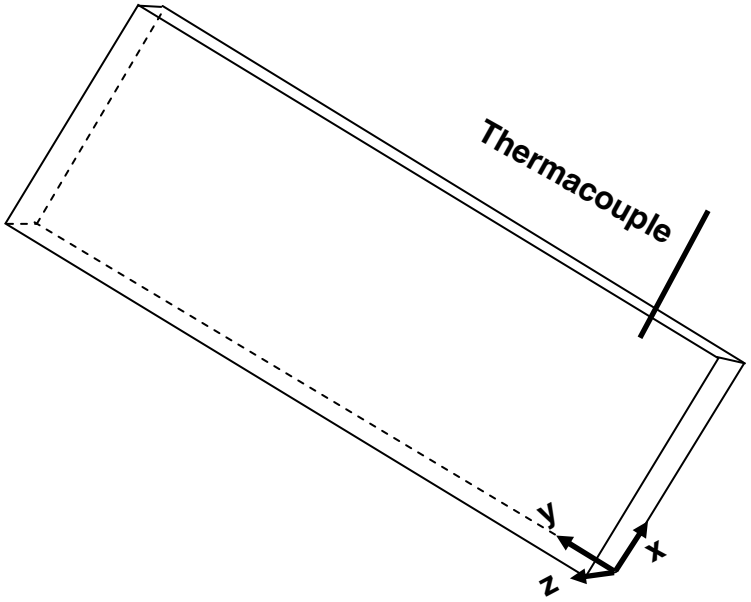

Figure B.1. Reactor block and coordinate system

Assumptions

- Steady state
- Top and bottom of the reactor are at set temperature
- There is no reaction
- There is no heat lost due to flow through the block

Governing Equations

The two dimensional heat equation

$$\frac{\partial^2 T}{\partial x^2} + \frac{\partial^2 T}{\partial y^2} = 0 \tag{B.1}$$

was used to model the temperature distribution across the x-y plane of the reactor block.

The Dirichlet boundary conditions used were as follows

$$T = 745.2°C \quad x = 0 \quad 0 \le y \le 29.4\ cm \quad 0 \le z \le 0.9\ cm \tag{B.2}$$

$$T = 745.2°C \quad x = 7.9\ cm \quad 0 \le y \le 29.4\ cm \quad 0 \le z \le 0.9\ cm \tag{B.3}$$

$$T = 745.2°C \quad y = 0 \quad 0 \le x \le 7.9\ cm \quad 0 \le z \le 0.9\ cm \tag{B.4}$$

$$T = 745.2°C \quad y = 29.4\ cm \quad 0 \le x \le 7.9\ cm \quad 0 \le z \le 0.9\ cm \tag{B.5}$$

$$T = 750.0°C \quad z = 0 \quad 0 \le x \le 7.9\ cm \quad 0 \le y \le 29.4\ cm \tag{B.6}$$

$$T = 750.0°C \quad z = 0.9\ cm \quad 0 \le x \le 7.9\ cm \quad 0 \le y \le 29.4\ cm \tag{B.7}$$

The boundary conditions in equations 1.2-1.5 were measured and the boundary conditions in Equations 1.6-1.7 were assumed to be at the set temperature of the controller.

Results

The results from the Matlab simulations indicate a temperature drop that starts on the boundaries of the x-plane. The temperature increases the farther you go into the x-plane until you hit the set temperature. The results for a set temperature of 750°C is presented in Figure B2. At the x-boundaries the measured temperature of the reactor block was 745.2°C. In the center of the z-plane, where the change in temperature per length in the x-direction is the smallest, the temperature reaches the set point approximately 1.5 centimeters into the reactor block in the x-direction. This affects the first two and last two channels of the reactor block, which will be lower than the set temperature. In conclusion the sides of the reactor block at any given set temperature will be approximately 0.6% lower than the desired set point of the reactor.

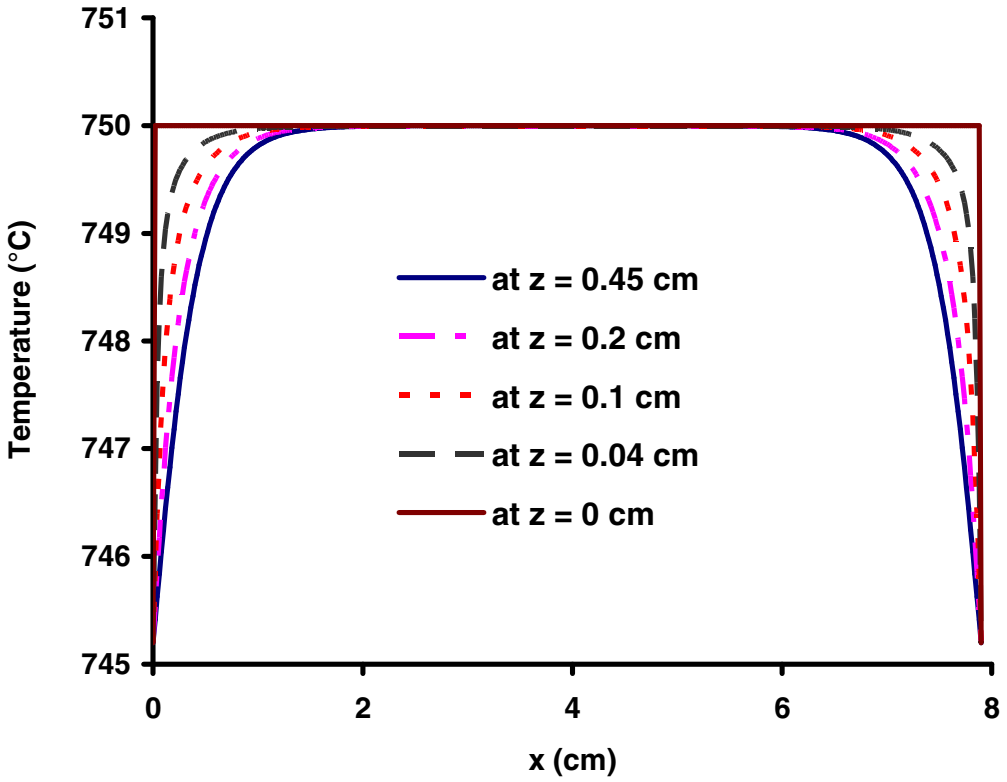

Figure B2. Temperature profiles across the x-plane of the reactor block at various locations in the z-plane

Modeling platform

Matlab was used as the modeling platform. A numerical solution was obtained using the Crank Nicolson difference approximation. The Matlab code used is as follows

```
clc
clear all
%Aaron Goodwin 6/6/2006
h=1/100;
X=7.9;
Y=0.9;
gpx=X/h+1;
gpy=Y/h+1;
U=zeros(gpx,gpy);
x=[0:h:X];
```

```
y=[0:h:Y];
w=4/(2+sqrt(4-(cos(pi/(gpx-1))+cos(pi/(gpy-1)))^2));
% I will now define the boundary conditions
U(1:gpx,1)=750;
U(1:gpx,gpy)=750;
U(1,1:gpy)=745.2;
U(gpx,1:gpy)=745.2;
%I will first write an iteration loop.
for k=1:400;
   Uold=U;
%I will now write a for loop to set up the i and j grid parameters i=x, and
%j=y
   for i=2:gpx-1
      for j=2:gpy-1
         %now I will write a for loop to update both the red and black entries
         if mod(i-j,2)==0
            U(i,j)=Uold(i,j)+w/4*(Uold(i-1,j)+Uold(i+1,j)+Uold(i,j-1)+Uold(i,j+1)-
4*Uold(i,j));
         end
      end
   end
   for i=2:gpx-1
      for j=2:gpy-1
         if mod(i-j,2)==1
            U(i,j)=Uold(i,j)+w/4*(U(i-1,j)+U(i+1,j)+U(i,j-1)+U(i,j+1)-4*Uold(i,j));
         end
      end
   end
    if((max(max(abs(U-Uold))))<0.0001)
            number_iterations=k
            break
    end
end
subplot(2,1,1)
    plot(x,U(:,gpy/2),'-',x,U(:,floor(gpy/4)),':',x,U(:,floor(gpy/6)),'-.',x,U(:,1),'--')
    axis([0 1.4 745 751])
    xlabel('x(cm)'), ylabel('Temp (°C)')
    title('Reactor Block Temperature Profile Based on Measured Boundary Conditions')
    legend('y=0.275','y=0.14','y=0.92', 'y=0')

    subplot(2,1,2)
    plot(x,U(:,gpy/2),'-',x,U(:,floor(gpy/4)),':',x,U(:,floor(gpy/6)),'-.',x,U(:,1),'--')
    axis([0 X 745 751])
    xlabel('x(cm)'), ylabel('Temp (°C)')
    title('Reactor Block Temperature Profile Based on Measured Boundary Conditions')
    legend('y=0.275','y=0.14','y=0.92', 'y=0')
```

Appendix C. Condenser Design Equations

Purpose

To determine the length of the condenser needed to quench the reaction from greater than 750°C to 30°C.

Design Equations

The length of the condenser was determined based on an energy balance bringing water from reactor temperatures to 30°C. The heat rate, $\dot{Q}$, needed to be taken out of the reactor effluent was calculated by

$$\dot{Q} = \Delta H = \dot{m}(\hat{H}_{H_2O,Out} - \hat{H}_{H_2O,In}) \tag{2.5}$$

where $\dot{m}$ is the mass flow rate of the effluent, $\hat{H}_{H_2O,In}$ is the enthalpy of the reactor effluent at the reactor conditions, and $\hat{H}_{H_2O,Out}$ is the enthalpy of the reactor effluent at ambient conditions. Steam tables were used to determine the inlet and outlet enthalpies due to its large excess in the reactor effluent. After calculating the amount of heat that needed to be taken out of the reactor effluent the following heat exchanger design equation was used to calculate the length of the condenser

$$L = \frac{\dot{Q}}{U_o * \Delta T_{lm} * \pi * d_o} \tag{2.6}$$

where d_o is the outer diameter of the inner tube, U_o is the overall heat transfer coefficient, and ΔT_{lm} is the log mean temperature given by

$$\Delta T_{lm} = \frac{(T_{in} - T_s) - (T_{out} - T_s)}{\ln(\frac{T_{in} - T_s}{T_{out} - T_s})} \tag{2.7}$$

In Equation 2.7 T_{in} is the reactor effluent temperature coming into the condenser, T_{out} is the reactor effluent temperature coming out of the condenser, and T_s is the temperature of the cooling water. A heat transfer coefficient of 0.023 J/cm^{2}sec°C was used, and the length of the condenser was designed to be 4 inches.